

# Investigating the Regulation of Ras Protein Prenylation

by

Desirée García-Torres

A dissertation submitted in partial fulfillment  
of the requirements for the degree of  
Doctor of Philosophy  
(Chemical Biology)  
in The University of Michigan  
2019

Doctoral Committee:

Professor Emerita Carol A. Fierke, Co-Chair  
Professor Anna K. Mapp, Co-Chair  
Assistant Professor Brent R. Martin  
Associate Professor Patrick J. O'Brien

Desirée García-Torres

dega@umich.edu

ORCID iD: 0000-0001-7293-9402

© Desirée García-Torres 2019

## ACKNOWLEDGMENTS

This thesis work would not have been possible without the support and guidance of many people throughout my scientific journey. First, I want to thank my thesis advisor, Dr. Carol A. Fierke, for her great mentorship, for allowing me to have the creative liberty to explore the scientific unknown, and for believing that I could successfully achieve this milestone. I want to thank my undergraduate research advisors, Dr. Carlos Cabrera, Dr. Carlos Hangarter, and Dr. Yihua Liu. You all instilled this never-ending sense of curiosity for science that contributed to my decision to pursue a doctoral degree. I also want to thank my committee members for their advice and assistance during my thesis research.

I want to thank past and present members of the Fierke laboratory. I want to give special thanks to Dr. Benjamin C. Jennings. You took me under your wing, shared with me that curiosity to know more about how small GTPases are regulated, and gave me the tools to pursue my research interests. I will never forget your words: “It is not about working hard, it is about working *smart*.” I also want to thank Kelsey Diffley, Andrea Stoddard, Dr. Katherine R. Leng, Dr. Carol Ann Castañeda, Dr. Nancy Wu, and Dr. Eric Sullivan. I appreciate your friendships and the many conversations about life and science, but mostly about experiments that didn’t work.

I am very grateful to my mother for her love and support during this process. I thank you for your many words of encouragement and for holding me up when I missed being back home in Puerto Rico and my strength wasn’t enough to think that I could continue. I also thank my family for the many phone calls, messages, and care packages. Even with the 2,000+ miles of distance, I could feel your warmth and love all the way in the Michigan tundra. My love and appreciation go to my husband, Jaime A. De Jesús-Rodríguez, for embarking on this journey with me, for respecting my voice and providing support and motivation to finish well.

Lastly, I want to acknowledge all the incredible women scientists that I have met during my life. You have immensely inspired me. With your examples, I have realized that there is a space for *all* of us in science.

## TABLE OF CONTENTS

<b>ACKNOWLEDGMENTS</b> .....	<b>ii</b>
<b>LIST OF FIGURES</b> .....	<b>vii</b>
<b>LIST OF TABLES</b> .....	<b>ix</b>
<b>ABSTRACT</b> .....	<b>x</b>
<b>CHAPTER 1. Introduction</b> .....	<b>1</b>
Overview .....	1
Ras proteins .....	2
Ras protein trafficking pathway.....	4
Modulation of Ras prenylation .....	7
DiRas proteins .....	11
Ras and human diseases .....	13
Cancer .....	13
RASopathies.....	14
Direct approaches to targeting Ras in human cancers .....	16
Objectives of this work.....	18
References .....	20
<b>CHAPTER 2. SmgGDS-607 Exhibits Dual Effects in Regulating Farnesylation of Small GTPases: Activation and Inhibition</b> .....	<b>29</b>
Introduction.....	29
Experimental Procedures .....	31
Materials .....	31

Preparation of Ras protein expression constructs .....	31
Preparation of human FTase and GGTase-I expression constructs .....	32
FTase and GGTase-I expression and purification .....	33
Biotinylated small GTPase expression and purification .....	34
Non-biotinylated small GTPase expression and purification .....	35
Radiolabel prenylation assay .....	35
Peptide prenylation assay .....	37
Binding assay .....	37
Results .....	38
SmgGDS-607 blocks farnesylation of DiRas1 but not KRas4B .....	38
SmgGDS-607 does not inhibit FTase reactivity .....	40
Differential binding affinities for SmgGDS-607 with FTase substrates.....	40
FTase binds to small GTPases with differential binding affinities .....	43
SmgGDS-607 blocks farnesylation of KRas4B when the CAAX ends in leucine .....	43
SmgGDS-607 enhances farnesylation of HRas.....	44
Discussion .....	47
Appendix .....	52
References .....	60

### **CHAPTER 3. Synergies Between the Upstream Polybasic Region and CAAX**

<b>Identity in Ras Dictate Specificity of Prenylation and Interaction with SmgGDS-607.....</b>	<b>63</b>
Introduction.....	63
Experimental Procedures .....	65
Materials .....	65
Preparation of KRas4B and HRas PBR chimera expression constructs..	65

Preparation of KRas4B and HRas CAAX chimera expression constructs	66
FTase expression and purification .....	66
Ras expression and purification.....	67
Steady-state kinetics.....	67
Transient kinetics.....	68
Binding assay .....	68
Results .....	69
The PBR sequence in Ras proteins enhances the steady-state kinetic parameters.....	69
PBR sequences enhance the transient kinetics catalyzed by FTase .....	72
Charge distribution in the PBR affects FTase kinetics .....	74
Synergies between CAAX and PBR dictate binding affinities of Ras substrates for SmgGDS-607.....	76
PBR in Ras influences SmgGDS-607-mediated regulation .....	77
Discussion .....	79
References .....	85
<b>CHAPTER 4. Conclusions and Future Directions.....</b>	<b>88</b>
The role of SmgGDS-607 in Ras prenylation .....	88
The role of the PBR in protein binding and catalysis .....	91
Implications of thesis work in cancer treatment .....	94
References .....	95

## LIST OF FIGURES

Figure 1.1. Map of Ras structural domains.....	2
Figure 1.2. Ras GTPase cycle .....	3
Figure 1.3. Ras membrane trafficking pathway .....	5
Figure 1.4. Post-translational lipid modifications that occur at the HVR of Ras isoforms	6
Figure 1.5. Structure of rat FTase complexed with an FPP analog and a KKKSKTKCVIM peptide .....	8
Figure 1.6. Electrostatic surface potential map of the SmgGDS crystal structure (PDB5XGC).....	9
Figure 1.7. DiRas proteins sequence alignment.....	11
Figure 1.8. Structure of the four FTI compounds most evaluated in clinical trials (108)	16
Figure 2.1. Farnesylation of FTase substrates in the presence of SmgGDS-607 .....	39
Figure 2.2. SmgGDS-607 binds directly to KRas4B, KRas4B M188L, and DiRas1, as measured by bio-layer interferometry .....	41
Figure 2.3. SmgGDS-607 blocks farnesylation of mutant KRas4B M188L, a less reactive FTase substrate.....	44
Figure 2.4. Farnesylation of HRas is enhanced in the presence of SmgGDS-607 .....	45
Figure 2.5. SmgGDS-607 enhances HRas farnesylation by stimulating both chemistry and product release .....	46
Figure 2.6. Proposed model for SmgGDS-607-mediated regulation of farnesylation of FTase substrates .....	49
Figure A1. Simulation of SmgGDS-607 concentration dependence for inhibition of small GTPase farnesylation using the KinTek Explorer Chemical Kinetics Software .....	56

Figure A2. SmgGDS-607 blocks the extent of geranylgeranylation of KRas4B ..... 57

Figure 3.1. Steady-state kinetics for FTase catalyzing prenylation of Ras substrates... 70

Figure 3.2. Comparison of the turnover constant  $k_{cat}$  for FTase-catalyzed prenylation of various Ras substrates..... 71

Figure 3.3. Single-turnover rate for farnesylation of Ras substrates ..... 73

Figure 3.4. Comparison of steady-state and single-turnover kinetic parameters of FTase-catalyzed prenylation of KRas4B and DiRas proteins..... 75

Figure 3.5. SmgGDS-607 exhibits differential effects on farnesylation of Ras substrates ..... 78

Figure 3.6. Kinetic Pathway for the FTase-catalyzed prenylation of Ras substrates..... 80

Figure 4.1. Proposed kinetic mechanisms for FTase catalytic cycle ..... 92

## LIST OF TABLES

Table 2.1. Tail sequences of FTase substrates used in this study .....	39
Table 2.2. Kinetic parameters for farnesylation of KRas4B CAAX peptide catalyzed by FTase .....	40
Table 2.3. Summary of thermodynamic values for SmgGDS-607 and FTase binding to different small GTPases .....	42
Table 2.4. Kinetic parameters for farnesylation of HRas catalyzed by FTase .....	47
Table A1. Summary of thermodynamic and kinetic values for SmgGDS-607 and prenyltransferases binding to different small GTPases .....	52
Table A2. Summary of parameters used for simulation of SmgGDS-607 concentration dependence for inhibition of small GTPase prenylation .....	53
Table 3.1. C-terminal sequence of FTase substrates used for this study .....	64
Table 3.2. Kinetic parameters for farnesylation of Ras proteins .....	69
Table 3.3. Kinetic parameters for farnesylation of DiRas proteins.....	75
Table 3.4. Binding affinity of SmgGDS-607 for Ras proteins.....	76

## ABSTRACT

Ras family small GTPases undergo prenylation for proper localization to the plasma membrane, where they carry out their signaling function. Prevalent mutations in these proteins that render them persistently active have attracted a lot of attention due to their association with disease and developmental syndromes, such as cancer and RASopathies. Protein farnesyltransferase (FTase) catalyzes the incorporation of a farnesyl moiety to the Cys residue in the C-terminal CAAX motif of Ras, stimulating proper membrane association. Small GTP-binding protein GDP-dissociation stimulator (SmgGDS) proteins are chaperones involved in binding and trafficking small GTPases. Recent data suggest that SmgGDS proteins also regulate prenylation of small GTPases *in vivo* in a substrate-selective manner. In addition to the CAAX motif, many Ras family members contain a polybasic region (PBR) upstream of the CAAX that is proposed to increase binding affinity to different protein interactors, including FTase and SmgGDS-607, and play a role in protein trafficking.

To investigate the role of SmgGDS-607 in Ras prenylation, we developed a model for regulation of farnesylation that highlights the importance of the PBR and CAAX motif on recognition and processing of full-length Ras proteins. Here we demonstrate that SmgGDS-607 differentially regulates farnesylation of several small GTPases. For some proteins, such as DiRas1, SmgGDS-607 inhibits farnesylation by sequestering the substrate and limiting modification catalyzed by FTase. The competitive binding affinities of the small GTPase for SmgGDS-607 and FTase dictate the extent of inhibition. Additionally, we demonstrate a novel function for SmgGDS-607, increasing the rate of farnesylation of HRas by enhancing product release from FTase. Since the cell contains multiple small GTPases regulated by SmgGDS, these differential interactions can lead to large changes in prenylation status.

We systematically studied the role of the PBR and CAAX motif in modulating substrate recognition by both FTase and SmgGDS-607 through use of a set of Ras chimeric mutants in kinetic and binding experiments. This work demonstrates that SmgGDS-607 binds to a broad range of small GTPases and does not require a PBR for recognition, although the presence of a PBR influences the strength of the SmgGDS:Ras interaction. These studies demonstrate that the PBR enhances catalytic efficiency, as higher values for both prenylation turnover ( $k_{\text{cat}}$ ) and substrate selectivity ( $k_{\text{cat}}/K_{\text{M}}$ ) are observed for substrates containing PBRs. Furthermore, the PBR plays an important role in facilitating product release. However, the CAAX identity also contributes to the extent of enhancement of  $k_{\text{cat}}$  and the single-turnover rate. Thus, the synergistic effects of the PBR and CAAX motif ultimately dictate whether SmgGDS-607 will inhibit or enhance prenylation. Together, this work provides mechanistic insight into the regulation of protein farnesylation of small GTPases, elucidating the role of the PBR and CAAX in farnesylation kinetics and demonstrating that SmgGDS-607 has multiple modes of substrate recognition, which can be of great importance for the development of novel anti-cancer therapeutics.

## CHAPTER 1

### Introduction

#### *Overview*

Small GTPases of the Ras family are associated with the development of cancer and a group of rare genetic conditions termed RASopathies. The involvement of Ras proteins with these health conditions stems from their signaling function that occurs at the plasma membrane. Prenylation is a post-translational modification that promotes membrane localization of Ras GTPases. This modification involves the addition of an isoprenoid, either a 15-carbon farnesyl or a 20-carbon geranylgeranyl group, to a cysteine residue located in the C-terminal CAAX motif of such proteins. CAAX-protein prenylation has been generally assumed to be constitutive. However, recently, SmgGDS (small GTP-binding protein GDP-dissociation stimulator) proteins have been identified as chaperone proteins that regulate prenylation of small GTPases. Many Ras and Ras-like GTPases contain an upstream polybasic region (PBR), which has been proposed to be recognized by both the prenyltransferase that catalyzes the attachment of the isoprenoid and SmgGDS proteins. This PBR has been observed to also aid in plasma membrane localization. The main goal of this work is to better understand how Ras proteins enter the prenylation pathway and the mechanism employed for regulation of prenylation. In this chapter, I will further describe Ras proteins and their function as small GTPases, touching on the significance of prenylation in the Ras membrane trafficking pathway, and the different proteins and mechanisms that contribute to the regulation of this post-translational modification. I will also discuss the involvement of Ras in various human pathologies.

## Ras proteins

Ras proteins regulate cellular signaling pathways responsible for gene expression, cell proliferation, survival and differentiation. Their primary role is to recruit transient signaling complexes at the plasma membrane to activate signal transduction pathways. In mammals, the expression of Ras proteins is encoded in three RAS genes: *HRAS*, *NRAS*, and *KRAS*. These genes give rise to four protein isoforms: HRas, NRas, KRas4A, and KRas4B. Structurally, Ras proteins can be defined by two domains (Figure 1.1). The largest one is known as the G domain (the first 165 amino acids) with >85% conserved sequence identity among the four mammalian proteins. The G domain contains five motifs that bind the guanosine nucleotide responsible for modulating Ras activity and an effector binding motif recognized by many binding partners. The second domain, which is the membrane targeting region, consists of the last 23-24 amino acids found at the C-terminus. This domain is characterized by a hypervariable region (HVR) and a CAAX motif.

Ras proteins belong to the large family of small GTPases, functioning as binary molecular switches that cycle between “on” and “off” states depending on the type of

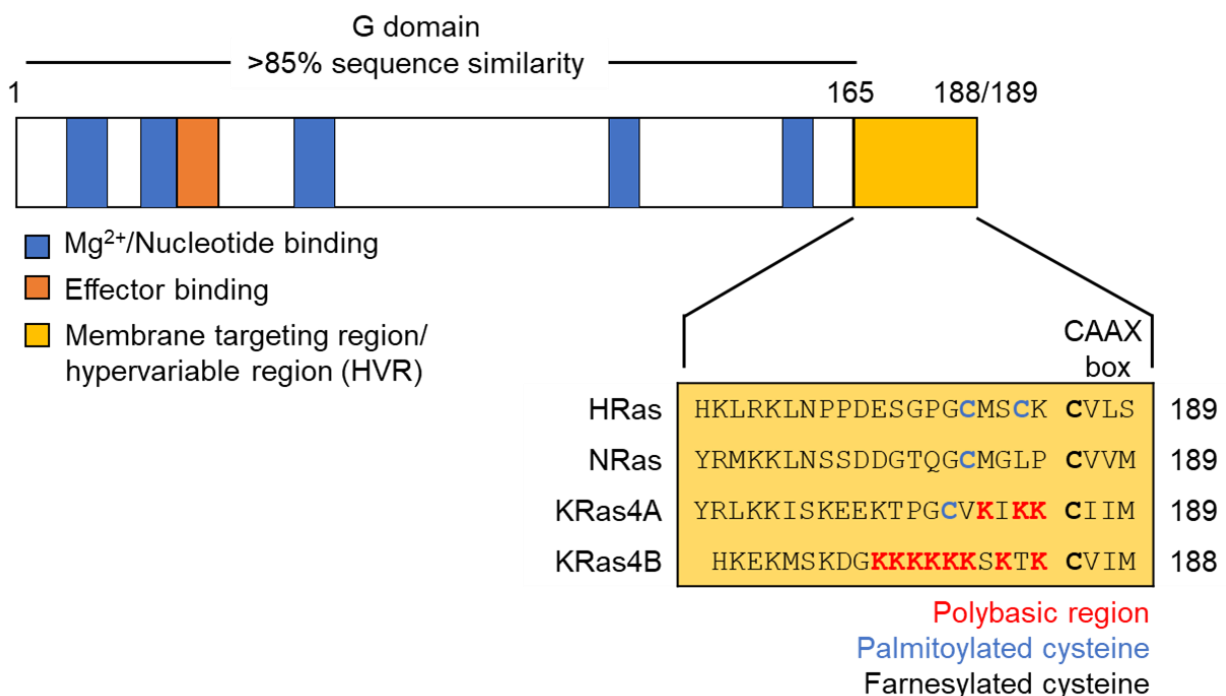


**Figure 1.1. Map of Ras structural domains.** The differences in amino acid sequence at the HVR dictate the different post-translational modifications that each isoform will undergo. Adapted from ref 107.

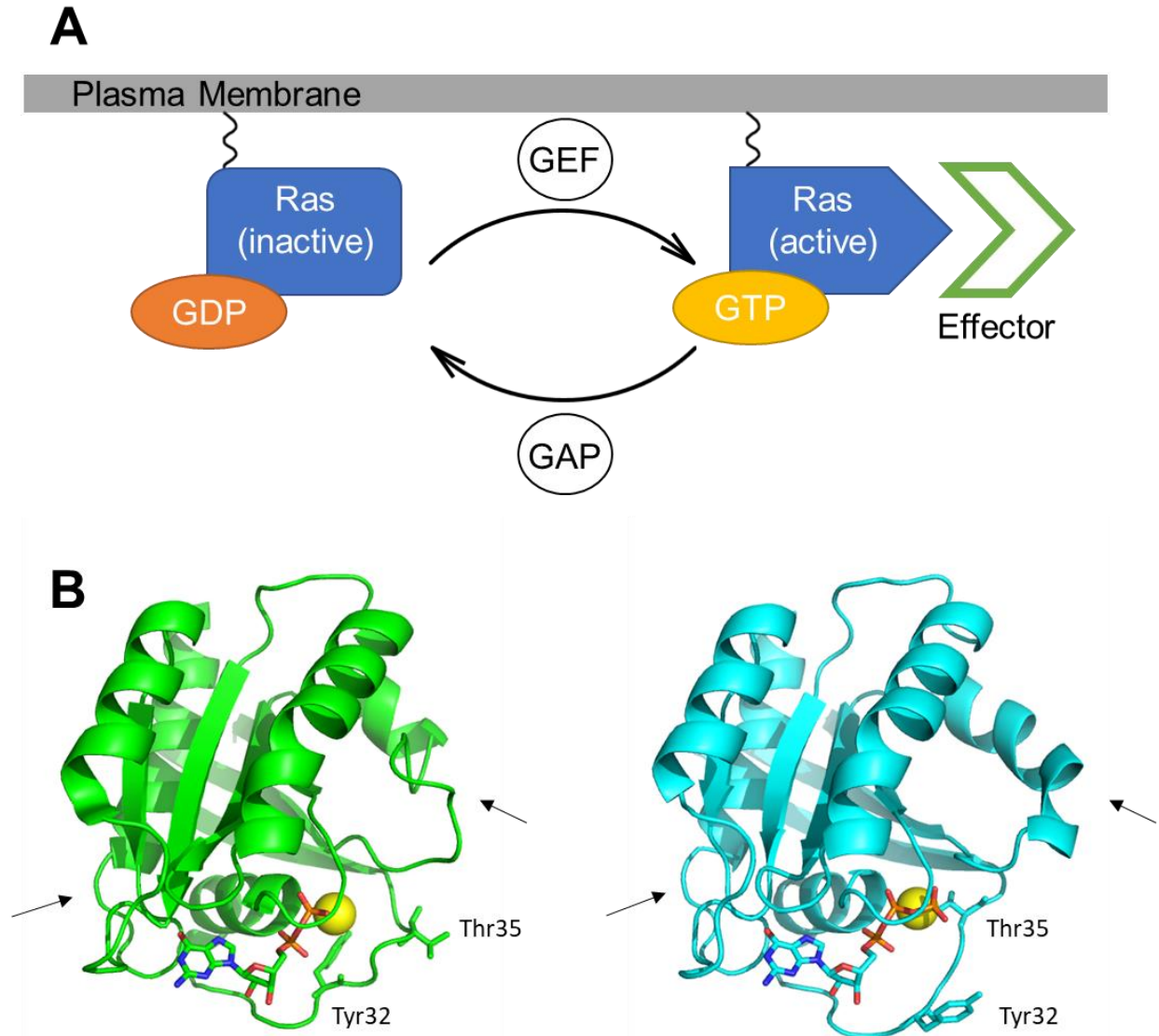


**Figure 1.2. Ras GTPase cycle.** A. Ras is activated when it binds a GTP molecule and inactivated when it binds a GDP molecule. Nucleotide exchange is stimulated by a GEF, while GTP hydrolysis is stimulated by a GAP. B. Structural changes in Ras upon nucleotide binding. Ras-GDP (PDB1Q21) is shown in green and Ras-GTP (PDB1QRA) is shown in cyan. The bound nucleotide is shown for both structures in stick figure and the bound  $Mg^{2+}$  in yellow. Secondary structure and loops that alter upon change in the bound nucleotide are shown with an arrow, highlighting the spatial orientation of Tyr32 and Thr35.

guanosine nucleotide bound (Figure 1.2A). Ras proteins are considered to be active when bound to guanosine triphosphate (GTP), allowing for a structural conformation that exposes an interaction surface that binds effectors with high affinity. In contrast, a guanosine diphosphate (GDP)-bound state leads to inactivation. The conversion from a GTP-bound to GDP-bound state occurs by means of the Ras hydrolase activity that catalyzes hydrolysis of the chemical bond of the  $\gamma$ -phosphorous atom in the GTP

molecule. After GTP hydrolysis, the Ras GTPase releases the resulting GDP molecule and binds a new GTP molecule to continue the cycle. However, the rates of intrinsic GTP hydrolysis ( $t_{1/2} = 17 \text{ min}$ ,  $k_{\text{off}} = 68 \times 10^{-5} \text{ s}^{-1}$ ) and GDP dissociation ( $t_{1/2} = 6 \text{ min}$ ,  $k_{\text{off}} = 2 \times 10^{-3} \text{ s}^{-1}$ ) are too slow for physiological relevance (1). Staying in either a GDP- or GTP-bound state for too long can disrupt the equilibrium of steps downstream of Ras activation, which can be deleterious for cell homeostasis. For efficient GTP hydrolysis, Ras proteins interact with GTPase-activating proteins (GAPs) that accelerate the GTP hydrolysis step by several orders of magnitude. To counteract this acceleration, guanine nucleotide exchange factors (GEFs) catalyze dissociation of GDP from Ras, allowing GTP to bind and maintain equilibrium in the GTP/GDP cycle. The type of guanosine nucleotide bound to Ras dictates the structural conformation of these proteins (Figure 1.2B). In the GDP-bound conformation, residues in the effector binding interface, such as Tyr32 and Thr35, are in a spatial conformation that is not optimal for interaction with binding partners. The change from GDP to GTP leads to a rearrangement of these residues, including formation of secondary structure, that enhances the affinity for binding partners, controlling the ability of Ras to interact with downstream effectors. Both nucleotide-bound status and membrane localization of these proteins serve a critical role in proper cell function, as both mediate the ability of Ras proteins to interact with signaling effectors and disruption can lead to the development of human diseases.

### ***Ras protein trafficking pathway***

Membrane association is essential for Ras proteins to initiate downstream signaling pathways. Previously, it was presumed that Ras signaling events happened exclusively at the plasma membrane. However, several studies have demonstrated that these signaling events can occur at intracellular membranes, including endosomes, the endoplasmic reticulum (ER), and the Golgi apparatus (2-7). The localization of Ras to the pertinent membrane platforms is mediated by a series of post-translational modifications (PTMs) that direct trafficking from the cytosolic surface of the ER to the inner surface of the plasma membrane (Figure 1.3) (8). All Ras protein isoforms contain a C-terminal consensus sequence known as the CAAX motif, where C is the cysteine to be modified, A is frequently an aliphatic residue, and the X residue is variable. After protein synthesis,

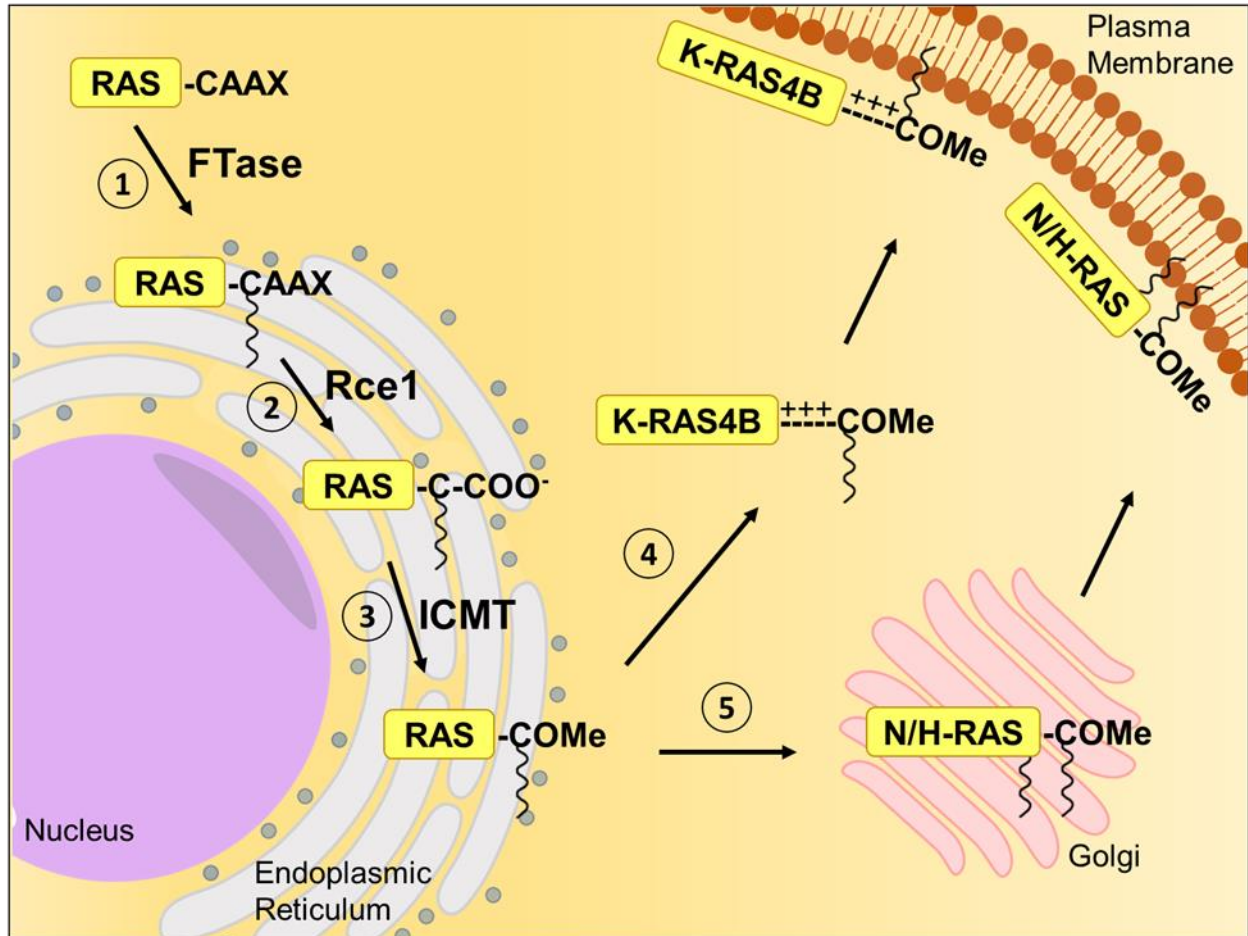


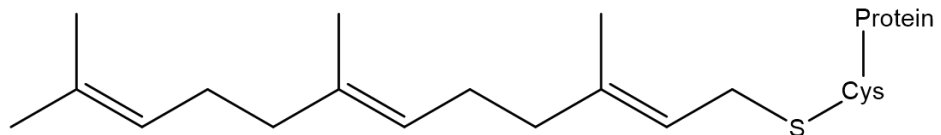
**Figure 1.3. Ras membrane trafficking pathway.** Ras proteins are synthesized in the cytosol, followed by farnesylation mediated by FTase (1). Proteolysis of -AAX residues (2) and O-methylation (3) of the Ras C-terminus catalyzed by Rce1 and ICMT, respectively, occurs at the cytosolic surface of the ER. KRas4B is shuttled directly to the plasma membrane where positively charged residues at the HVR enhance localization (4). NRas and HRas proceed to the cytosolic surface of the Golgi apparatus to be palmitoylated by the DHH9—GCP16 complex (5), followed by vesicular transport to the plasma membrane.

this CAAX motif is generally sequentially processed in three main steps: farnesylation, proteolysis, and methylation. The first step, farnesylation, is the irreversible attachment of a 15-carbon farnesyl moiety to the cysteine thiol catalyzed by protein farnesyltransferase (FTase) (9). For some Ras isoforms, under conditions where farnesylation is inhibited, the alternative attachment of a 20-carbon geranylgeranyl moiety is catalyzed by protein geranylgeranyltransferase type 1 (GGTase-I) (10). Following lipid attachment, a prenyl protein protease in the ER membrane, RAS-converting CAAX endopeptidase 1 (Rce1), catalyzes cleavage of the last three residues (–AAX) of the GTPase CAAX proteins. Finally, in step three, isoprenylcysteine carboxylmethyltransferase (ICMT) catalyzes the addition of a methyl group to the newly

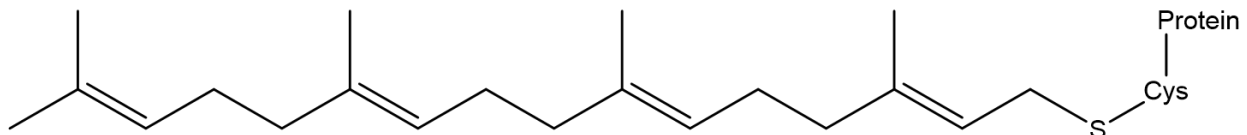
exposed carboxy-terminus, making the C-terminus more hydrophobic and capable of insertion into cellular membranes (9,11). Although CAAX processing allows for association of Ras with ER membranes, this modification alone is insufficient for stable association with the plasma membrane.

Depending on the small GTPase identity, the protein may undergo additional PTMs before trafficking to the plasma membrane. After prenylation, both HRas and NRas are shuttled through vesicular transport from the ER to the Golgi, where they are palmitoylated by the palmitoyl acyltransferase (PAT) identified as DHHC9–GCP16 protein complex (12). Unlike farnesylation, palmitoylation is a reversible process that consists of the covalent attachment of a 16-carbon palmitoyl chain on cysteine residues (Figure 1.4) (13). HRas has two cysteine residues that are palmitoylated (Cys181 and Cys184), whereas NRas has only one (Cys181). The addition of a single palmitoyl chain has been demonstrated to increase the affinity of these Ras isoforms for membranes by 100-fold (14,15). Therefore, palmitoylation helps in trapping Ras to the endomembrane compartments and subsequently transporting them to the plasma membrane via transport vesicles. KRas4A is also palmitoylated at Cys181 by a PAT that has yet to be identified. However, KRas4A bypasses the Golgi and is transported directly to the plasma membrane where the basic residues in the HVR help stabilize the membrane interaction

### Farnesyl



### Geranylgeranyl



### Palmitoyl

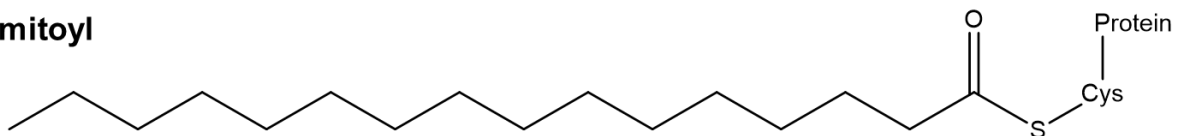


**Figure 1.4. Post-translational lipid modifications that occur at the HVR of Ras isoforms.** All Ras isoforms require the incorporation of a farnesyl group to the C-terminal Cys residue to continue through the membrane trafficking pathway. The incorporation of a geranylgeranyl group can occur for NRas, KRas4B and KRas4A under conditions in which farnesylation is inhibited. Attachment of a palmitoyl group is required for plasma membrane localization of NRas and HRas.

(16). Unlike the other Ras isoforms, KRas4B is not palmitoylated, but contains tandem lysine repeats in the HVR that facilitate membrane association (17). This stretch of positively charged residues found in the HVR of many small GTPases is also known as a polybasic region (PBR) and can be composed of varying lysine and arginine combinations and repetitions. The presence of a PBR in KRas4B enables electrostatic interactions with the negatively charged headgroups of the lipids that compose the plasma membrane, allowing for stronger membrane affinity and bypassing transport to the Golgi. The mode of transport from the ER to the plasma membrane of KRas4B is still unknown. However, all Ras proteins need to contain at least a prenyl group as an anchor to the membrane, where they fulfill their biological role. Hence, CAAX lipidation plays a crucial role in small GTPase function (18,19). In this work, the central focus will be around prenylation catalyzed by FTase.

### ***Modulation of Ras prenylation***

One of the most distinctive features of Ras isoforms is the presence of polybasic residues in the HVR, characteristically termed the polybasic (PBR) region. Interestingly, HRas is the only Ras isoform that lacks a PBR. Understanding the differences between the Ras isoforms that contain a PBR and HRas has sparked significant interest since the discovery of the Ras proteins. As previously mentioned, the PBR, and lack thereof, in Ras isoforms plays a crucial function in dictating how these proteins associate with membranes and what PTMs occur. Furthermore, there is striking evidence that the PBR also regulates the interaction of Ras with other proteins (20-28). One such interaction is that of FTase with Ras isoforms. James and colleagues demonstrated through *in vitro* experiments that the PBR contributes to higher affinity binding of FTase and KRas4B, compared to HRas (24). When the C-terminal sequence of HRas is substituted with the PBR of KRas4B, a lower concentration similar to that of KRas4B is required to saturate FTase with this HRas chimera. The co-crystal structure of FTase with a KRas4B-derived 11-mer peptide substrate demonstrates that FTase makes several direct contacts with the PBR. Most of the interactions occur between  $\beta$ -subunit residues (Asp91, Glu94, Arg358, Arg359) and lysine residues in the peptide (Figure 1.5) (26). Additionally, previous members in the Fierke laboratory have studied the role of the PBR in modulating

prenyltransferase kinetics with peptide substrates. These data indicate that the presence of a PBR allows for alternative prenylation of KRas4B by decreasing the catalytic efficiency of FTase to a level comparable to that of geranylgeranylation catalyzed by GGTase-I (29).

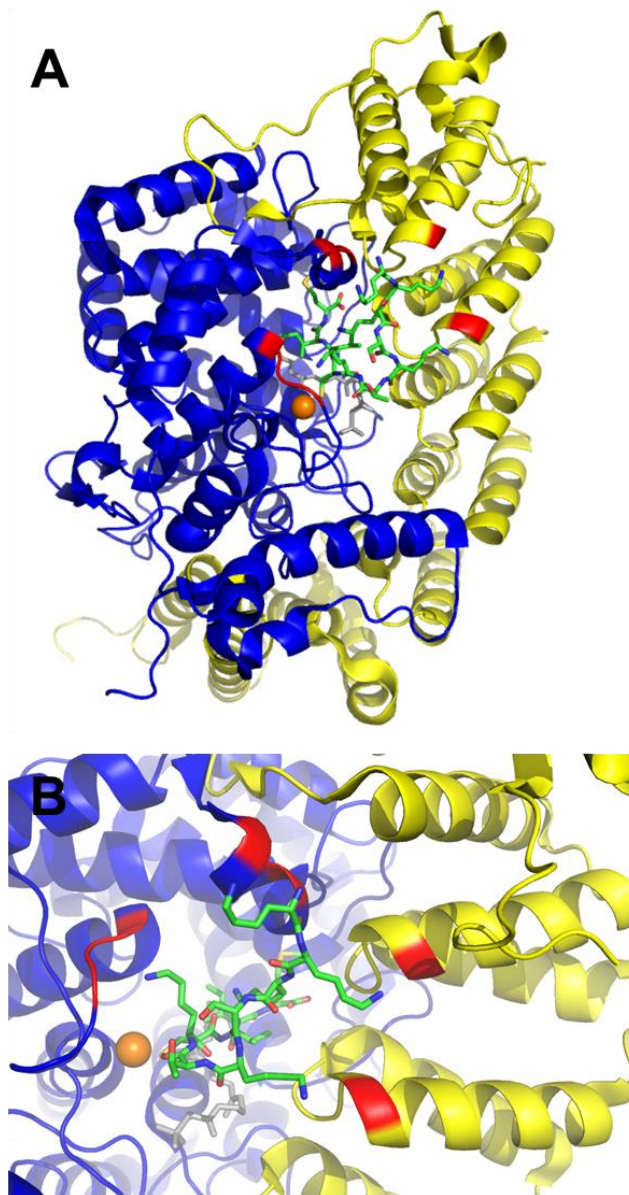


**Figure 1.5. Structure of rat FTase complexed with an FPP analog and a KKKSCTKCVIM peptide.** A. The rat FTase heterodimer (PDB1D8D) is shown with the  $\alpha$ -subunit in yellow and the  $\beta$ -subunit in blue. The bound FPP analog (gray) and 11-mer peptide are represented in stick figures. Residues at the FTase interface that make polar interactions with the upstream lysine residues in the KRas4B-derived peptide are highlighted in red. B. View of the substrate binding cavity. The 11-mer peptide is bound in such a conformation where Cys coordinates with  $Zn^{2+}$ , while FPP analog binds  $Mg^{2+}$  (in orange). The upstream lysine residues (Lys1, Lys2, Lys5, and Lys7) make polar contacts with residues at the FTase interface.

Another interaction that appears to be modulated by the PBR is that of Ras and the small G protein GDP dissociation stimulator (SmgGDS). The entry of Ras proteins to the membrane trafficking pathway was originally proposed to be constitutive. After farnesylation, Ras proteins gain affinity for membranes, particularly the ER membranes, where subsequent CAAX modifications are catalyzed. However, until recently the transport mechanism for farnesylated Ras proteins from the cytosol to the ER membranes was a mystery. In recent studies, small GTPases were proposed to interact with two splice variants of SmgGDS, termed SmgGDS-607 and SmgGDS-558, which served as chaperones to traffic modified Ras proteins to the plasma membrane (20,21,30). SmgGDS proteins are structurally characterized by a unique fold consisting of armadillo (ARM) repeats (31). However, SmgGDS-607 and SmgGDS-558 differ by one armadillo repeat, which leads to the reported differential binding preference for prenylated and non-prenylated small GTPases (20,22,32). SmgGDS contains an electronegative patch that interacts with the PBR of many binding partners, including Ras proteins (Figure 1.6) (17, 30, 40). Mutations of the conserved acidic residues that make up the electronegative patch in SmgGDS-607 diminish the ability of SmgGDS-607 to interact with RhoA and

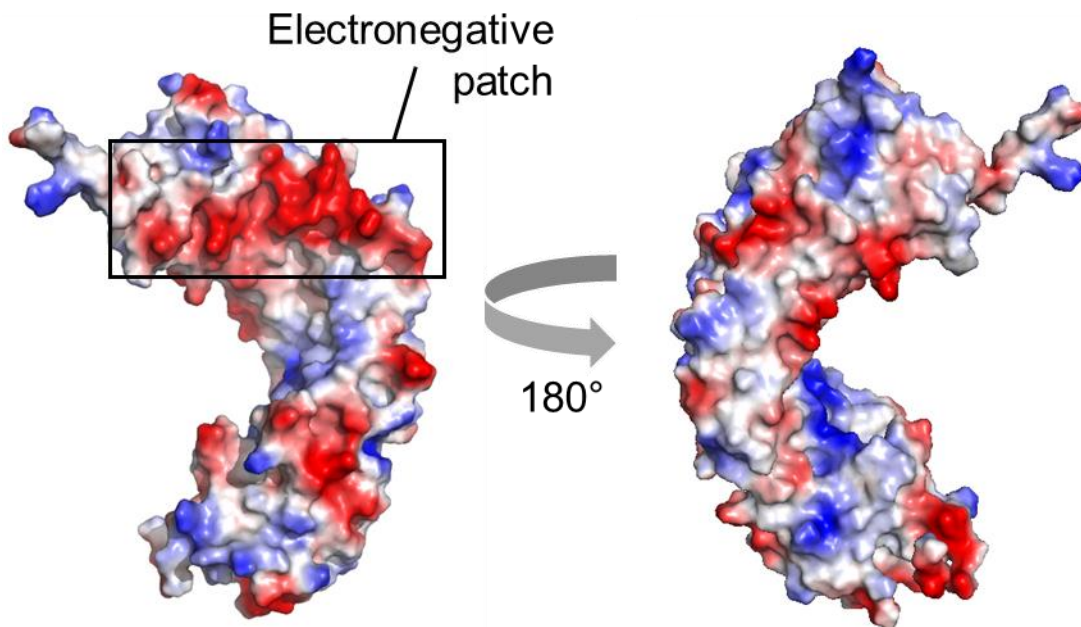


**Figure 1.6. Electrostatic surface potential map of the SmgGDS crystal structure (PDB5XGC).** The negatively charged and positively charged regions are shown in red and blue, respectively. The electronegative patch that interacts with the PBR of small GTPases is indicated by the black rectangle. Adapted from ref 31.

promote GDP release (33). Similarly, truncation of the PBR or mutations in the PBR that disrupt the positive charge result in an inability to form a high affinity complex between SmgGDS-607 and RhoA, confirming the importance of this domain for high affinity interaction with SmgGDS. This electrostatic interaction is not only important for RhoA, but also seems to be crucial for stable complex formation between SmgGDS and other small GTPases, including KRas4B, DiRas1, and DiRas2 (23, 33-36). Additionally, the SmgGDS splice variants contain a highly conserved binding pocket on its surface, in which multiple small GTPases can bind (31,33,34).

Initially, SmgGDS proteins were classified as small GTPase activators that promote GDP/GTP exchange in a distinct manner from GEFs and GAPs (37-39). Yet, a recent *in vitro* study performed with a panel of distinct small GTPases demonstrated that SmgGDS is solely able to activate RhoA and RhoC (33), suggesting that SmgGDS proteins may play different roles depending on the identity of the small GTPase. Nevertheless, cell-based experiments suggest that the splice variants of SmgGDS work together as chaperone proteins to promote the passage of small GTPases through the prenylation pathway. Pull-down experiments demonstrate that SmgGDS-607 binds newly synthesized, non-prenylated small GTPases and may escort them to the prenyltransferase (20,22,40). In contrast, SmgGDS-558 binds to the prenylated small GTPases and potentially helps trafficking to the ER (20,22,32). The binding interaction between SmgGDS-607 and the non-prenylated small GTPases reduces their levels of prenylation (20, 40), suggesting a mode of regulation in which SmgGDS-607 sequesters newly synthesized small GTPases in the cytoplasm from prenylation until receiving a signal. After prenylation, SmgGDS-558 might promote the release of newly prenylated small GTPase from the prenyltransferase and also aid in transport to the ER. Although SmgGDS-607 binds non-prenylated small GTPases, it was found that SmgGDS-607 regulates the prenylation of small GTPases that are geranylgeranylated more effectively than those that are farnesylated, such as KRas4B (20). Detailed biochemical analysis has demonstrated that SmgGDS-607 follows a substrate sequestration model for regulation of RhoA geranylgeranylation (40), suggesting that the entry of other small GTPases into the prenylation pathway may be regulated in a similar fashion. Overexpression of SmgGDS has been found to promote malignancy in multiple cancers including prostate

cancer (41), non-small cell lung carcinoma (42), and breast cancer (43). Since SmgGDS-607 binds a wide variety of small GTPases and exhibits GEF activity for a select number of them, understanding the mechanism that dictates the small GTPase selectivity of SmgGDS will provide insight into the development of novel drug targets to treat the implicated cancer types.

### **DiRas proteins**

In the early 2000s, DiRas proteins were identified and characterized as Ras-like proteins that belong to a distinct subgroup of the Ras superfamily (44, 45). The DiRas family is composed of three small GTPases, including DiRas1 (also known as Rig), DiRas2 and DiRas3 (also referred to as NOEY2 and ARHI). DiRas1 and DiRas2 share 30-40% overall sequence identity with Ras family members, and ~40% sequence identity with DiRas3. In contrast, DiRas3 shares 20-25% sequence identity with Ras family members. Similar to other Ras family members, DiRas proteins contain a highly conserved GTP-binding domain, a putative effector domain, and a membrane targeting region at the C-terminus. However, studies have shown that DiRas proteins possess different biochemical and functional properties compared to other Ras family members (44).

DiRas1	1	-----MPEQSN DYRVVVF	GAGGVGKSS	LVLRFVKG	30	
DiRas2	1	-----MPEQSN DYRVAVF	GAGGVGKSS	LVLRFVKG	30	
DiRas3	1	MGNASFGSKEQKLLKRLRLLPALLILRAFKPHRKIRDYRVVVF	GTAGVGKST	LLHKWASG	60	
DiRas1	31	TFRDTYIPTIEDTYRQVISCDKSVCTLQITDT	TGSHQ	FPAMQRLSISKGHAFILVFSVTS	90	
DiRas2	31	TFRESYIPTVEDTYRQVISCDKSICTLQITDT	TGSHQ	FPAMQRLSISKGHAFILVYSITS	90	
DiRas3	61	NFRHEYLPTIENTYCQLLGC SHGVL SLHITD	SKSGDG	NRALQRHVIARGHAFVLVSVTK	120	
DiRas1	91	KQSLEELGPIYKLIVQIKGS-VEDIPVMLVGNKCD	ET-QREVD	TREAQAVAQEWKCAFME	148	
DiRas2	91	RQSLEELKPIYEQICEIKGD-VESIPIMLVGNKCD	ESPSREVQSSEAEALARTWKCAFME		149	
DiRas3	121	KETLEELKAFYELICKIKGNNLHKFP	IVLVGNKSD	DT-HREVALNDGATCAMEWNC	179	
DiRas1	149	TSAKMNYNVKELFQELLTLETRRNSLNIDG	KRSGKQKR	TD	RVKGKCTLM	
DiRas2	150	TSAKLNHNVKELFQELLNLEKRRTVSLQIDG	KKS	KQQKRKE	KLKGKCVIM	
DiRas3	180	ISAKTDVNVQELFHMLLNYKKKPTTGLQEPE	KKS	QMPN	TEKLLDKC	IIM

■ Putative Mg<sup>2+</sup>/nucleotide binding      ■ Putative effector binding

**Figure 1.7. DiRas proteins sequence alignment.** Highlighted in yellow are the residues found in the putative DiRas nucleotide binding or effector binding motifs that differ from those found in HRas; in red and bold are the positively charged residues that make up the respective PBRs.

The divergence in biochemistry and functionality of DiRas can be attributed to amino acid differences in the protein sequences that also lead to structural alterations (Figure 1.7). Within the GTP-binding domain, the residues corresponding to Ala59 and Gln61 in HRas are substituted by Thr63 and Ser65 for both DiRas1 and DiRas2. In DiRas3, the residues corresponding to Gly12 and Gln61 in HRas, which are required for nucleotide binding, are substituted by Ala46 and Gly95. Regarding the effector domain, DiRas differs from most Ras members in that Ile37 (both DiRas1 and DiRas2) and Leu67 (DiRas3) replace Asp33 in HRas. Additionally, Val40 (DiRas2) and Asn72 (DiRas3) are at a position corresponding to Ile36 and Asp38 in HRas. Most interestingly, DiRas3 contains a unique extension of 34 amino acids at the N-terminus, which is required for its tumor suppressive function (44,46). As a result of these substitutions, DiRas proteins exhibit low levels of GTPase activity and can be found in a GTP-bound conformation under physiological conditions (44). Furthermore, substitutions in the effector domain are proposed to alter the way DiRas isoforms associate with effector molecules (44).

Unlike Ras proteins, which are involved in the progression of cancers, DiRas isoforms have been identified as tumor suppressors in various cancer types. For example, DiRas1 has been recognized as a potential human neural and kidney tumor suppressor (45,47). DiRas3 has been identified as a tumor suppressor in ovarian and breast carcinomas (48). One way in which these proteins exert their tumor suppressive function is by antagonizing Ras-mediated signaling. Baljuls and colleagues demonstrated that DiRas3 could target Ras/RAF signaling by associating with HRas and its effector C-RAF. This association causes a disruption of HRas-induced heterodimerization of C-RAF with B-RAF and suppresses the kinase activity of C-RAF (49). DiRas1 was also shown to antagonize the RAS-mediated ERK/MAPK signaling pathway, as less Ras-mediated activation of Elk-1 was observed with the overexpression of DiRas1 (45). Other cases in which DiRas proteins interfere with signaling pathways have been observed for JAK/STAT, FAK, PI-3K/AKT, mTOR, and NF- $\kappa$ B signal transduction (50-54). Additionally, Bergom *et al.* described a tumor suppressive mechanism for DiRas1 where the activity of Ras and Rho family members is altered by antagonizing their interaction with SmgGDS (34).

## ***Ras and human diseases***

### ***Cancer***

Ras proteins have become one of the most intensively studied oncogenes because of the widespread prevalence of *RAS* gene mutations in human cancer. On average, missense mutations at one of the three mutational hotspots (G12, G13, Q61) in all *RAS* genes are found in 16% of human cancers (55). The oncogenic effects stem from the inability of the mutated Ras protein to perform GAP-mediated GTP hydrolysis, resulting in an accumulation of active GTP-bound Ras in cells (56, 57). Although all three Ras proteins have high (82-90%) sequence homology and conserved structural and biochemical properties, there is striking evidence of isoform-specific prevalence in cancer. When it comes to Ras-related cancers, KRas is the most frequently mutated isoform (86%), followed by NRas (11%) and HRas (3%) (55). Furthermore, mutations in specific isoforms have been linked to specific cancer types. For example, pancreatic ductal, lung and colorectal carcinomas are almost exclusively attributed to KRas mutations, while NRas is the most frequent isoform mutated in cutaneous melanomas and leukemias (58). Although HRas mutations are less frequent, they are predominantly associated with head and neck squamous cell carcinomas (59).

The complexity of Ras-related cancer types is significantly increased when considering the mutation frequency at each of the three hotspots. The majority of KRas mutations occur at codon G12 (83%), followed by G13 (14%) and Q61 (2%) mutations. KRas mutations in pancreatic ductal and lung adenocarcinoma are dominated by G12 mutations, while there is a relatively high frequency of G13 mutations in colorectal carcinomas. HRas exhibits comparable mutation frequencies across all three codons. In contrast, most (60%) of the NRas mutations occur at Q61, compared with G12 (23%) and G13 (12%). Mutations in codon Q61 in NRas encompass the most frequently mutated hotspot in melanoma, whereas G12 mutations are predominant in acute myeloid leukemia. Furthermore, the specific amino acid substitution at the mutational hotspots also contributes to significant differences between cancer types. For example, at G12, the predominant substitution in pancreatic ductal adenocarcinomas and colorectal carcinomas is G12D, followed by G12V; while in non-small cell lung carcinoma, the

predominant substitution is G12C (59). These patterns suggest that different Ras mutations and specific amino acid substitutions have different functional consequences.

Why there is bias for specific Ras isoforms and Ras mutation frequencies in cancer types is still a matter of speculation. One possible explanation revolves around the relative abundance of Ras isoforms in the cell. Through pull-down experiments, it was demonstrated that KRas and NRas are the two most abundant isoforms, while lower levels of HRas are expressed in different cancer cell lines (60). Furthermore, the Ras isoforms exhibit differences in membrane compartmentalization, with KRas associating almost exclusively with the cell surface whereas NRas displays a prominent ER/Golgi pool (60). Because different pools of regulators and effectors reside in the different cellular compartments, the alterations in membrane localization of the Ras isoforms are proposed to regulate how and when the different interactions take place. For example, it was shown that a variety of growth factors stimulate Ras at the ER and Golgi. Particularly, ER-localized Ras is capable of stimulating transformation and proliferation equivalent to that seen for oncogenic HRas, suggesting that HRas-related cancers might stem from signaling at the ER (61, 62). Due to these complexities in Ras-mediated tumor progression, for the past 30+ years, researchers all over the world have been employing diverse strategies to target these proteins for cancer therapies, as discussed in a later section.

### ***RASopathies***

The disruption of proper Ras signaling by mutations in genes that encode for proteins associated with the Ras/MAPK pathway gives rise to a class of developmental disorders categorized as congenital RASopathies. These mutations provide additional insight into Ras signaling pathways. Although each mutation exhibits unique phenotypic traits, many share characteristic features including craniofacial dysmorphism, cardiac defects, developmental and growth abnormalities, and varying degrees of neurocognitive impairment. Noonan syndrome (NS) is the most common syndrome, affecting between 1:1,000 and 1:2,500 newborns (63). Most of the germline mutations in NS cases occur in *PTPN11*, *SOS1*, *RAF1*, and *KRAS* genes (64-67), all important modulators of the RAS pathway. The *KRAS* mutations associated with NS result in either a reduction in GAP-

mediated GTP hydrolysis or interference in binding guanine nucleotides by KRas (67, 68). These effects lead to accumulation of active GTP-bound KRas, resulting in increased signaling of the Ras/MAPK pathway albeit at lesser levels than in cancer (67). Exhibiting a similar phenotype to NS, Noonan syndrome with multiple lentigines (NSML) (formerly called Leopard syndrome) is a distinct syndrome caused by heterozygous missense mutations in *PTPN11* and *RAF1* genes (66, 69).

A less common syndrome is Neurofibromatosis type 1 (NF1), affecting approximately 1 in 3,500 newborns (91). This disorder is caused by loss-of-function mutations in the *NF1* gene, which encodes for neurofibromin, a GAP that regulates Ras (70-72). Abolition of neurofibromin function results in reduction of Ras GTP hydrolysis, which increases signaling down the Ras/MAPK pathway. Legious syndrome, a milder form of NF1, occurs due to loss-of-function mutations in *SPRED1* (73). SPRED proteins are essential for the interaction between neurofibromin and Ras in the plasma membrane (74). Hence, disruption of SPRED-neurofibromin interaction leads to reduction of Ras GTPase activity. Costello syndrome (CS) is the rarest of the RASopathies, affecting about 300 people worldwide. Unlike the other RASopathies, only germline mutations in *HRAS* cause CS. Interestingly, similar to oncogenic Ras, the most frequent HRas mutations in CS occur in codon G12. More than 80% of cases occur due to a G12S substitution, followed by G12A (75). These mutations decrease GTPase activity, leading to an accumulation of active GTP-bound HRas. Cardio-facio-cutaneous syndrome (CFC) shares many phenotypic features with both NS and CS. Most germline mutations in CFC are activating mutations in *BRAF* (76). Less frequently, mutations occur in *KRAS*, *MEK1* and *MEK2* (76, 77). The role of mutant KRas in CFC has not been determined yet. However, it appears that mutant KRas might conserve GTPase activity, while being insensitive to GAPs (67).

Collectively, RASopathies make one of the largest known groups of malformation syndromes. In most cases, the implicated mutations result in constitutive activation of the Ras/MAPK pathway. Although more extensive studies are needed to understand the full spectrum of associated genes and implications of gene mutations, several therapeutics are being developed and some are even undergoing clinical trials (78,79). Since Ras prenylation is essential for proper trafficking and activation of the MAPK pathway, further

exploration of the regulation of Ras prenylation could pave the way for novel and effective therapies.

### ***Direct approaches to targeting Ras in human cancers***

Due to its central function in recruiting signaling complexes at the different membranes and its implications in malignant transformation, most current efforts to abolish aberrant Ras signaling leading to cancer have focused on the development of drugs that target Ras proteins or Ras effector pathways. Three key approaches have been used to directly target Ras signaling, such as altering the Ras-GTP/Ras-GDP balance, blocking the Ras-effector interaction, and disrupting Ras processing/localization. Although great progress

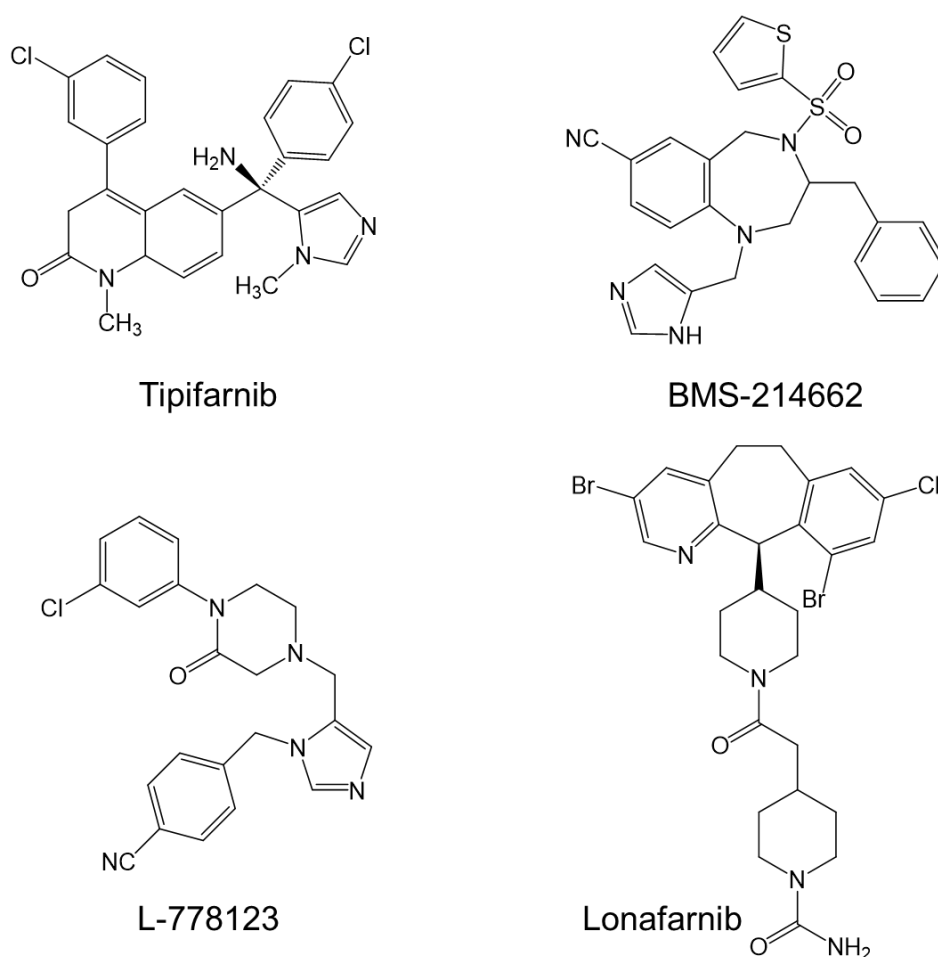


**Figure 1.8. Structure of the four FTI compounds most evaluated in clinical trials (108).** Tipifarnib is currently under phase I, II and III clinical trials for various cancer types. BMS-214662 is currently under phase I clinical trials for different leukemias and myelodysplastic syndromes. L-778123 is currently under a phase I clinical trial for refractory solid malignancies. Lonafarnib is currently under phase II clinical trials for various cancer types.

has been made in understanding the mechanism employed by Ras proteins in tumor cell growth, they still remain very challenging to target. SCH-53239 was one of the first small molecules designed to inhibit guanine nucleotide exchange in Ras (80). Its discovery led to the development of more soluble small molecule analogs (81). These initial studies propelled an overwhelming amount of efforts towards the discovery of small molecules or peptide mimics that target nucleotide exchange. However, this approach has encountered a lack of success due to the high binding affinity for GTP and GDP at picomolar levels combined with the high cellular concentrations of these analytes (82,83). Efforts to block multiple Ras-effector interactions by either allosteric modulators (84-87) or inhibitors of specific protein-protein interactions, such as Ras:Raf (88-91) and Ras:Sos1 (92, 93), have been successful. However, the vast majority of compounds lack potency and require further improvements to generate a useful Ras inhibitor.

Because of the relative low success in developing therapies that directly target oncogenic Ras, alternative strategies have been pursued in targeting Ras PTMs required for proper membrane localization (6, 94-96). This strategy has led to the development of highly potent FTase inhibitors (FTIs), with four moving on to clinical trials: tipifarnib, lonafarnib, BMS-214662 and L-778123 (Figure 1.8) (97). Unfortunately, these compounds have yet to prove to be efficacious in the clinic to treat tumors driven by mutations in NRas and KRas, the two isoforms mostly associated with human cancer. This is partly because GGTase-I can catalyze geranylgeranylation of both isoforms in cells, although not as efficiently as farnesylation by FTase (10, 98-100). Upon FTI exposure, oncogenic Ras is not suppressed given that alternative geranylgeranylation allows Ras to reach the target membranes where signaling occurs. Lau and colleagues demonstrated that modification catalyzed by ICMT has a crucial role in malignant transformation and tumor maintenance. Through *in vitro* and *in vivo* studies, they demonstrate that ICMT loss-of-function mutation abolishes the ability of KRas and NRas to initiate tumor development in various cancer cell lines (101). Various ICMT inhibitors have shown promise in preclinical testing and alter methylation of proteins containing either a farnesyl or geranylgeranyl modification (102, 103). Similarly, efforts to target the protease (Rce1) function have been reported (104). However, one of the main concerns

in targeting ICMT and Rce1 is the fact that Ras is only one of many proteins that are modified by these enzymes, increasing the number of potential off-target effects from these inhibitors. Palmitoylation is another PTM that has been investigated as a potential anti-Ras target (105, 106). Yet, there have not been as extensive efforts in developing small molecules and peptide mimics to target this modification due to the complexity of the enzymology of Ras palmitoylation and the fact that the most frequently mutated Ras isoform (KRas4B) is not palmitoylated in cells.

### ***Objectives of this work***

Although Ras proteins have been extensively studied for the past three decades, many questions remain. Better understanding of regulation of Ras PTMs and their roles in disease states can serve to improve strategies to treat such diseases. The main goal of this work is to elucidate the factors that regulate entry of Ras proteins into the prenylation pathway and the mechanism employed for such regulation. In this work, two areas are addressed to shed light into Ras prenylation: (1) the role of SmgGDS-607 in regulation of Ras protein farnesylation, and (2) the effect of polybasic residues in the HVR of full-length substrates on the FTase-catalyzed reaction and SmgGDS-607 interaction.

To evaluate the role of SmgGDS-607 in regulation of Ras and Ras-like protein farnesylation, competition experiments were conducted with full-length protein substrates. Binding affinities between Ras substrates and the two modulators, SmgGDS-607 and FTase, were determined to shed light into the strength of the different protein interactions. These experiments led to the development of a differential binding mechanism for SmgGDS-mediated regulation whereby the relative affinity of Ras for SmgGDS-607 and FTase determines the extent of inhibition of farnesylation. In addition, for the first time, SmgGDS-607 is also shown to enhance farnesylation of a small GTPase lacking a PBR, suggesting that SmgGDS-607 forms a ternary complex between FTase and HRas. These data clearly demonstrate that SmgGDS-607 plays important and differential roles in regulating farnesylation of Ras isoforms.

To evaluate the role of the PBR and CAAX motifs in modulating Ras prenylation, I measured the steady state kinetic parameters  $k_{cat}/K_M$ ,  $k_{cat}$ , and  $K_M$  for farnesylation of Ras

chimeric mutants and DiRas proteins and the binding affinity of Ras proteins for SmgGDS-607. The set of Ras chimeric mutants used include various combinations of G domain, HVR and CAAX sequences between the KRas4B and HRas isoforms. Kinetic analysis of the Ras and Ras-like substrates revealed that the PBR enhances product release of farnesylated-Ras proteins from FTase and that the extent of enhancement is dependent on the sequence identity of the PBR and CAAX motifs. The binding data of SmgGDS-607 with the Ras substrates prove that the PBR motif is essential for a high affinity interaction. Yet, synergies between PBR and CAAX sequences also contribute to the strength of this interaction. Additionally, through competition experiments, I demonstrated that SmgGDS-607 can restore PBR-mediated enhancement of farnesylation for substrates that lack a PBR. This work provides insight into how the differential effects of SmgGDS-607 together with FTase kinetics dictate the dynamics and levels of Ras farnesylation in the cell.

## REFERENCES

1. Hunter, J. C., Manandhar, A., Carrasco, M. A., Gurbani, D., Gondi, S., Westover, K. D. (2015) Biochemical and structural analysis of common cancer-associated KRAS mutations. *Mol. Cancer Res.* **13**, 1325–1335.
2. Choy, E., Chiu, V. K., Silletti, J., Feoktistov, M., Morimoto, T., Michaelson, D., Ivanov, I. E., and Philips, M. R. (1999) Endomembrane trafficking of ras. The CAAX motif targets proteins to the ER and Golgi. *Cell* **98**, 69–80.
3. Chiu, V. K., Bivona, T., Hach, A., Sajous, J. B., Silletti, J., Wiener, H., Johnson, R. L., 2nd, Cox, A. D., Philips, M. R. (2002) Ras signaling on the endoplasmic reticulum and the Golgi. *Nat. Cell Biol.* **4**, 343–350.
4. Rocks, O., Peyker, A., Kahms, M., Verveer, P. J., Koerner, C., Lumbierres, M., Kuhlmann, J., Waldmann, H., Wittinghofer, A., Bastiaens, P. I. (2005) An acylation cycle regulates localization and activity of palmitoylated Ras isoforms. *Science* **307**, 1746–1752.
5. Mor, A., Philips, M. R. (2006) Compartmentalized Ras/MAPK signaling. *Annu. Rev. Immunol.* **24**, 771–800.
6. Wright, L. P., Philips, M. R. (2006) Thematic review series. Lipid post-translational modifications. CAAX modification and membrane targeting of Ras. *J. Lipid Res.* **47**, 883–891.
7. Fehrenbacher, N., Bar-Sagi, D., Philips, M. (2009) Ras/MAPK signaling from endomembranes. *Mol. Oncol.* **3**, 297–307.
8. Hancock, J. F., Parton, R. G. (2005) Ras plasma membrane signalling platforms. *Biochem. J.* **389**, 1–11.
9. Ashby, M. N. (1998) CaaX converting enzymes. *Curr. Opin. Lipidol.* **9**, 99–102.
10. Whyte, D. B., Kirschmeier, P., Hockenberry, T. N., Nunez-Oliva, I., James, L., Catino, J. J., Bishop, W. R., Pai, J. K. (1997) K- and N-Ras are geranylgeranylated in cells treated with farnesyl protein transferase inhibitors. *J. Biol. Chem.* **272**, 14459–14464.
11. Winter-Vann, A. M., and Casey, P. J. (2005) Post-prenylation-processing enzymes as new targets in oncogenesis. *Nat. Rev. Cancer* **5**, 405–412.
12. Swarthout, J. T., Lobo, S., Farh, L., Croke, M. R., Greentree, W. K., Deschenes, R. J., Linder, M. E. (2005) DHHC9 and GCP16 constitute a human protein fatty acyltransferase with specificity for H- and N-Ras. *J. Biol. Chem.* **280**, 31141–31148.
13. Magee, A. I., Gutierrez, L., McKay, I. A., Marshall, C. J., Hall, A. (1987) Dynamic fatty acylation of p21N-ras. *EMBO J.* **6**, 3353–3357.
14. Shahinian, S., Silviu, J. R. (1995) Doubly-lipid-modified protein sequence motifs exhibit long-lived anchorage to lipid bilayer membranes. *Biochemistry* **34**, 3813–3822.
15. Schroeder, H., Leventis, R., Rex, S., Schelhaas, M., Nägele, E., Waldmann, H., Silviu, J. R. (1997) S-Acylation and plasma membrane targeting of the farnesylated carboxyl-terminal peptide of N-ras in mammalian fibroblasts. *Biochemistry* **36**, 13102–13109.
16. Laude, A. J., Prior, I. A. (2008) Palmitoylation and localization of RAS isoforms are modulated by the hypervariable linker domain. *J. Cell Sci.* **121**, 421–427.

17. Hancock, J. F., Cadwallader, K., Marshall, C. J. (1991) Methylation and proteolysis are essential for efficient membrane binding of prenylated p21K-ras(B) *EMBO J.* **10**, 641–646.
18. Zhang, F. L., and Casey, P. J. (1996) Protein Prenylation: Molecular mechanisms and functional consequences. *Annual Review Biochemistry* **65**, 1–29.
19. Gelb, M. H., Brunsveld, L., Hrycyna, C. A., Michaelis, S., Tamanoi, F., Van Voorhis, W. C., and Waldmann, H. (2006) Therapeutic intervention based on protein prenylation and associated modifications. *Nat. Chem. Biol.* **2**, 518–528.
20. Berg, T. J., Gastonguay, A. J., Lorimer, E. L., Kuhnmuench, J. R., Li, R., Fields, A. P., Williams, C. L. (2010) Splice variants of SmgGDS control small GTPase prenylation and membrane localization. *J. Biol. Chem.* **285**, 35255–35266.
21. Williams, C. L. (2013) A new signaling paradigm to control the prenylation and trafficking of small GTPases. *Cell cycle* **12**, 2933–2934.
22. Schuld, N. J., Vervacke, J. S., Lorimer, E. L., Simon, N. C., Hauser, A. D., Barbieri, J. T., Distefano, M. D., Williams, C. L. (2014) The chaperone protein SmgGDS interacts with small GTPases entering the prenylation pathway by recognizing the last amino acid in the CAAX motif. *J. Biol. Chem.* **289**, 6862–6876.
23. Vikis, H. G., Stewart, S., Guan, K. L. (2002) SmgGDS displays differential binding and exchange activity towards different Ras isoforms. *Oncogene* **20**, 2425–2432.
24. James, G. L., Goldstein, J. L., Brown, M. S. (1995) Polylysine and CVIM sequences of K-RasB dictate specificity of prenylation and confer resistance to benzodiazepine peptidomimetic in vitro. *J. Biol. Chem.* **270**, 6221–6226.
25. Chen, Z., Otto, J. C., Bergo, M. O., Young, S. G., Casey, P. J., (2000) The C-terminal polylysine region and methylation of K-Ras are critical for the interaction between K-Ras and microtubules. *J. Biol. Chem.* **275**, pp. 41251–41257.
26. Long, S. B., Casey, P. J., Beese, L. S. (2000) The basis for K-Ras4B binding specificity to protein farnesyltransferase revealed by 2 Å resolution ternary complex structures. *Structure* **8**, 209–222.
27. Santillo, M., Mondola, P., Serù, R., Annella, T., Cassano, S., Ciullo, I., Tecce, M. F., Iacomino, G., Damiano, S., Cuda, G., Paternò, R., Martignetti, V., Mele, E., Feliciello, A., Avvedimento, E. V. (2001) Opposing functions of Ki- and Ha-Ras genes in the regulation of redox signals. *Curr. Biol.* **11**, 614–619.
28. Abraham, S. J., Nolet, R. P., Calvert, R. J., Anderson, L. M., Gaponenko, V. (2009) The hypervariable region of K-Ras4B is responsible for its specific interactions with calmodulin. *Biochemistry* **48**, 7575–7583.
29. Hicks, K. A., Hartman, H. L., Fierke, C. A. (2005) Upstream polybasic region in peptides enhances dual specificity for prenylation by both farnesyltransferase and geranylgeranyltransferase type I. *Biochemistry* **44**, 15325–15333.
30. Ntantie, E., Gonyo, P., Lorimer, E. L., Hauser, A. D., Schuld, N., McAllister, D., Kalyanaraman, B., Dwinell, M. B., Auchampach, J. A., Williams, C. L. (2013) An adenosine-mediated signaling pathway suppresses prenylation of the GTPase Rap1B and promotes cell scattering. *Sci Signal.* **6**, ra39.
31. Shimizu, H., Toma-Fukai, S., Saijo, S., Shimizu, N., Kontani, K., Katada, T., Shimizu, T. (2017) Structure-based analysis of the guanine nucleotide exchange factor SmgGDS reveals armadillo-repeat motifs and key regions for activity and GTPase binding. *J. Biol. Chem.* **292**, 13441–13448.

32. Shimizu, H., Toma-Fukai, S., Kontani, K., Katada, T., Shimizu, T. (2018) GEF mechanism revealed by the structure of SmgGDS-558 and farnesylated RhoA complex and its implication for a chaperone mechanism. *Proc. Natl. Acad. Sci. U S A.* **115**, 9563–9568.
33. Hamel, B., Monaghan-Benson, E., Rojas, R. J., Temple, B. R. S., Marston, D. J., Burrige, K., Sondek, J. (2011) SmgGDS is a guanine nucleotide exchange factor that specifically activates RhoA and RhoC. *J. Biol. Chem.* **286**, 12141–12148.
34. Bergom, C., Hauser, A. D., Rymaszewski, A., Gonyo, P., Prokop, J. W., Jennings, B. C., Lawton, A. J., Frei, A., Lorimer, E. L., Aguilera-Barrantes, I., Mackinnon, A. C., Noon, K., Fierke, C. A., Williams, C. L. The tumor-suppressive small GTPase DiRas1 binds the noncanonical guanine nucleotide exchange factor SmgGDS and antagonizes SmgGDS interactions with oncogenic small GTPases. *J. Biol. Chem.* **291**, 6534–6545.
35. Lanning, C. C., Ruiz-Velasco, R., Williams, C. L. (2003) Novel mechanism of the co-regulation of nuclear transport of SmgGDS and Rac1. *J. Biol. Chem.* **278**, 12495–12506.
36. Ogita, Y., Egami, S., Ebihara, A., Ueda, N., Katada, T., Kontani, K. (2015) Di-Ras2 protein forms a complex with SmgGDS protein in brain cytosol in order to be in a low affinity state for guanine nucleotides. *J. Biol. Chem.* **290**, 20245–20256.
37. Kaibuchi, K., Mizuno, T., Fujioka, H., Yamamoto, T., Kishi, K., Fukumoto, Y., Hori, Y., Takai, Y. (1991) Molecular cloning of the cDNA for stimulatory GDP/GTP exchange protein for smg p21s (ras p21-like small GTP-binding proteins) and characterization of stimulatory GDP/GTP exchange protein. *Mol. Cell Biol.* **11**, 2873–2880.
38. Yamamoto, T., Kaibuchi, K., Mizuno, T., Hiroyoshi, M., Shirataki, H., Takai, Y. (1990) Purification and characterization from bovine brain cytosol of proteins that regulate the GDP/GTP exchange reaction of smg p21s, ras p21-like GTP-binding proteins. *J. Biol. Chem.* **265**, 16626–16634.
39. Mizuno, T., Kaibuchi, K., Yamamoto, T., Kawamura, M., Sakoda, T., Fujioka, H., Matsuura, Y., Takai, Y. (1991) A stimulatory GDP/GTP exchange protein for smg p21 is active on the post-translationally processed form of c-Ki-ras p21 and RhoA p21. *Proc. Natl. Acad. Sci. U S A.* **88**, 6442–6446.
40. Jennings, B. C., Lawton, A. J., Rizk, Z., Fierke, C. A. (2018) SmgGDS-607 regulation of RhoA GTPase prenylation is nucleotide-dependent. *Biochemistry* **57**, 4289–4298.
41. Zhi, H., Yang, X., Kuhnmuench, J., Berg, T., Thill, R., Yang, H., See, W., Becker, C., Williams, C., Li, R. (2009) SmgGDS is up-regulated in prostate carcinoma and promotes tumour phenotypes in prostate cancer cells. *J. Pathol.* **217**, 389–397.
42. Tew, G. W., Lorimer, E. L., Berg, T. J., Zhi, H., Li, R., Williams, C. L. (2008) SmgGDS regulates cell proliferation, migration, and NF-kappa B transcriptional activity in non-small cell lung carcinoma. *J. Biol. Chem.* **283**, 963–976.
43. Hauser, A. D., Bergom, C., Schuld, N. J., Chen, X., Lorimer, E. L., Huang, J., Mackinnon, A. C., Williams, C. L. (2013). The SmgGDS splice variant SmgGDS-558 is a key promoter of tumor growth and RhoA signaling in breast cancer. *Mol. cancer res: MCR*, **12**, 130–142.

44. Kontani, K., Tada, M., Ogawa, T., Okai, T., Saito, K., Araki, Y., Katada, T. (2002) Di-Ras, a distinct subgroup of Ras family GTPase with unique biochemical properties. *J. Biol. Chem.* **277**, 41070–41078.
45. Ellis, C. A., Vos, M. D., Howell, H., Vallecorsa, T., Fults, D. W., Clark, G. J. (2002) Rig is a novel Ras-related protein and potential neural tumor suppressor. *Proc. Natl. Acad. Sci. U S A.* **99**, 9876–9881.
46. Luo, R. Z., Fang, X., Marquez, R., Liu, S. Y., Mills, G. B., Liao, W. S., Yu, Y., Bast, R. C. (2003) ARHI is a Ras-related small G-protein with a novel N-terminal extension that inhibits growth of ovarian and breast cancers. *Oncogene* **22**, 2897–2909.
47. Xu, X., Li, J., Wang, S., Zheng, X., Xie, L. (2018) RNAa and vector-mediated overexpression of DiRas1 suppresses tumor growth and migration in renal cell carcinoma. *Mol. Ther. Nucleic Acids* **12**, 845–853.
48. Yu, Y., Xu, F., Peng, H., Fang, X., Zhao, S., Li, Y., Cuevas, B., Kuo, W. L., Gray, J. W., Siciliano, M., Mills, G. B., Bast, R. C. Jr. (1999) NOEY2 (ARHI), an imprinted putative tumor suppressor gene in ovarian and breast carcinomas. *Proc. Natl. Acad. Sci. U S A.* **96**, 214–219.
49. Baljuls, A., Beck, M., Oenel, A., Robubi, A., Kroschewski, R., Hekman, M., Rudel, T., Rapp, U. R. (2012) The tumor suppressor DiRas3 forms a complex with H-Ras and C-RAF proteins and regulates localization, dimerization, and kinase activity of C-RAF. *J. Biol. Chem.* **287**, 23128–23140.
50. Badgwell, D. B., Lu, Z., Le, K., Gao, F., Yang, M., Suh, G. K., Bao, J. J., Das, P., Andreeff, M., Chen, W., Yu, Y., Ahmed, A. A., S-L Liao, W., Bast, R. C. Jr. (2012) The tumor-suppressor gene ARHI (DIRAS3) suppresses ovarian cancer cell migration through inhibition of the Stat3 and FAK/Rho signaling pathways. *Oncogene* **31**, 68–79.
51. Lu, Z., Luo, R. Z., Lu, Y., Zhang, X., Yu, Q., Khare, S., Kondo, S., Kondo, Y., Yu, Y., Mills, G. B., Liao, W. S., Bast, R.C. Jr. (2008) The tumor suppressor gene ARHI regulates autophagy and tumor dormancy in human ovarian cancer cells. *J. Clin. Invest.* **118**, 3917–3929.
52. Nishimoto, A., Yu, Y., Lu, Z., Mao, X., Ren, Z., Watowich, S. S., Mills, G. B., Liao, W. S., Chen, X., Bast, R. C. Jr., Luo, R. Z. (2005) A Ras homologue member I directly inhibits signal transducers and activators of transcription 3 translocation and activity in human breast and ovarian cancer cells. *Cancer Res.* **65**, 6701–6710.
53. Hu, Y. Q., Si, L. J., Ye, Z. S., Lin, Z. H., Zhou, J. P. (2013) Inhibitory effect of ARHI on pancreatic cancer cells and NF-kappa B activity. *Mol. Med. Rep.* **7**, 1180–1184.
54. Pei, X. H., Yang, Z., Liu, H. X., Qiao, S. S. (2011) Aplasia Ras homologue member I overexpression induces apoptosis through inhibition of survival pathways in human hepatocellular carcinoma cells in culture and in xenograft. *Cell Biol. Int.* **35**, 1019–1024.
55. Forbes, S. A., Bindal, N., Bamford, S., Cole, C., Kok, C. Y., Beare, D., Jia, M., Shepherd, R., Leung, K., Menzies, A., Teague, J. W., Campbell, P. J., Stratton, M. R., Futreal, P. A. (2011) COSMIC: mining complete cancer genomes in the Catalogue of Somatic Mutations in Cancer. *Nucleic Acids Res.* **39**, D945-D950.

56. Pylayeva-Gupta, Y., Grabocka, E., Bar-Sagi, D. (2011) RAS oncogenes: weaving a tumorigenic web. *Nat. Rev. Cancer* **11**, 761–774.
57. Ostrem, J. M., Shokat, K. M. (2016) Direct small-molecule inhibitors of KRAS: from structural insights to mechanism-based design. *Nat. Rev. Drug Discov.* **15**, 771–785.
58. Prior, I. A., Lewis, P. D., Mattos, C. (2012). A comprehensive survey of Ras mutations in cancer. *Cancer Res.* **72**, 2457–2467.
59. Cox, A. D., Fesik, S. W., Kimmelman, A. C., Luo, J., Der, C. J. (2014) Drugging the undruggable RAS: mission possible? *Nat. Rev. Drug Discov.* **13**, 828–851.
60. Omerovic, J., Hammond, D. E., Clague, M. J., Prior, I. A. (2008) Ras isoform abundance and signalling in human cancer cell lines. *Oncogene* **27**, 2754–2762.
61. Chiu, V. K., Bivona, T., Hach, A., Sajous, J. B., Silletti, J., Wiener, H., Johnson, R. L., 2nd, Cox, A. D., Philips, M. R. (2002) Ras signalling on the endoplasmic reticulum and the Golgi. *Nat. Cell Biol.* **4**, 343–350.
62. Matallanas, D., Sanz-Moreno, V., Arozarena, I., Calvo, F., Agudo-Ibáñez, L., Santos, E., Berciano, M. T., Crespo, P. (2006) Distinct utilization of effectors and biological outcomes resulting from site-specific Ras activation: Ras functions in lipid rafts and Golgi complex are dispensable for proliferation and transformation. *Mol. Cell Biol.* **26**, 100–116.
63. Simanshu, D. K., Nissley, D. V., McCormick, F. (2017) RAS proteins and their regulators in human disease. *Cell* **170**, 17–33.
64. Tartaglia, M., Mehler, E. L., Goldberg, R., Zampino, G., Brunner, H. G., Kremer, H., van der Burgt, I., Crosby, A. H., Ion, A., Jeffery, S., Kalidas, K., Patton, M. A., Kucherlapati, R. S., Gelb, B. D. (2001) Mutations in PTPN11, encoding the protein tyrosine phosphatase SHP-2, cause Noonan syndrome. *Nat. Genet.* **29**, 465–468.
65. Roberts, A. E., Araki, T., Swanson, K. D., Montgomery, K. T., Schiripo, T. A., Joshi, V. A., Li, L., Yassin, Y., Tamburino, A. M., Neel, B. G., Kucherlapati, R. S. (2007) Germline gain-of-function mutations in SOS1 cause Noonan syndrome. *Nat. Genet.* **39**, 70–74.
66. Pandit, B., Sarkozy, A., Pennacchio, L. A., Carta, C., Oishi, K., Martinelli, S., Pogna, E. A., Schackwitz, W., Ustaszewska, A., Landstrom, A., Bos, J. M., Ommen, S. R., Esposito, G., Lepri, F., Faul, C., Mundel, P., López Siguero, J. P., Tenconi, R., Selicorni, A., Rossi, C., Mazzanti, L., Torrente, I., Marino, B., Digilio, M. C., Zampino, G., Ackerman, M. J., Dallapiccola, B., Tartaglia, M., Gelb, B. D. (2007) Gain-of-function RAF1 mutations cause Noonan and LEOPARD syndromes with hypertrophic cardiomyopathy. *Nat. Genet.* **39**, 1007–1012.
67. Schubbert, S., Zenker, M., Rowe, S. L., Boll, S., Klein, C., Bollag, G., van der Burgt, I., Musante, L., Kalscheuer, V., Wehner, L. E., Nguyen, H., West, B., Zhang, K. Y., Siermans, E., Rauch, A., Niemeyer, C. M., Shannon, K., Kratz, C. P. (2006) Germline KRAS mutations cause Noonan syndrome. *Nat. Genet.* **38**, 331–336.
68. Schubbert, S., Bollag, G., Lyubynska, N., Nguyen, H., Kratz, C. P., Zenker, M., Niemeyer, C. M., Molven, A., Shannon, K. (2007) Biochemical and functional characterization of germline KRAS mutations. *Mol. Cell Biol.* **27**, 7765–7770.
69. Digilio, M. C., Conti, E., Sarkozy, A., Mingarelli, R., Dottorini, T., Marino, B., Pizzuti, A., Dallapiccola, B. (2002) Grouping of multiple-lentiginos/LEOPARD and Noonan syndromes on the PTPN11 gene. *Am. J. Hum. Genet.* **71**, 389–394.

70. Wallace, M. R., Marchuk, D. A., Andersen, L. B., Letcher, R., Odeh, H. M., Saulino, A. M., Fountain, J. W., Brereton, A., Nicholson, J., Mitchell, A. L., Brownstein, B. H., Collins, F. S. (1990) Type 1 neurofibromatosis gene: identification of a large transcript disrupted in three NF1 patients. *Science* **249**, 181–186.
71. Cawthon, R. M., O'Connell, P., Buchberg, A. M., Viskochil, D., Weiss, R. B., Culver, M., Stevens, J., Jenkins, N. A., Copeland, N. G., White, R. (1990) Identification and characterization of transcripts from the neurofibromatosis 1 region: the sequence and genomic structure of EVI2 and mapping of other transcripts. *Genomics* **7**, 555–565.
72. Viskochil, D., Buchberg, A. M., Xu, G., Cawthon, R. M., Stevens, J., Wolff, R. K., Culver, M., Carey, J. C., Copeland, N. G., Jenkins, N. A., White, R., O'Connell, P. (1990) Deletions and a translocation interrupt a cloned gene at the neurofibromatosis type 1 locus. *Cell* **62**, 187–192.
73. Brems, H., Chmara, M., Sahbatou, M., Denayer, E., Taniguchi, K., Kato, R., Somers, R., Messiaen, L., De Schepper, S., Fryns, J. P., Cools, J., Marynen, P., Thomas, G., Yoshimura, A., Legius, E. (2007) Germline loss-of-function mutations in SPRED1 cause a neurofibromatosis 1-like phenotype. *Nat. Genet.* **39**, 1120–1126.
74. Stowe, I. B., Mercado, E. L., Stowe, T. R., Bell, E. L., Oses-Prieto, J. A., Hernández, H., Burlingame, A. L., McCormick, F. (2012) A shared molecular mechanism underlies the human rasopathies Legius syndrome and Neurofibromatosis-1. *Genes Dev.* **26**, 1421–1426.
75. Tidyman, W. E., Rauen, K. A. (2008) Noonan, Costello and cardio-facio-cutaneous syndromes: dysregulation of the Ras-MAPK pathway. *Expert Rev. Mol. Med.* **10**, e37.
76. Rodriguez-Viciana, P., Tetsu, O., Tidyman, W. E., Estep, A. L., Conger, B. A., Cruz, M. S., McCormick, F., Rauen, K. A. (2006) Germline mutations in genes within the MAPK pathway cause cardio-facio-cutaneous syndrome. *Science* **311**, 1287–1290.
77. Niihori, T., Aoki, Y., Narumi, Y., Neri, G., Cave, H., Verloes, A., Okamoto, N., Hennekam, R. C., Gillissen-Kaesbach, G., Wiczorek, D., Kavamura, M. I., Kurosawa, K., Ohashi, H., Wilson, L., Heron, D., Bonneau, D., Corona, G., Kaname, T., Naritomi, K., Baumann, C., Matsumoto, N., Kato, K., Kure, S., Matsubara, Y. (2006) Germline KRAS and BRAF mutations in cardio-facio-cutaneous syndrome. *Nat. Genet.* **38**, 294–296.
78. Krab, L. C., de Goede-Bolder, A., Aarsen, F. K., Pluijm, S. M., Bouman, M. J., van der Geest, J. N., Lequin, M., Catsman, C. E., Arts, W. F., Kushner, S. A., Silva, A. J., de Zeeuw, C. I., Moll, H. A., Elgersma, Y. (2008) Effect of simvastatin on cognitive functioning in children with neurofibromatosis type 1: a randomized controlled trial. *JAMA.* **300**, 287–294.
79. Acosta, M. T., Kardel, P. G., Walsh, K. S., Rosenbaum, K. N., Gioia, G. A., Packer, R. J. (2011) Lovastatin as treatment for neurocognitive deficits in neurofibromatosis type 1: phase I study. *Pediatr. Neurol.* **45**, 241–245.
80. Taveras, A. G., Remiszewski, S. W., Doll, R. J., Cesarz, D., Huang, E. C., Kirschmeier, P., Pramanik, B. N., Snow, M. E., Wang, Y.S., del Rosario, J. D., Vibulbhan, B., Bauer, B. B., Brown, J. E., Carr, D., Catino, J., Evans, C. A.,

- Girjavallabhan, V., Heimark, L., James, L., Liberles, S., Nash, C., Perkins, L., Senior, M. M., Tsarbopoulos, A., Ganguly, A. K., Aust, R., Brown, E., Delisle, D., Fuhrman, S., Hendrickson, T., Kissinger, C., Love, R., Sisson, W., Villafranca, E., Webber, S. E. (1997) Ras oncoprotein inhibitors: The discovery of potent, ras nucleotide exchange inhibitors and the structural determination of a drug-protein complex. *Bioorg. Med. Chem.* **5**, 125–133.
81. Peri, F., Airoidi, C., Colombo, S., Martegani, E., van Neuren, A. S., Stein, M., Marinzi, C., Nicotra, F. (2005) Design, synthesis and biological evaluation of sugar-derived Ras inhibitors. *Chembiochem.* **6**, 1839–1848.
82. John, J., Sohmen, R., Feuerstein, J., Linke, R., Wittinghofer, A., Goody, R. S. (1990) Kinetics of interaction of nucleotides with nucleotide-free H-ras p21. *Biochemistry* **29**, 6058–6065.
83. Goody, R. S., Frech, M., Wittinghofer, A. (1991) Affinity of guanine nucleotide binding proteins for their ligands: facts and artefacts. *Trends Biochem. Sci.* **16**, 327–328.
84. Rosnizeck, I. C., Graf, T., Spoerner, M., Tränkle, J., Filchtinski, D., Herrmann, C., Gremer, L., Vetter, I. R., Wittinghofer, A., König, B., Kalbitzer, H. R. (2010) Stabilizing a weak binding state for effectors in the human ras protein by cyclen complexes. *Angew. Chem. Int. Ed. Engl.* **49**, 3830–3833.
85. Grant, B. J., Lukman, S., Hocker, H. J., Sayyah, J., Brown, J. H., McCammon, J. A., Gorfe, A. A. (2011) Novel allosteric sites on Ras for lead generation, *PLoS One* **6**, e25711.
86. Buhrman, G., O'Connor, C., Zerbe, B., Kearney, B. M., Napoleon, R., Kovrigina, E. A., Vajda, S., Kozakov, D., Kovrigin, E. L., Mattos, C. (2011) Analysis of binding site hot spots on the surface of Ras GTPase, *J. Mol. Biol.* **413**, 773–789.
87. Welsch, M. E., Kaplan, A., Chambers, J. M., Stokes, M. E., Bos, P. H., Zask, A., Zhang, Y., Sanchez-Martin, M., Badgley, M. A., Huang, C. S., Tran, T. H., Akkiraju, H., Brown, L. M., Nandakumar, R., Cremers, S., Yang, W. S., Tong, L., Olive, K. P., Ferrando, A., Stockwell, B. R. (2017) Multivalent small-molecule pan-RAS inhibitors. *Cell* **168**, 878–889.e29.
88. Kato-Stankiewicz, J., Hakimi, I., Zhi, G., Zhang, J., Serebriiskii, I., Guo, L., Edamatsu, H., Koide, H., Menon, S., Eckl, R., Sakamuri, S., Lu, Y., Chen, Q. Z., Agarwal, S., Baumbach, W. R., Golemis, E. A., Tamanoi, F., Khazak, V. (2002) Inhibitors of Ras/Raf-1 interaction identified by two-hybrid screening revert Ras-dependent transformation phenotypes in human cancer cells. *Proc. Natl. Acad. Sci. U S A.* **99**, 14398–14403.
89. Lu, Y., Sakamuri, S., Chen, Q. Z., Keng, Y. F., Khazak, V., Illgen, K., Schabbert, S., Weber, L., Menon, S. R. (2004) Solution phase parallel synthesis and evaluation of MAPK inhibitory activities of close structural analogues of a Ras pathway modulator. *Bioorg. Med. Chem. Lett.* **14**, 3957–3962.
90. Gonzalez-Perez, V., Reiner, D. J., Alan, J. K., Mitchell, C., Edwards, L. J., Khazak, V., Der, C. J., Cox, A. D. (2010) Genetic and functional characterization of putative Ras/Raf interaction inhibitors in *C. elegans* and mammalian cells. *J. Mol. Signal* **5**, 2.
91. Shima, F., Yoshikawa, Y., Ye, M., Araki, M., Matsumoto, S., Liao, J., Hu, L., Sugimoto, T., Ijiri, Y., Takeda, A., Nishiyama, Y., Sato, C., Muraoka, S., Tamura,

- A., Osoda, T., Tsuda, K., Miyakawa, T., Fukunishi, H., Shimada, J., Kumasaka, T., Yamamoto, M., Kataoka, T. (2013) In silico discovery of small-molecule Ras inhibitors that display antitumor activity by blocking the Ras-effector interaction. *Proc. Natl. Acad. Sci. U S A* **110**, 8182–8187.
92. Patgiri, A., Yadav, K. K., Arora, P. S., Bar-Sagi, D. (2011) An orthosteric inhibitor of the Ras-Sos interaction. *Nat. Chem. Biol.* **7**, 585–587.
93. Maurer, T., Garrenton, L. S., Oh, A., Pitts, K., Anderson, D. J., Skelton, N. J., Fauber, B. P., Pan, B., Malek, S., Stokoe, D., Ludlam, M. J., Bowman, K. K., Wu, J., Giannetti, A. M., Starovasnik, M. A., Mellman, I., Jackson, P. K., Rudolph, J., Wang, W., Fang, G. (2012) Small-molecule ligands bind to a distinct pocket in Ras and inhibit SOS-mediated nucleotide exchange activity. *Proc. Natl. Acad. Sci. USA.* **109**, 5299–5304.
94. Philips, M. R., Cox, A. D. (2007) *Geranylgeranyltransferase I as a target for anti-cancer drugs.* *J. Clin. Invest.* **117**, 1223–1225.
95. Winter-Vann, A. M., Casey, P. J. (2005) *Post-prenylation-processing enzymes as new targets in oncogenesis.* *Nature Rev. Cancer* **5**, 405–412.
96. Holstein, S. A., Hohl, R. J. (2012) Is there a future for prenyltransferase inhibitors in cancer therapy? *Curr. Opin. Pharmacol.* **12**, 704–709.
97. Berndt, N., Hamilton, A. D., Sebti, S. M. (2011) Targeting protein prenylation for cancer therapy. *Nat. Rev. Cancer* **11**, 775–791.
98. Lerner, E. C., Zhang, T. T., Knowles, D. B., Qian, Y., Hamilton, A. D., Sebti, S. M. (1997) Inhibition of the prenylation of K-Ras, but not H- or N-Ras, is highly resistant to CAAX peptidomimetics and requires both a farnesyltransferase and a geranylgeranyltransferase I inhibitor in human tumor cell lines. *Oncogene* **15**, 1283–1288.
99. Rowell, C. A., Kowalczyk, J. J., Lewis, M. D., Garcia, A. M. (1997) Direct demonstration of geranylgeranylation and farnesylation of Ki-Ras *in vivo*. *J. Biol. Chem.* **272**, 14093–14097.
100. Sun, J., Qian, Y., Hamilton, A. D., Sebti, S. M. (1998) Both farnesyltransferase and geranylgeranyltransferase I inhibitors are required for inhibition of oncogenic K-Ras prenylation but each alone is sufficient to suppress human tumor growth in nude mouse xenografts. *Oncogene* **16**, 1467–1473.
101. Lau, H. Y., Tang, J., Casey, P. J., Wang, M. (2017). Isoprenylcysteine carboxylmethyltransferase is critical for malignant transformation and tumor maintenance by all RAS isoforms. *Oncogene* **36**, 3934–3942.
102. Lau, H. Y., Ramanujulu, P. M., Guo, D., Yang, T., Wirawan, M., Casey, P. J., Go, M. L., Wang, M. (2014) An improved isoprenylcysteine carboxylmethyltransferase inhibitor induces cancer cell death and attenuates tumor growth *in vivo*. *Cancer Biol. Ther.* **15**, 1280–1291.
103. Winter-Vann, A. M., Baron, R. A., Wong, W., de la Cruz, J., York, J. D., Gooden, D. M., Bergo, M. O., Young, S. G., Toone, E. J., Casey, P. J. (2005) A small-molecule inhibitor of isoprenylcysteine carboxyl methyltransferase with antitumor activity in cancer cells. *Proc. Natl. Acad. Sci. U S A* **102**, 4336–4341.
104. Schlitzer, M., Winter-Vann, A., Casey, P. J. (2001) Non-peptidic, non-prenylic inhibitors of the prenyl protein-specific protease Rce1. *Bioorg. Med. Chem. Lett.* **11**, 425–427.

105. Resh, M. D. (2017) Palmitoylation of proteins in cancer. *Biochem Soc. Trans.* **45**, 409–416.
106. Ko, P. J., Dixon, S. J. (2018) Protein palmitoylation and cancer. *EMBO Rep.* **19**, e46666.
107. Prior, I. A., Hancock, J. F. (2012) Ras trafficking, localization and compartmentalized signalling. *Semin. Cell Dev. Biol.* **23**, 145–153.
108. ClinicalTrials.gov. U.S. National Library of Medicine; Bethesda, MD. Accessible from <https://clinicaltrials.gov/>

## CHAPTER 2

### **SmgGDS-607 Exhibits Dual Effects in Regulating Farnesylation of Small GTPases: Activation and Inhibition**

#### INTRODUCTION

For over 30 years, Ras proteins (KRas4A, KRas4B, NRas and HRas) have attracted attention due to their connection to human cancer. Oncogenic Ras mutations, the most prominent occur at G12, G13, and Q61, can reduce or eliminate the inherent GTPase activity, leading to constitutive GTP binding and therefore activation of signaling pathways (1-3). Such Ras mutants are not inactivated by normal cellular mechanisms, and unchecked activity is associated with human tumor pathogenesis. KRas is the isoform that is mutated most often (85%) in cancers with a Ras missense mutation, followed by NRas (12%) and HRas (3%) (4). One of many efforts to control aberrant GTPase signaling focuses on impeding Ras localization to the plasma membrane by targeting FTase prenylation through small-molecule inhibitors (1). One caveat of FTase inhibitors (FTIs) is their inability to block prenylation of KRas and NRas. In the presence of FTIs, GGTase-I catalyzes geranylgeranylation of KRas and NRas, which allows for normal function in the cell (5-7). The cross-reactivity of these proteins with both prenyltransferases is related to the sequence of the CAAX box which includes a methionine at the X position (-CaaM) (8). Combination treatment with both FTIs and GGTase inhibitors (GGTIs) has been shown to block prenylation of KRas and NRas in mice, but only at lethally high doses (9,10). Thus, a novel strategy that can prevent membrane association of oncogenic Ras proteins might aid in cancer treatment.

CAAX-protein prenylation has been generally assumed to be unregulated in the cell (11). However, recent studies indicate that splice variants of SmgGDS (small GTP-

binding protein GDP-dissociation stimulator) proteins bind small GTPases and regulate their entry into the prenylation pathway (12,13). There are two splice variants of SmgGDS, SmgGDS-607 and SmgGDS-558, and both bind multiple Ras and Rho family members by recognizing their C-terminal polybasic regions (PBRs) and CAAX boxes (12-15). Previous data suggest that SmgGDS-607 binds newly synthesized, non-prenylated GTPases, while SmgGDS-558 binds prenylated GTPases, potentially helping them traffic to the plasma membrane (12). Recent *in vitro* studies show that SmgGDS-607 inhibits the geranylgeranylation of RhoA in a nucleotide-dependent manner, and this inhibition occurs through RhoA substrate sequestration rather than inhibition of GGTase-I (13). Because SmgGDS-607 binds non-prenylated GTPases and inhibits prenylation, this protein is proposed to function as a gatekeeper by regulating small GTPase entry into the prenylation pathway.

While the role of SmgGDS-607 in inhibiting geranylgeranylation is well-established (13), the role of this protein in regulating the farnesylation pathway is still not known. So far, five small GTPases that go through the farnesylation pathway (KRas4B, HRas, NRas, DiRas1 and DRas2) have been demonstrated to associate with SmgGDS-607 in cells (14-17). Pulldown experiments have demonstrated that SmgGDS-607 associates with wild-type, constitutively active (G12V), and dominant negative (S17N) KRas4B and that this association appears to be mediated by the PBR moiety (12,14). Additionally, more KRas4B pulls down with SmgGDS-607 when cells are treated with an FTI, compared to cells that are untreated (15). To further characterize the role of SmgGDS-607 in regulating farnesylation, we assayed the effects of SmgGDS-607 on *in vitro* prenylation of three representative FTase substrate, KRas4B, HRas, and DiRas1. These three substrates capture the different types of C-terminal tails in the FTase substrates recognized by SmgGDS-607. Furthermore, we measured the binding affinities of Ras proteins for the prenyltransferases and SmgGDS-607. These data demonstrate that SmgGDS-607 does not significantly affect the rate of farnesylation of KRas4B while inhibiting farnesylation of DiRas1, a Ras-like protein homologous to KRas4B. These differential effects are explained by the relative binding affinities of the small GTPase for SmgGDS-607 and FTase. Surprisingly, SmgGDS-607 enhances the rate of farnesylation of HRas, an effect that has never been seen before with any other small GTPase, by increasing the rate of

product dissociation from FTase. These results elucidate a novel cellular mechanism for regulation of protein farnesylation. This mechanism suggests that SmgGDS-607 enhances entry of certain small GTPases into the farnesylation pathway, implying that small molecules targeting the SmgGDS-607 and Ras interaction may have therapeutic value.

## EXPERIMENTAL PROCEDURES

### ***Materials***

Purified, his-tagged SmgGDS-607 and biotinylated SmgGDS-607 were a gift from Dr. Benjamin C. Jennings (University of Michigan). Dr. Carol L. Williams (Medical College of Wisconsin) provided human DiRas1 cDNA. Dr. Arul M. Chinnaiyan (University of Michigan) provided human KRas4B and HRas cDNAs. Tritium labeled farnesyl pyrophosphate ( $[^3\text{H}]$ -FPP) was purchased from American Radiolabeled Chemicals, Inc. Primers were purchased from Integrated DNA Technologies.

### ***Preparation of Ras protein expression constructs***

Bacterial His<sub>6</sub>-TEV expression constructs for KRas4B (pBJ176), HRas (pBJ162), and DiRas1 (pBJ173) were previously prepared by Dr. Benjamin Jennings by cloning the Ras and DiRas genes into pETM-11 vectors to encode the small GTPases with a TEV protease cleavage site and an N-terminal His<sub>6</sub> tag. To construct plasmid pBJ176, the KRas4B gene was amplified by PCR with primers F1: 5'-GAGTCCATATGAC TGAATATAAACTTGTGG and F2: 5'-GATAGGCTTACCTTCGAAC. To construct plasmid pBJ162, the HRas gene was amplified by PCR with primers F3: 5'-GAGTCCATATGACGGAATATAAGCTTGTGTTG and F4: 5'-GCTAGCTCGAGTCAG GAGAGCACACACTTG. To construct plasmid pBJ173, the DiRas1 gene was amplified by PCR with primers F5: 5'-AGGCACAGTCGAGGCTGATCAG and F6: 5'-GAGTCCA TATGCCGGAACAGAGTAACGATTACCG. All PCR products were individually gel purified and digested with *Nde*I and *Xho*I. The DNA fragments were then individually ligated into *Nde*I/*Xho*I-digested pETM-11 vectors. DNA sequencing verified the correct protein coding sequence.

To construct expression plasmids encoding for an Avi-tag, a pair of primers were designed for insertion of the Avi-tag sequence to the pETM-11 vectors harboring the three different Ras genes (pBJ176, pBJ162, and pBJ173). Primers (F7: 5'-CTACTGAGAATCTTTATTTTCAGGGCGGCCTGAACGACATCTTCGAGGCTCAGAAAATCGAATGGCACGAACATATGACTGAATATAAACTTGTGGTAG; F8: 5'-CTACCACAA GTTTATATTCAGTCATATGTTTCGTGCCATTCGATTTTCTGAGCCTCGAAGATGTCCGAGGCCGCCCTGAAAATAAAGATTCTCAGTAG) were used to amplify the three Ras genes with the inserted Avi-tag, resulting in His<sub>6</sub>-TEV-Avi-tag expression constructs. DNA sequencing verified the correct protein coding sequence.

### ***Preparation of human FTase and GGTase-I expression constructs***

Human FTase and GGTase-I expression plasmids were constructed in pETM-11 vectors with genes encoding the FTase subunits (pDG135) and the GGTase-I subunits (pDG140) in the order  $\alpha$ - $\beta$ . DNA fragments encoding the  $\alpha$  subunit shared by both enzymes and the different  $\beta$  subunits for each enzyme were synthesized by Invitrogen. To construct plasmid pDG135, a pair of primers was designed to amplify the  $\alpha$  subunit coding region (F1: 5'-ATTGTCGACAGGAGGTATCACATGGCATCACCGTCTAGCTTC; F2: 5'-CAATCTCGAGTCAAGCATCGGTCCGCGTTCGG). Another pair of primers was used to amplify the FTase  $\beta$  subunit (F3: 5'-ATGCCATGGCCGCCACCGAA; F4: 5'-CTTGTCGACTTATTGCTGGACGTT). The resulting PCR product for the  $\alpha$  subunit was digested with *SalI/XhoI* and the resulting PCR product for the  $\beta$  subunit was digested by *SalI/NcoI*. The two DNA fragments were then ligated into a *NcoI/XhoI*-digested pETM-11 vector.

To construct plasmid pDG140, a pair of primers was designed to amplify the GGTase-I  $\beta$  subunit coding region (F5: 5'-CAATAAGTCGACAGGAGGTATAACATGGCGGCGACGGAAGATGAACG; F6: 5'-GCTTACCGAATTCTTGTTAAACTCCTCCTGGGTGGAAATATGCACG). The resulting PCR product for the  $\beta$  subunit was digested by *SalI/EcoRI*. The DNA fragment was then ligated into *SalI/EcoRI*-digested pDG135, which contains the shared  $\alpha$  subunit between FTase and GGTase-I. DNA sequencing verified the correct protein coding sequence.

### ***FTase and GGTase-I expression and purification***

Recombinant human FTase was overexpressed and purified as previously described with a few modifications (34). BL21(DE3) cells were transformed with pDG135 plasmid for His<sub>6</sub>-tagged protein. Cells were grown in 2 L of TB media (24 g tryptone, 48 g yeast extract, 7.5 g NaCl, 0.4% glycerol, 10  $\mu$ M MgCl<sub>2</sub>, 0.17 M KH<sub>2</sub>PO<sub>4</sub>, 0.72 M K<sub>2</sub>HPO<sub>4</sub>) supplemented with kanamycin (50  $\mu$ g/ml) and 100  $\mu$ M ZnCl<sub>2</sub> at 37°C until reaching an OD<sub>600</sub> of 1. Isopropyl  $\beta$ -D-1-thiogalactopyranoside (IPTG) was added to a final concentration of 0.8 mM to induce protein expression. Cells were grown for an additional 18 hours post-induction at 25°C until harvesting (10,000 x g, 30 min., 4°C). The cell pellet was stored at -80°C until purification.

Cell pellets were resuspended in chilled lysis buffer (20 mM Tris pH 7.6, 200 mM NaCl, 5% glycerol, 5 mM imidazole, 2 mM tris(2-carboxyethyl)phosphine, TCEP) supplemented with Pierce protease inhibitor cocktail tablets (Thermo Fisher). The resuspended cells were lysed using a microfluidizer (Microfluidics). Nucleic acids were precipitated by addition of 0.1% polyethylenimine, and the lysate was cleared by centrifugation (35,000 x g, 25 min., 4°C). The supernatant was then loaded on a 4 mL His-Pur<sup>TM</sup> Ni-NTA affinity column (Thermo Scientific). The column was washed with 5 column volumes of wash buffer (20 mM Tris pH 7.6, 200 mM NaCl, 10  $\mu$ M ZnCl<sub>2</sub>, 5% glycerol, 10 mM imidazole, 1 mM TCEP), and protein was eluted with a stepwise imidazole gradient (25, 50, 75, 100, 150, 200, and 250 mM imidazole). Fractions were pooled and dialyzed overnight against buffer containing 20 mM Tris pH 7.6, 200 mM NaCl, 10  $\mu$ M ZnCl<sub>2</sub>, 5% glycerol, and 1 mM TCEP. Protein was concentrated using Amicon Ultra concentrator (30K MWCO, Millipore), aliquoted, and stored at -80°C.

Human GGTase-I was expressed and purified similarly to FTase with a few modifications. BL21(DE3) cells were transformed with pDG140. Protein expression was induced at OD<sub>600</sub> of 0.65, and the cells were grown for an additional 18 hours post-induction at 22°C. After protein elution from a His-Pur<sup>TM</sup> Ni-NTA column with an imidazole stepwise gradient as described for FTase, active fractions were pooled, TEV protease was added at a 1:10 ratio (mg TEV:mg GGTase-I), and the sample was dialyzed (20K MWCO) overnight. After his-tag cleavage, the sample was centrifuged (2,700 x g, 15 min.,

4°C) to remove precipitated TEV protease. Cleaved GGTase-I was loaded onto a 4 mL His-Pur™ Ni-NTA affinity column and eluted with a stepwise imidazole gradient (0, 10, 20, 40, 80, 160, and 300 mM imidazole). Active fractions were pooled, concentrated, aliquoted, and stored at -80°C.

### ***Biotinylated small GTPase expression and purification***

The expression and purification of recombinant biotinylated small GTPases was completed as previously described with a few modifications (35). BL21-A1 cells harboring pBirAcm and pRARE plasmids were co-transformed with recombinant vector (pDG137, pDG138, pDG141, pDG143) for His<sub>6</sub>-TEV-Avi-tag GTPase (KRas4B, KRas4B M188L, DiRas1, HRas), and then grown at 37°C in 50 mL of TB media supplemented with kanamycin (25 µg/ml), chloramphenicol (10 µg/ml) and streptomycin (50 µg/ml). After reaching an OD<sub>600</sub> of 0.6, the culture was cooled to 22°C for 1 hour. Protein expression was induced by adding 1.5 mM IPTG, followed by the addition of 50 µM biotin in bicine buffer (pH 8.3) and 0.2% arabinose. Cells were grown for an additional 18 hours post-induction at 22°C until harvesting (2,700 x g, 30 min., 4°C). The bacterial pellet was resuspended in lysis buffer (25 mM Tris pH 7.6, 300 mM NaCl, 5% glycerol, 5 mM imidazole, 2 mM benzamidine, 1 mM PMSF, 1 µM pepstatin), and cells were lysed by sonication. After the lysate was cleared by centrifugation (10,800 x g, 40 min, 4°C), the supernatant was batch loaded onto a 500 µL His-Pur™ Ni-NTA resin suspension for 2 hours while shaking at 4°C. The resin was transferred to a disposable Poly-Prep chromatography column (Bio-Rad) and washed with lysis buffer. Biotinylated protein bound to the resin was eluted with lysis buffer containing 300 mM imidazole. After protein elution, TEV protease was added at a 1:10 ratio (mg TEV:mg GTPase), and the sample was dialyzed (3.5K MWCO) overnight against 20 mM HEPES pH 7.8, 200 mM NaCl, 5% glycerol, 1 mM TCEP. After cleavage, the sample was centrifuged (2,700 x g, 15 min, 4°C) to remove precipitated TEV protease. The supernatant was batch loaded to 500 µL of His-Pur™ Ni-NTA resin suspension for 1 hour with shaking at 4°C. Cleaved protein was batch eluted with 2 column volumes of lysis buffer in a stepwise imidazole gradient (0, 100, 300 mM). Fractions were analyzed by SDS-PAGE. Protein fractions were pooled, aliquoted, and stored at -80°C.

### ***Non-biotinylated small GTPase expression and purification***

Small GTPases were expressed in BL21(DE3) *E.coli* cells cultured in 2 L of LB media (20 g tryptone, 10 g yeast extract, 20 g NaCl, 10 mM MgCl<sub>2</sub>, 0.5% glucose, 50 µg/mL kanamycin) by transforming with recombinant vectors encoding for KRas4B, KRas4B M188L, DiRas1, and HRas (pBJ176, pDG136, pBJ173, pBJ162). Cells were grown at 34°C until OD<sub>600</sub> 0.6-0.8. Culture was cooled to 18°C, and protein expression was induced with addition of 0.1 mM IPTG. Cells were grown for an additional 18 hours post-induction at 18°C until harvesting (10,000 x g, 30 min, 4°C). The cell pellet was stored at -80°C until purification.

Following protein expression, recombinant small GTPases were purified similarly to FTase with a few modifications. After protein elution from a His-Pur™ Ni-NTA column with an imidazole stepwise gradient, fractions were analyzed by SDS-PAGE and fractions containing desired protein were pooled. TEV protease was added at a 1:10 ratio (mg TEV:mg GGTase-I) and the sample was dialyzed (20K MWCO) overnight against buffer containing 20 mM HEPES pH 7.8, 200 mM NaCl, 5% glycerol, and 1 mM TCEP. After his-tag cleavage, the sample was centrifuged (2,700 x g, 15 min., 4°C) to remove precipitated TEV protease. Cleaved protein was loaded onto a 4 mL His-Pur™ Ni-NTA affinity column and eluted with a stepwise imidazole gradient, as described for GGTase-I. Protein fractions were pooled, concentrated using Amicon Ultra concentrator (10K MWCO, Millipore), aliquoted, and stored at -80°C.

### ***Radiolabel prenylation assay***

Recombinant small GTPases were incubated in assay buffer (50 mM HEPPSO pH 7.8, 5 mM TCEP, 5 mM MgCl<sub>2</sub>, 0.1% Triton X-100) with GDP before addition of recombinant human FTase and varying concentrations of SmgGDS-607. Tritium labeled farnesyl diphosphate (<sup>3</sup>H-FPP, American Radiolabeled Chemicals Inc.) was diluted to 10% with unlabeled FPP in assay buffer. Reactions were initiated by the addition of radiolabeled FPP mixture and incubated at 30°C before quenching the reactions by the addition of Laemmli sample buffer. Incubation times for the farnesylation reaction varied depending on the small GTPase to ensure the measurement was under initial velocity conditions (<10% reaction): KRas4B (5 min), KRas4B M188L (30 min), DiRas1 (6 min),

HRas (5 min). Unless indicated otherwise, final concentrations were 2.5  $\mu\text{M}$  small GTPase, 25  $\mu\text{M}$  GDP, 25 nM FTase, and 4  $\mu\text{M}$   $^3\text{H}$ -FPP. After quenching, samples were heated for 2 min at 70°C before resolving by SDS-PAGE, followed by Coomassie Blue staining and de-staining. The small GTPase bands were cut out, placed in scintillation vials, and dissolved by incubating in 500  $\mu\text{L}$  of 34%  $\text{H}_2\text{O}_2$ , 0.2 mM  $\text{CuSO}_4$  at 35°C overnight. Samples were counted on a Beckman LS 6500 liquid scintillation counter after addition of 4.5 mL of BioSafe II scintillation cocktail (Research Products International). The pmol of prenylated product was determined using the specific activity (dpm/pmol) of tritium.

For steady-state kinetic studies, activity was measured by an increase in radioactivity upon farnesylation of the small GTPase. Assays were performed at 30°C in 50 mM HEPES, pH 7.8, 5 mM TCEP, 5 mM  $\text{MgCl}_2$ , 20  $\mu\text{M}$  GDP. FTase (50 nM) and HRas (0.5, 1, 2.5, 5, or 10  $\mu\text{M}$ ) were incubated in the absence or presence of 10  $\mu\text{M}$  SmgGDS-607. Reactions were initiated by the addition of radiolabeled FPP at twice the concentration of HRas and incubated at 30°C before quenching the reactions at various time points ( $n = 8$ ) with Laemmli sample buffer. The initial rate of incorporation of radioactivity was determined by fitting a line to the time dependence of product formation ( $\mu\text{M}$  prenylated GTPase/seconds) and the standard error was calculated and shown as error bars. The values for  $k_{\text{cat}}$  and  $K_{\text{M}}$  were determined by fitting the Michaelis-Menten equation to the concentration dependence of the initial velocity ( $V/E$ ) using nonlinear regression in GraphPad Prism with the standard errors reported.

$$\frac{\text{Velocity}}{[\text{FTase}]} = \frac{k_{\text{cat}} \times [\text{substrate}]}{K_{\text{M}} + [\text{substrate}]} \quad \text{Equation 1}$$

Single turnover experiments were performed for FTase and HRas in the presence and absence of SmgGDS-607. Reactions were carried out at 30°C in 50 mM HEPES, pH 7.8, 5 mM TCEP, 5 mM  $\text{MgCl}_2$ , 20  $\mu\text{M}$  GDP. The reactions contained 500 nM FTase pre-incubated with 250 nM  $^3\text{H}$ -FPP, 2.5  $\mu\text{M}$  HRas, with or without 10  $\mu\text{M}$  SmgGDS-607. Reactions initiated with the addition of FPP were allowed to proceed for up to 1 hour. Time points were taken by quenching the reaction at different time intervals with Laemmli sample buffer. The rate constant for product formation ( $k_{\text{obs}}$ ) was determined by fitting

equation 2 to the time dependence of product formation ( $\mu\text{M}$  prenylated HRas/second), where  $P_t$  is the product formed at time  $t$ , and  $P_{\text{max}}$  is the reaction endpoint.

$$P_t = P_{\text{max}} \times (1 - e^{-k_{\text{obs}}t}) \quad \text{Equation 2}$$

### **Peptide prenylation assay**

For steady-state kinetic studies performed with peptide, FTase activity was measured by an increase in fluorescence intensity ( $\lambda_{\text{ex}} = 340 \text{ nm}$ ,  $\lambda_{\text{em}} = 520 \text{ nm}$ ) upon farnesylation of dansylated peptide using a previously published assay (27). Experiments were carried out using dansyl-TKCVIM peptide, which mimics the CAAX box of KRas4B. Assays were performed at  $30^\circ\text{C}$  in  $50 \text{ mM}$  HEPES,  $\text{pH } 7.8$ ,  $5 \text{ mM}$  TCEP,  $5 \text{ mM}$   $\text{MgCl}_2$ , and  $20 \mu\text{M}$  FPP. FTase ( $50 \text{ nM}$ ) and dansyl-TKCVIM ( $0.2$ ,  $0.4$ ,  $0.8$ ,  $1.6$ ,  $2.4$ , and  $4.8 \mu\text{M}$ ) were incubated in the absence or presence of  $5 \mu\text{M}$  SmgGDS-607. Reactions were measured every  $30 \text{ s}$  for  $1.5 \text{ h}$ . The initial rate of farnesylation was determined by fitting a line to the time dependence of product formation, resulting in units of RFU/s. To obtain the initial rate of farnesylation in units of  $\mu\text{M/s}$ , equation 3 was used, where  $V$  is the initial velocity of the reaction in units of  $\mu\text{M/s}$ ,  $R$  is the initial velocity of the reaction in units of RFU/s,  $P$  is the max concentration of the substrate, and  $F_{\text{max}}$  is the max fluorescence intensity at the endpoint.

$$V = \frac{RP}{F_{\text{max}}} \quad \text{Equation 3}$$

The values for  $k_{\text{cat}}$  and  $K_M$  were determined by fitting the Michaelis-Menten equation to the concentration dependence of the initial velocity ( $V/E$ ) using nonlinear regression in GraphPad Prism with the standard errors reported.

### **Binding assay**

Binding affinities were measured by biolayer interferometry (BLI) using the OctetRed96 instrument (Forte Bio). Assays were performed at  $30^\circ\text{C}$  in 96-well plates. Streptavidin (SA) biosensors were loaded with biotinylated KRas4B, KRas4B M188L, DiRas1 or HRas in  $50 \text{ mM}$  HEPES  $\text{pH } 7.8$ ,  $150 \text{ mM}$   $\text{NaCl}$ ,  $2 \text{ mM}$   $\text{MgCl}_2$ ,  $20 \mu\text{M}$   $\text{GDP}$ ,  $2 \text{ mM}$  TCEP, and  $0.25 \text{ mg/ml}$  BSA. The loaded biosensors were washed in the same buffer before cycling through increasing concentrations of SmgGDS-607 or FTase. For FTase,

the binding studies were performed in the presence of the FPT inhibitor II (I2, Millipore), an inactive FPP analogue, at double the concentration of FTase. Controls included a sensor probe without biotinylated small GTPase that was incubated with either SmgGDS-607 or FTase and a sensor probe loaded with biotinylated small GTPase that was incubated only with buffer. Controls were subtracted from the binding data to correct for non-specific binding. Kinetic parameters  $k_{on}$  and  $k_{off}$  were determined by fitting Equation 4 and Equation 5, respectively, to the time dependence of complex association and dissociation. R refers to the BLI response (nm), IR is the initial BLI response (nm), Amp represents the amplitude of the BLI response change,  $k_{on}$  ( $M^{-1} s^{-1}$ ) represents the rate constant of complex formation,  $k_{off}$  ( $s^{-1}$ ) represents the rate constant of complex dissociation, and FR (nm) is the final BLI response.

$$R = IR + \text{Amp} (1 - e^{-k_{on}t}) \quad \text{Equation 4}$$

$$R = \text{Amp} (e^{-k_{off}t}) + \text{FR} \quad \text{Equation 5}$$

The dissociation constant,  $K_D$ , was determined by fitting the responses at equilibrium ( $R_{eq}$ ) for each SmgGDS-607 or prenyltransferase concentration to a binding isotherm (Equation 6), where  $K_D$  is the dissociation constant and X is the concentration of either SmgGDS-607 or prenyltransferase. The data were fit using nonlinear regression in GraphPad Prism with the standard errors reported.

$$R_{eq} = \frac{R_{max}[X]}{K_D + [X]} \quad \text{Equation 6}$$

## RESULTS

### ***SmgGDS-607 blocks farnesylation of DiRas1 but not KRas4B***

SmgGDS-607 inhibits geranylgeranylation of RhoA catalyzed by GGTase-I by binding to and blocking the prenylation site (13). Furthermore, SmgGDS-607 was previously demonstrated to pull down with small GTPases ending in methionine, such as KRas4B, only in the presence of an FTI that leads to alternative geranylgeranylation (15). However, SmgGDS-607 has not been demonstrated to regulate farnesylation of small GTPases.

To test SmgGDS-607-mediated regulation, we used a radiolabel-incorporation assay to monitor levels of farnesylation of small GTPases, specifically KRas4B and DiRas1, in the presence of SmgGDS-607. While DiRas1 and KRas4B belong to different branches of the Ras family, they share 36% sequence identity, end in methionine (Table 2.1), and are modified by FTase (18). Additionally, Bergom and colleagues demonstrated that DiRas1 antagonizes the interaction of SmgGDS-558 with KRas4B (16).

**Table 2.1 Tail sequences of FTase substrates used in this study.**

Small GTPase	Polybasic region	CAAX box	No. of amino acids in sequence
KRas4B	DGKKKKKKSKTK	CVIM	188
KRas4B M188L	DGKKKKKKSKTK	CVIL	188
DiRas1	GKQKRTDRVKGK	CTLM	198
HRas <sup>a</sup>	PDESGPGCMSCK	CVLS	189

<sup>a</sup>Conrary to the other GTPases tested, HRas does not contain a recognizable polybasic region.

Under *in vitro* conditions, addition of increasing concentrations of SmgGDS-607 minimally inhibits the extent of farnesylation of KRas4B, with 32% inhibition at 20  $\mu\text{M}$  SmgGDS-607 after 5 min of incubation. In contrast, addition of SmgGDS-607 drastically

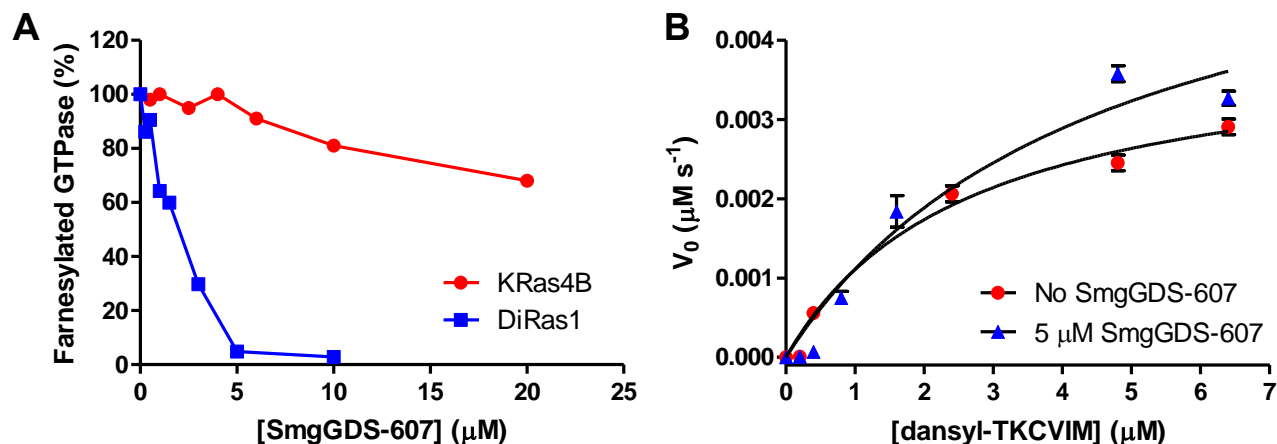


**Figure 2.1. Farnesylation of FTase substrates in the presence of SmgGDS-607.** (A) SmgGDS-607 blocks the extent of farnesylation of DiRas1, but not KRas4B, in a dose-dependent manner. Both KRas4B and DiRas1 end with a methionine in their CAAX box, consistent with the observed farnesylation catalyzed by FTase. KRas4B or DiRas1 (2.5  $\mu\text{M}$  final) was incubated with GDP (25  $\mu\text{M}$ ), FTase (25 nM), [<sup>3</sup>H]-FPP (4  $\mu\text{M}$ ), and eight different concentrations of SmgGDS-607. The reactions were stopped after 5 min (KRas4B) or 6 min (DiRas1), and incorporation of radiolabeled farnesyl was measured as described in the methods. The data points are from single reactions at each SmgGDS-607 concentration. The results are representative of three independent experiment. (B) Addition of 5  $\mu\text{M}$  SmgGDS-607 has little effect on the kinetics of farnesylation of dansyl-TKCVIM peptide. FTase (50 nM) was incubated with 20  $\mu\text{M}$  FPP and various concentrations of peptide in the presence and absence of 5  $\mu\text{M}$  SmgGDS-607. The amount of farnesylated peptide was ascertained by measuring an increase in fluorescence upon farnesyl attachment as described in the methods. The initial rate of farnesylation ( $V_0$ ) and standard error were determined by fitting a line (GraphPad Prism) to multiple determinations of product formation as a function of time. The Michaelis-Menten equation was fit to the data to determine values for  $k_{cat}$ ,  $K_M$  and standard error, listed in Table 2.2.

decreases farnesyl incorporation in DiRas1, with more than 90% inhibition at 5  $\mu\text{M}$  SmgGDS-607 (Figure 2.1A) as compared to ~10% inhibition for KRas4B under similar conditions. Together, these data demonstrate that SmgGDS-607 can directly block farnesylation of an FTase substrate that ends in methionine and does not require the presence of an FTI.

### ***SmgGDS-607 does not inhibit FTase reactivity***

To investigate whether the observed inhibition of farnesylation by SmgGDS-607 is due to SmgGDS-607 directly inhibiting FTase reactivity, we tested the effect of SmgGDS-607 on the farnesylation rate of a dansylated peptide substrate (dansyl-TKCVIM) that mimics the CAAX box of KRas4B and has high affinity for FTase ( $0.86 \pm 0.08$  nM) (20). Addition of 5  $\mu\text{M}$  SmgGDS-607 did not significantly affect FTase activity (Figure 2.1B). Both kinetic parameters,  $K_M$  and  $k_{\text{cat}}$ , were unchanged by the presence of SmgGDS-607 (Table 2.2). These data demonstrate that SmgGDS-607 does not directly inhibit FTase. Rather, the observed inhibition (Figure 2.1A) occurs by competition for binding the FTase substrate.

**Table 2.2. Kinetic parameters for farnesylation of KRas4B CAAX peptide catalyzed by FTase<sup>a</sup>.**

[SmgGDS-607]	$k_{\text{cat}}$ ( $\text{s}^{-1}$ )	$K_M$ ( $\mu\text{M}$ )
---	$0.08 \pm 0.01$	$3 \pm 1$
5 $\mu\text{M}$	$0.12 \pm 0.04$	$4 \pm 3$

<sup>a</sup>FTase activity was measured by monitoring changes in fluorescence intensity upon farnesylation of dansylated peptide. Steady-state parameters were determined by a nonlinear regression fit of the Michaelis- Menten equation to the dependence of the initial rate on the substrate concentration using GraphPad Prism as described in the Experimental Procedures and the standard errors calculated from these fits are reported.

### ***Differential binding affinities for SmgGDS-607 with FTase substrates***

To determine a possible mechanism to explain the differential effects of SmgGDS-607 on blocking farnesylation of DiRas1 compared to KRas4B, we measured the affinities of SmgGDS-607 for several small GTPases using bio-layer interferometry (BLI, OctetRed96) with biotinylated small GTPases and varying concentrations of SmgGDS-607 (19). BLI data for SmgGDS-607 binding to KRas4B, including the kinetic association rate constant ( $k_{\text{on}}$ ), the kinetic dissociation rate constants ( $k_{\text{off}}$ ), and the equilibrium endpoint are shown in Fig. 2.2. The dissociation constants ( $K_D$ ) for KRas4B, KRas4B M188L, DiRas1 and HRas were determined from the fit of a single binding isotherm to the

endpoint data (Fig. 2.2B-C). Binding data for all small GTPases are summarized in Table 2.3.

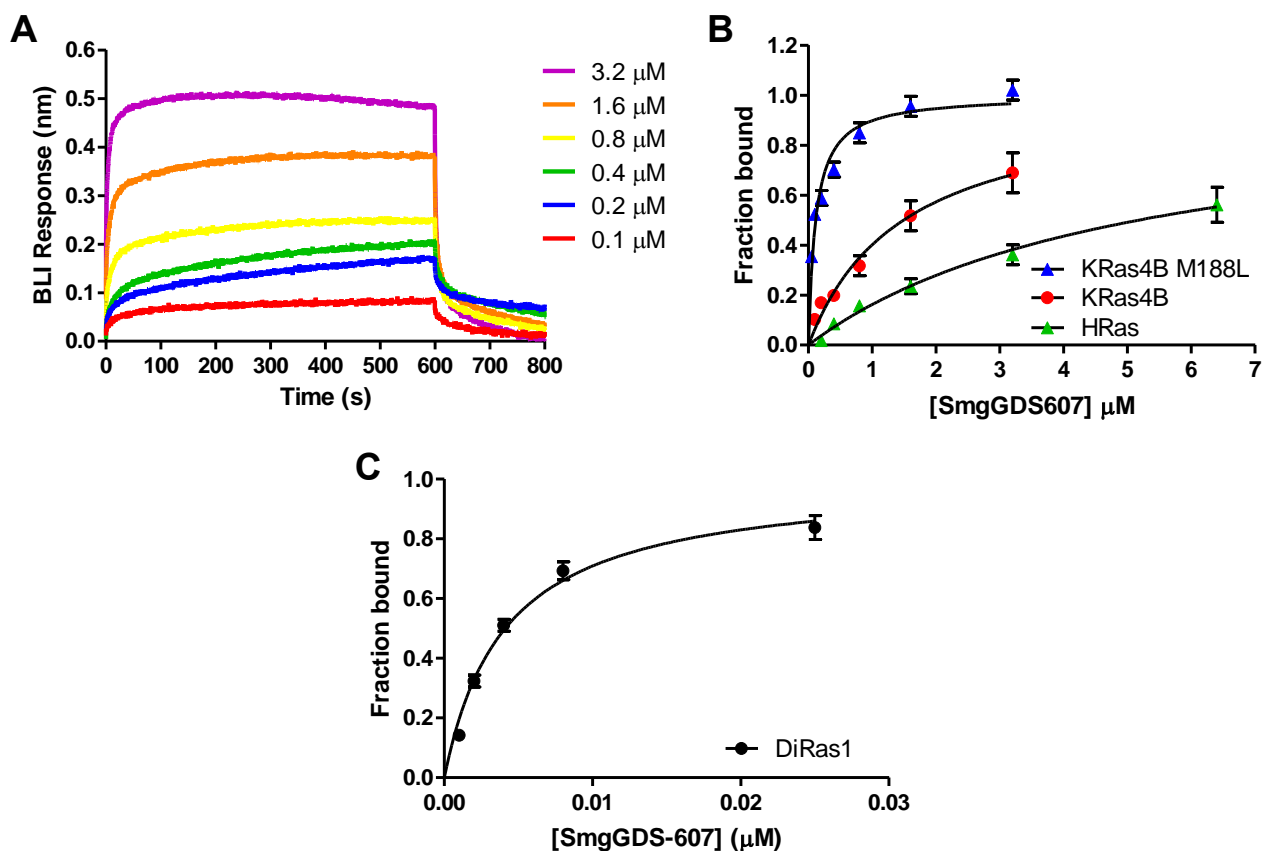


**Figure 2.2. SmgGDS-607 binds directly to KRas4B, KRas4B M188L, and DiRas1, as measured by bio-layer interferometry.** (A) Representative binding assay between SmgGDS-607 and biotinylated KRas4B (adhered to the streptavidin biosensor tip) depicting the association (0-600 s) and dissociation (600-800 s) reactions at six different SmgGDS-607 concentrations after correcting for nonspecific binding. Equations 4 and 5 were fit to the association and dissociation data using GraphPad Prism, respectively, resulting in the following values with the calculated standard error:  $k_{\text{on}} = 0.14 \pm 0.02 \mu\text{M}^{-1} \text{s}^{-1}$  and  $k_{\text{off}} = 0.01 \pm 0.02 \text{s}^{-1}$ . (B and C) Representative data for SmgGDS-607 binding to KRas4B, KRas4B M188L, HRas and DiRas1. The data points and reported standard errors are from the BLI endpoints obtained from the nonlinear regression fit to the binding association step as presented in panel A. These data points were normalized to the BLI response at saturation. The value of  $K_D$  and standard error was determined by a fit of Equation 6 to these data using GraphPad Prism, resulting in a  $K_D$  for KRas4B of  $1.5 \pm 0.4 \mu\text{M}$ , KRas4B M188L of  $0.11 \pm 0.02 \mu\text{M}$ , HRas of  $>9 \mu\text{M}$  and DiRas1 of  $0.0047 \pm 0.0009 \mu\text{M}$ . The results are representative of two independent studies.

An electronegative patch in the structure of SmgGDS-607 is predicted to be pivotal for interactions with the positive charges in the PBR of small GTPases (12,16). In the KRas4B PBR, tandem repeats of lysine residues provide a highly positively-charged region that could interact with the electronegative patch in SmgGDS-607, as compared to the more dispersed positive charges in the PBR of DiRas1 (Table 2.1). Based on this we predicted that KRas4B would bind to SmgGDS-607 with high affinity. However, the

affinity of KRas4B for SmgGDS-607 is  $1.5 \pm 0.4 \mu\text{M}$ , which is >300-fold weaker than the DiRas1 affinity at  $4.7 \pm 0.9 \text{ nM}$ , suggesting a more complicated model of substrate recognition.

**Table 2.3. Summary of thermodynamic values for SmgGDS-607 and FTase binding to different small GTPases<sup>a</sup>.**

	CAAX identity	$K_D$ (nM)	$K_D^{\text{SmgGDS-607}} / K_D^{\text{FTase}}$
<b>Binding to SmgGDS-607</b>			
KRas4B	CVIM	$1500 \pm 370$	$700 \pm 300$
KRas4B M188L	CVIL	$110 \pm 20$	$0.10 \pm 0.04$
DiRas1	CTLM	$4.7 \pm 0.9$	$0.12 \pm 0.02$
HRas	CVLS	>9,000	ND <sup>b</sup>
<b>Binding to FTase</b>			
KRas4B	CVIM	$2.2 \pm 0.7$	
KRas4B M188L	CVIL	$1100 \pm 370$	
DiRas1	CTLM	$40 \pm 2$	

<sup>a</sup>Measured by biolayer interferometry as described in the Experimental Procedures and the legend of Figure 2.2.  $K_D$  was determined from a hyperbolic equation fit to the endpoint data from the BLI response obtained during the association step between the small GTPases and SmgGDS-607 or FTase. The errors in the  $K_D$  values are from the standard error of the fit of the binding isotherm to the data. The uncertainty in the ratio was calculated by error propagation (37). <sup>b</sup>Not determined.

Previous data indicated that SmgGDS-607 pulls down higher levels of KRas4B when the terminal amino acid is altered to leucine from methionine (KRas4B M188L) (15). To investigate this phenomenon, we repeated the binding assay using KRas4B M188L, demonstrating a 13-fold increased affinity for SmgGDS-607 (Table 2.3). We next measured the affinity of SmgGDS-607 for HRas, a small GTPase that does not contain a canonical PBR and ends with a different CAAX (-CVLS) sequence. The affinity of HRas for SmgGDS-607 is >9  $\mu\text{M}$ , which is >6-fold weaker than KRas4B and >1,000-fold weaker than DiRas1, indicating that HRas has the weakest binding affinity out of all the substrates tested. The contrasting affinity of HRas to KRas4B indicates that the PBR might regulate the interaction with SmgGDS-607. Furthermore, these data suggest that the PBR motif in KRas4B may not optimally interact with SmgGDS-607. The enhanced binding affinity for the KRas4B M188L mutant supports the proposal that SmgGDS-607 recognizes the last residue in KRas4B and that the amino acid sequence of the CAAX box is an important determinant of binding affinity and substrate selectivity.

### ***FTase binds to small GTPases with differential binding affinities***

Measurement of direct binding affinities between FTase and full-length small GTPases has proven a challenge previously. To solve this issue, we have used BLI to measure, for the first time, direct real-time binding of FTase to KRas4B and DiRas1 to determine dissociation constants for these full-length proteins. Previously, affinities for rat FTase binding CAAX peptides with varied terminal residues were determined; a peptide corresponding to the C-terminus of KRas4B (TKCVIM) has a  $K_D$  value of  $0.86 \pm 0.08$  nM (20). Using BLI, we measured the affinity of human FTase for KRas4B as  $K_D = 2.2 \pm 0.7$  nM (Table 2.3), comparable to the value measured for the peptide. Interestingly, when the native CAAX sequence CVIM is replaced with CVIL, the affinity for human FTase decreases by 500-fold ( $K_D = 1.1 \pm 0.3$   $\mu$ M). This result was unexpected since for peptides there is minimal difference in the rat FTase dissociation constants for TKCVIL compared to TKCVIM ( $1.1 \pm 0.1$  nM and  $0.86 \pm 0.08$  nM, respectively) (20). These data indicate that the change in affinity for the full-length protein is not determined solely by an altered interaction of FTase with the CAAX tail. For full-length DiRas1 (CAAX = CTLM), the measured dissociation constant for human FTase is  $40 \pm 2$  nM (Table 2.3) which is 8-fold weaker than the measured  $K_D$  for rat FTase with the TKCTLM peptide ( $5.2 \pm 0.8$  nM) (21). These data also suggest that other factors, such as interaction with the PBR region and/or steric hindrance of the C-terminal tail by the full-length protein, explain this weaker affinity.

### ***SmgGDS-607 blocks farnesylation of KRas4B when the CAAX ends in leucine***

To further test whether the ability of SmgGDS-607 to block farnesylation of small GTPases depends on the relative affinities of FTase and SmgGDS-607, we measured whether SmgGDS-607 blocks farnesylation of KRas4B M188L (Figure 2.3); this mutant decreases the affinity for human FTase by 500-fold and enhances SmgGDS-607 affinity by 14-fold leading to an increase in the  $K_D^{FTase} / K_D^{SmgGDS-607}$  for the mutant compared to wild-type of >5,000-fold. Consistent with this, 2.5  $\mu$ M SmgGDS-607 inhibits >90% of the farnesylation of KRas4B M188L compared to ~10% of wild-type KRas4B under comparable conditions. Contrary to KRas4B, for KRas4B M188L the reactions were allowed to proceed for 30 min since farnesylation of this mutant is slower. At 30 min, the amount of product formed is comparable to that of KRas4B after a 5 min incubation. This

result provides additional evidence that SmgGDS-607 regulation of farnesylation of KRas4B, and likely other small GTPases, is driven by differences in binding affinities for FTase and SmgGDS-607. To further examine this mechanism, we simulated the SmgGDS-607 concentration dependence of inhibition of GTPase farnesylation using the KinTek Explorer Chemical Kinetics Software with a differential binding model (Figure A1; Appendix). Our modeling provides qualitative dose-response curves consistent with those obtained empirically (Figures 2.1 and 2.3), confirming that SmgGDS-mediated regulation for KRas4B and DiRas1 can be explained by a differential binding model. Furthermore, taken together, these data demonstrate that regulation of farnesylation by SmgGDS-607 is driven by the differential binding affinities, suggesting that in a cellular context SmgGDS-607 competes with FTase for binding of small GTPases.

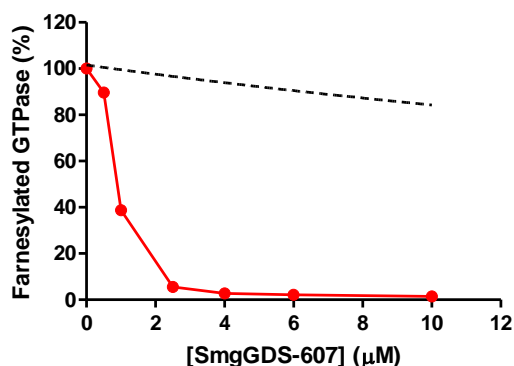


**Figure 2.3. SmgGDS-607 blocks farnesylation of mutant KRas4B M188L, a less reactive FTase substrate.** Radiolabel prenylation assay was performed similarly to Figure 2.1A. KRas4B M188L (2.5 µM final) was incubated with GDP (25 µM), FTase (25 nM), [<sup>3</sup>H]-FPP (4 µM), and eight different concentrations of SmgGDS-607. The reactions were stopped after 30 min incubation. The dotted line represents the effects of SmgGDS-607 on KRas4B farnesylation from Figure 2.1A. Data points are from single reactions at each SmgGDS-607 concentration. The results are representative of three independent experiments.

### ***SmgGDS-607 enhances farnesylation of HRas***

To date, there has been no evidence that SmgGDS-607 regulates prenylation of small GTPases without a PBR sequence. To examine this, we measured the effect of SmgGDS-607 on prenylation of HRas which contains no identified PBR and has a CAAX sequence that ends in serine (CVLS). Previous pull-down data suggested that SmgGDS-607 interacts with both dominant negative and nucleotide free forms of HRas (14). However, no one has examined the effects of SmgGDS-607 on farnesylation of HRas. Unexpectedly, addition of 10 µM SmgGDS-607 enhanced farnesylation of HRas by ~5-fold, while having almost no effect on geranylgeranylation (Figure 2.4A). Minimal

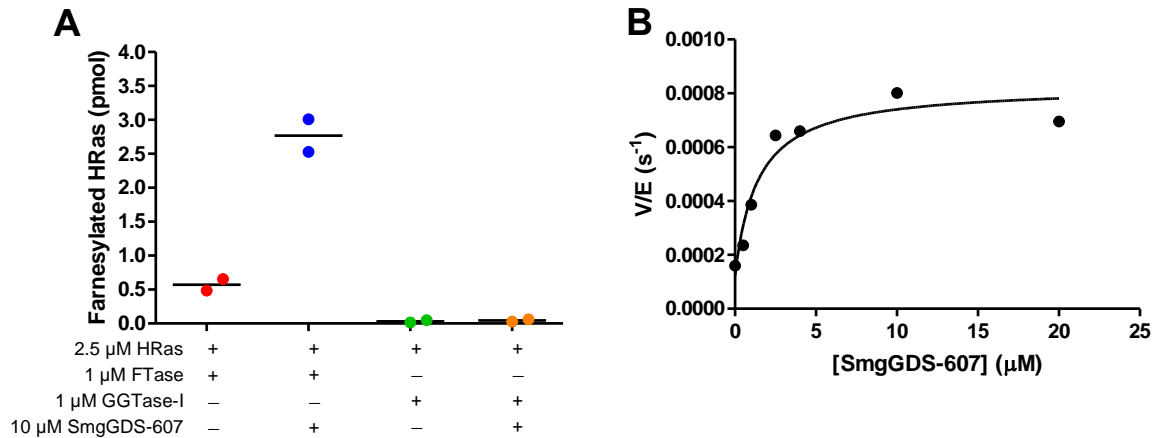


**Figure 2.4. Farnesylation of HRAs is enhanced in the presence of SmgGDS-607.** (A) SmgGDS-607 enhances the extent of farnesylation of HRAs, but not geranylgeranylation. GDP-bound HRAs (2.5 μM) was preincubated with the different components and then labeled with [<sup>3</sup>H]-FPP (4 μM) for 6 min or [<sup>3</sup>H]-GGPP (4 μM) for 20 min. Incorporation of radiolabeled prenyl group was measured as described in the methods. The graph depicts the results from two independent experiments. (B) Concentration dependence of SmgGDS-607 enhancement of farnesylation of HRAs catalyzed by FTase. Seven different concentrations of SmgGDS-607 were incubated with HRAs (2.5 μM final), GDP (25 μM), FTase (50 nM), and [<sup>3</sup>H]-FPP (4 μM). The reactions were stopped after 5 min, and incorporation of radiolabeled farnesyl into HRAs measured as described in the methods. A hyperbolic equation was fit to the data in GraphPad Prism to obtain the value of  $K_{1/2}$  for activation,  $k_{max}$  at saturating SmgGDS-607, and standard errors. The data points are from single reactions at each SmgGDS-607 concentration. The results are representative of three independent experiments.

modification (<1%) was observed after a 20 min incubation of 2.5 μM HRAs with 1 μM GGTase-I; addition of 10 μM SmgGDS-607 did not increase geranylgeranylation. To better understand this farnesylation enhancement, we measured the effect of SmgGDS-607 on the rate of steady-state turnover (Figure 2.4B). Increasing concentrations of SmgGDS-607 enhance the rate constant for farnesylation of 2.5 μM HRAs by 4.4-fold (Figure 2.4A), with a  $k_{max}$  of  $0.00071 \pm 0.00009 \text{ s}^{-1}$  and a  $K_{1/2}$  of  $1.4 \pm 0.7 \text{ μM}$ .

The enhancement of HRAs farnesylation by SmgGDS-607 could be due to either or both: (1) decreasing the  $K_M$  for HRAs and/or (2) increasing turnover ( $k_{cat}$ ) of farnesylated-HRAs catalyzed by FTase. To distinguish between these alternatives, we measured the effect of SmgGDS-607 on the multiple turnover (MTO) kinetic parameters  $k_{cat}$  and  $K_M$  for FTase-catalyzed modification of HRAs using the radiolabel-incorporation assay with HRAs concentrations that were at least 2 times below and above the  $K_M$  (Figure 2.5A). These kinetic data reveal that SmgGDS-607 has a minimal effect on the value of  $K_M$  while increasing the values of  $k_{cat}$  and  $k_{cat}/K_M$  by >5-fold (Table 2.4). For peptide substrates, the farnesylation step is rapid and product release is rate-limiting for turnover (22,23); however, this has not been evaluated for protein substrates. To test whether the effect of

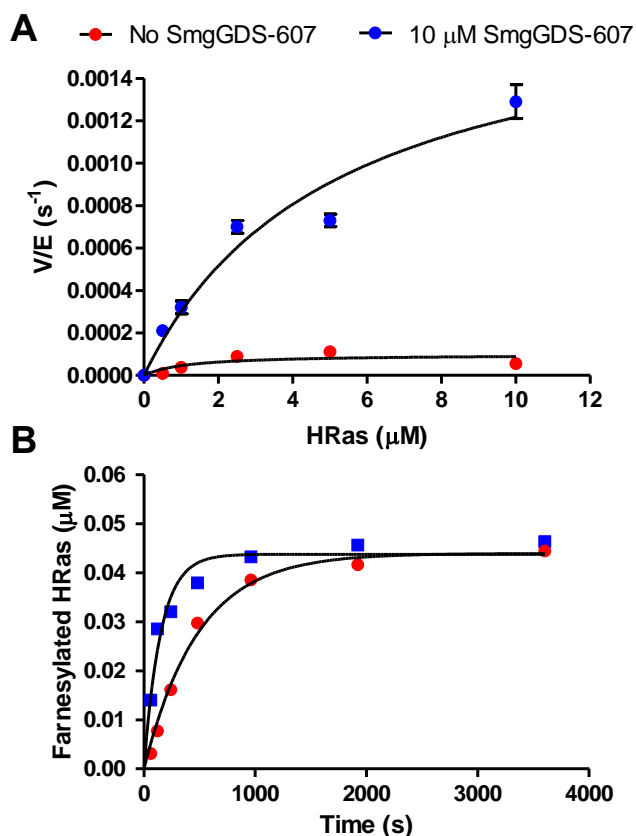


**Figure 2.5. SmgGDS-607 enhances HRas farnesylation by stimulating both chemistry and product release.** (A) Concentration dependence of farnesylation of HRas catalyzed by FTase in the presence of SmgGDS-607. The initial velocity for the reaction of 50 nM FTase, eight different concentrations of HRas, 25 μM GDP, <sup>3</sup>H-FPP at twice the concentration of HRas, and either 0 or 10 μM SmgGDS-607 was measured from the time dependent change in incorporation of the radiolabel into HRas, as described in the methods section. The initial rate of farnesylation (V/E) and standard error were determined by fitting a line (GraphPad Prism) to eight measurements of product formation at different times. The Michaelis-Menten equation was fit to these data to determine values for  $k_{cat}$ ,  $K_M$ ,  $k_{cat}/K_M$ , and standard errors, listed in Table 2.4. (B) Single-turnover kinetics for farnesylation of HRas in the absence and presence of 10 μM SmgGDS-607. Under these conditions, FTase (500 nM) reacts with 2.5 μM HRas, 25 μM GDP, and limiting <sup>3</sup>H-FPP (250 nM). The farnesylation rate constant  $k_{obs}$  and standard error were calculated by a fit (GraphPad Prism) of equation 2 to the data as  $0.0021 \pm 0.0002$  and  $0.007 \pm 0.001$  s<sup>-1</sup> for without and with SmgGDS-607, respectively.

SmgGDS-607 on  $k_{cat}$  is due to enhancement of product release or chemistry, we measured farnesylation of HRas under single turnover (STO) conditions, where FTase and HRas concentrations are in excess of the FPP concentration. Under these conditions, the observed rate constant,  $k_{obs}$ , for farnesylation of HRas is  $0.0021 \pm 0.0002$  s<sup>-1</sup>, which is 16-fold faster than the value of  $k_{cat}$ , indicating that a step after farnesylation, such as product release, is the rate-limiting step for turnover. Addition of 10 μM SmgGDS-607 increases the observed STO rate constant for farnesylation of HRas by 3-fold but this rate remains 4-fold faster than the MTO turnover rate constant (Figure 2.5B, Table 2.4). These data indicate that SmgGDS-607 has a modest effect on binding and/or catalysis while

also increasing the rate of product dissociation. The effects on turnover and product dissociation suggest that SmgGDS-607 forms a ternary complex with HRas and FTase.

**Table 2.4. Kinetic parameters for farnesylation of HRas catalyzed by FTase<sup>a</sup>**

[SmgGDS-607]	$k_{\text{cat}}$ (s <sup>-1</sup> )	$K_{\text{M}}$ (μM)	$k_{\text{cat}}/K_{\text{M}}$ (M <sup>-1</sup> s <sup>-1</sup> )	$k_{\text{obs}}$ (s <sup>-1</sup> ) <sup>b</sup>
---	0.00013 ± 0.00002	1.9 ± 0.8	68	0.0021 ± 0.0002
10 μM	0.0019 ± 0.0004	5 ± 2	380	0.007 ± 0.001

<sup>a</sup>FTase activity was measured and catalytic efficiencies were determined as described in the methods and the legend of Figure 2.5. All values are reported with the standard error of the fit to the data.

<sup>b</sup> $k_{\text{obs}}$  is the single-turnover rate constant for production of farnesylated HRas under limiting FPP conditions.

## DISCUSSION

Recent studies suggest that SmgGDS-607 can regulate geranylgeranylation of small GTPases by binding to and sequestering the non-prenylated form of the GTPase to inhibit prenylation (12,15). Until now, a similar regulatory mechanism for farnesylation has not been observed. Our studies demonstrate that SmgGDS-607 can regulate farnesylation of FTase substrates by blocking the small GTPase from interacting with FTase. This mode of regulation is dictated by the differential binding affinities of the small GTPases between FTase and SmgGDS-607. Furthermore, unexpectedly our studies demonstrate that SmgGDS-607 increases farnesylation of HRas (and likely other small GTPases) by enhancing both catalysis and product release. These findings provide new insight into the regulation of small GTPases before and during the farnesylation pathway.

The structural architecture for small GTPases is defined by a globular body and a floppy tail that contains the PBR domain and the CAAX box. The tail, in particular, has been demonstrated to be crucial for recognition by the prenyltransferases (24-28). On the other hand, cellular data implicate both the tail and the body in SmgGDS recognition (14). Although pull down experiments have been used to determine the relative affinity of SmgGDS-607 with small GTPases, the thermodynamic measurements for SmgGDS-607 and small GTPases that undergo farnesylation have not been reported. Previously, binding studies for SmgGDS-607 have been performed with RhoA, a GGTase-I substrate (13,28). Here, we sought to identify the determinants of SmgGDS-607 recognition of FTase substrates by assaying three different GTPases, KRas4B, DiRas1, and HRas. Our *in vitro* experiments demonstrate that the last residue in the CAAX box of KRas4B affects

the binding affinity for SmgGDS-607, confirming cell-based work indicating the importance of this residue for selectivity (15). In cell experiments, wild-type KRas4B did not pull down with SmgGDS-607. However, when the C-terminal methionine was mutated to leucine, SmgGDS-607 co-immunoprecipitated with unprenylated KRas4B (15). Our data corroborate this finding since SmgGDS-607 binds the M188L mutant >300-fold more tightly than wild-type KRas4B, thus demonstrating that the CAAX box sequence is important for recognition. Additionally, our data suggest that other factors also regulate binding affinity, as indicated by the enhanced affinity of DiRas1 compared to KRas4B (Table 2.3). Recent studies suggest that the negatively-charged region in SmgGDS-607 interacts with the PBR-CAAX motif of small GTPases (28, 29). The sequence of the PBR and the length of the tail are factors that could affect the direct contact with SmgGDS and/or the conformation of such GTPases, altering interaction with SmgGDS-607. Although both GTPases end in methionine, KRas4B and DiRas1 differ in their PBR sequence and tail length. The PBR domain of KRas4B contains tandem lysine repeats, which might not be optimal for binding to the dispersed electronegative region in SmgGDS-607, whereas the positive charges in the PBR domain of DiRas1 are more dispersed and include arginine residues (Table 2.1). Additionally, DiRas1 has a longer tail, which might provide optimal distal contacts with SmgGDS-607. Besides the different features found on the tail of small GTPases, studies have shown that the bound nucleotide status of RhoA significantly influences the affinity for SmgGDS-607 (12, 13, 28, 36). In contrast, the affinity of SmgGDS-607 for DiRas1 increases modestly (2-fold) when the bound nucleotide is GTP compared to GDP (data not shown). These data suggest that the factors dictating binding affinity with SmgGDS-607 are complex, and specific to each small GTPase.

Our binding studies demonstrate that the sequence of the C-terminal tails of small GTPases leads to differential affinities for SmgGDS-607 and FTase. Our model indicates that although SmgGDS-607 can bind to GTPases that undergo either farnesylation or geranylgeranylation, the regulation of prenylation is dictated by the relative binding affinities of each GTPase for SmgGDS-607 and the prenyltransferase (Figure 2.6). For DiRas1 and KRas4B M188L, SmgGDS-607 inhibits farnesylation due to the higher affinity of the GTPase for SmgGDS-607 compared to FTase ( $K_D^{\text{SmgGDS-607}}/K_D^{\text{FTase}} \sim 0.1$ , Table

2.3). However, SmgGDS-607 does not effectively inhibit farnesylation of KRas4B due to a combination of decreased affinity for SmgGDS-607 and increased affinity for FTase ( $K_D^{\text{SmgGDS-607}}/K_D^{\text{FTase}} \sim 700$ , Table 2.3). In contrast, geranylgeranylation of KRas4B is inhibited by SmgGDS-607 due to the enhanced affinity for SmgGDS-607 relative to GGTase-I (Table A1, Figure A2; Appendix). Consistent with this model, previous data demonstrate that treatment of cells with a FTI increases the co-immunoprecipitation of

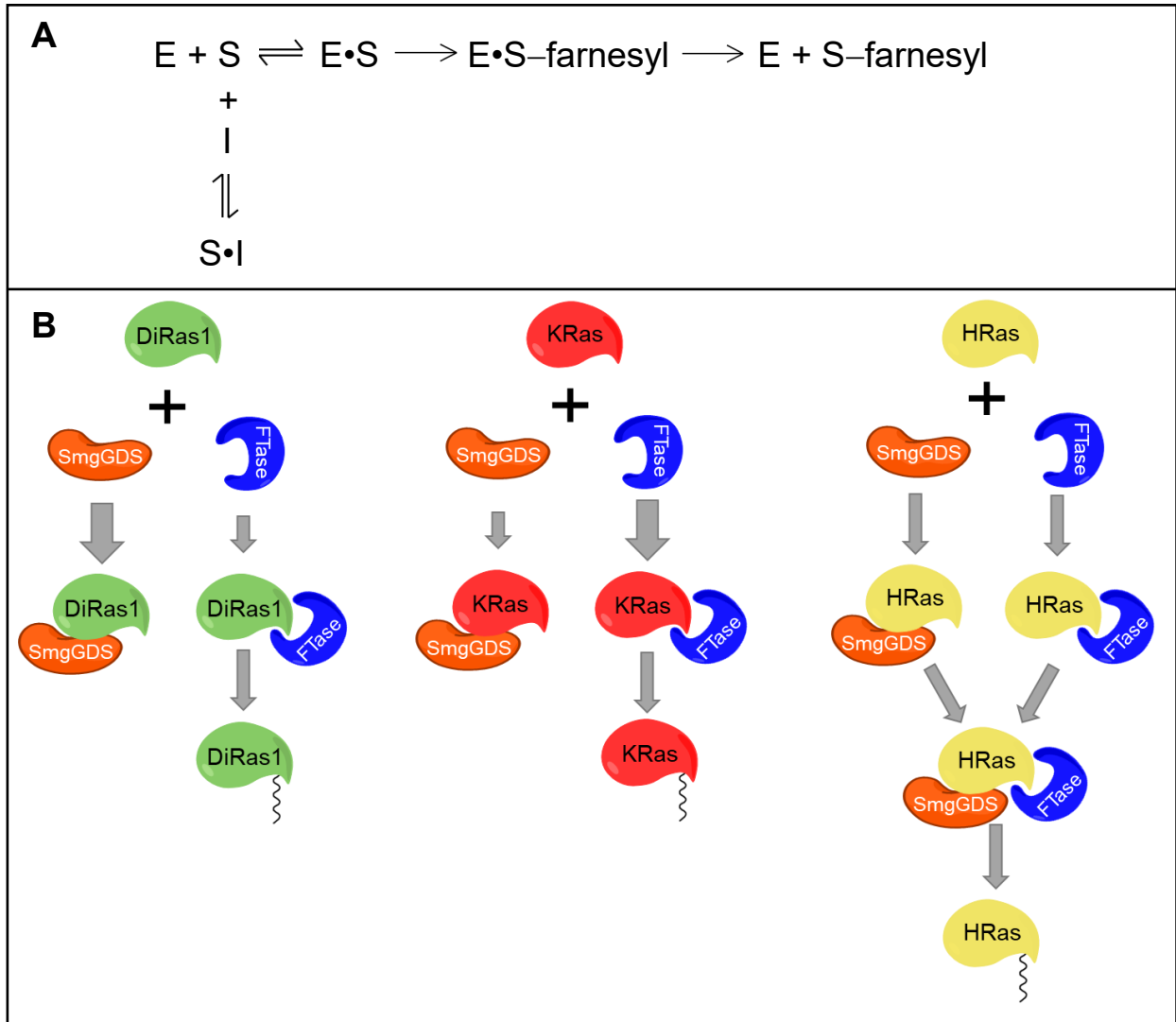


**Figure 2.6. Proposed model for SmgGDS-607-mediated regulation of farnesylation of FTase substrates.** (A) Differential binding model for inhibition of FTase (E)-catalyzed prenylation of small GTPases (S) containing a PBR motif in the presence of SmgGDS-607 (I). (B) Under thermodynamic conditions, the small GTPases that have higher affinity for SmgGDS-607 compared to FTase, such as DiRas1, form a stable SmgGDS-607•GTPase complex (heavy arrow) to inhibit farnesylation. For KRas4B, the affinity for FTase is thermodynamically favored (heavy arrow) compared to SmgGDS-607, therefore the SmgGDS-607•GTPase complex does not build up and farnesylation is not inhibited. Regulation for DiRas1 and KRas4B is mostly determined by the preference of the small GTPase for binding either SmgGDS-607 or FTase. For substrates lacking a PBR, such as HRas, SmgGDS-607 forms a ternary complex that facilitates farnesylation and product release.

SmgGDS-607 and KRas4B (15). Under these conditions, KRas4B can be alternatively geranylgeranylated. Since the binding affinity of KRas4B for GGTase-I is weaker than for SmgGDS-607 (Table A1), KRas4B preferentially binds to SmgGDS-607 and geranylgeranylation is inhibited. It is important to note that these events happen in a cellular environment where other small GTPases compete with KRas4B for binding to the prenyltransferases and SmgGDS-607. Particularly, cell-based competition experiments with DiRas1 demonstrate that DiRas1 decreases the amount of KRas4B that immunoprecipitates with SmgGDS-558 (16). Similarly, our binding data show that DiRas1 binds SmgGDS-607 >300-fold tighter than KRas4B, which predicts that increased unfarnesylated DiRas1 concentrations should antagonize SmgGDS-607 binding KRas4B in cells. Therefore, the prenylation pathways are constantly regulated by the levels of small GTPases and other binding partners. Furthermore, the PBR and CAAX sequences of a given GTPase are optimized for this regulatory function in the cell. Alteration of the association between small GTPases, such as KRas4B, and SmgGDS-607 by small molecules could be a novel target for effective therapeutics against small GTPase-associated cancers.

The data presented in this study, together with previous data (13, 15), show that SmgGDS-607 functions as a regulator of small GTPase geranylgeranylation by binding to non-prenylated small GTPases and blocking prenylation. Originally, SmgGDS was reported as a guanine nucleotide exchange factor (GEF) for multiple small GTPases that contain a PBR. However, recently, SmgGDS was demonstrated to function as a GEF for only select GTPases, RhoA and RhoC (30). Other studies have reported that the PBR domain of small GTPases plays an important role for both nucleotide exchange and affinity for SmgGDS-607 (14, 31). Until now, no one has determined whether SmgGDS-607 also regulates small GTPases without a PBR, such as HRas. In this study, we demonstrate that SmgGDS-607 also enhances farnesylation of a non-canonical SmgGDS substrate, HRas. Our *in vitro* data support a model in which SmgGDS-607 forms a complex with both HRas and FTase that enhances both farnesylation and product release (Figure 2.6B). Previous kinetic studies have demonstrated that the product dissociation is the rate determining step in FTase turnover of peptides (22,32). Furthermore, an additional FPP molecule binds to FTase to enhance dissociation of the

prenylated peptide by trapping the farnesyl moiety in an alternate conformation in the “exit groove” (33). We hypothesize that SmgGDS-607 could enhance product release in a similar way. By interacting with both HRas and FTase, SmgGDS-607 could stabilize the alternate product conformation, which allows for enhanced turnover. Contrary to the other FTase substrates tested in this study, HRas does not contain a PBR on its tail and has modest affinity for SmgGDS-607 alone. Enhancement of prenylation has not been observed with GTPases that contain a PBR. Additionally, our kinetic study with dansylated peptide indicates that SmgGDS-607 does not directly interact with FTase. Hence, it suggests that the formation of a ternary FTase•Protein•SmgGDS-607 complex might be specific for GTPases lacking a PBR.

Furthermore, the differential effects of SmgGDS-607 on farnesylation of small GTPases intensify the observed effects for a given substrate. Because FTase has multiple substrates in the cell, the specificity constant ( $k_{cat}/K_M$ ) is the best index to compare the preference of FTase for reacting with different substrates. At 10  $\mu$ M SmgGDS-607, the values of  $k_{cat}/K_M$  for farnesylation of small GTPases are affected as follows: DiRas1 decreases  $\geq 10$ -fold, KRas4B remains essentially unchanged and HRas increases 6-fold. Therefore, the ratio of  $k_{cat}/K_M$  values for HRas compared to DiRas1 changes by a factor of  $\geq 60$ -fold. This calculation illustrates how the presence of SmgGDS-607 significantly alters the dynamics and levels of Ras farnesylation in the cell.

These data support a model in which SmgGDS-607 regulates the farnesylation of small GTPases and this regulation is mediated by differential binding affinities. Although past studies have shown SmgGDS-607 regulates GTPases undergoing the geranylgeranylation pathway, we have shown that SmgGDS-607 regulation extends to the farnesylation pathway. Additionally, we have identified a novel function for SmgGDS-607 in facilitating product release of the farnesylated HRas (and possibly other small GTPases lacking a PBR) from protein farnesyltransferase. Further investigation into the synergies between the PBR and CAAX identity for farnesylation and regulation should be explored to assess their potential as novel targets for anti-cancer therapeutics.

## APPENDIX

This appendix contains supporting tables, figures, and methods for Chapter 2.

**Table A1. Summary of thermodynamic and kinetic values for SmgGDS-607 and prenyltransferases binding to different small GTPases<sup>a</sup>.**

	CAAX identity	$K_D$ (nM)	$k_{on}$ ( $\mu\text{M}^{-1} \text{s}^{-1}$ )	$k_{off}$ ( $\text{s}^{-1}$ )	$K_{calc}$ (nM)
<b>Binding to SmgGDS-607</b>					
KRas4B	CVIM	$1500 \pm 370$	$0.14 \pm 0.02$	$0.01 \pm 0.02$	$\leq 210$
KRas4B M188L	CVIL	$110 \pm 20$	$0.41 \pm 0.01$	$0.0015 \pm 0.0004$	$4 \pm 1$
DiRas1	CTLM	$4.7 \pm 0.9$	$0.19 \pm 0.01$	$0.0008 \pm 0.0001$	$4.2 \pm 0.6$
<b>Binding to FTase</b>					
KRas4B	CVIM	$2.2 \pm 0.7$	$0.60 \pm 0.02$	$0.0016 \pm 0.0001$	$2.7 \pm 0.2$
KRas4B M188L	CVIL	$1100 \pm 370$	$0.13 \pm 0.08$	$0.32 \pm 0.07$	$3000 \pm 2000$
DiRas1	CTLM	$40 \pm 2$	$0.49 \pm 0.03$	$0.009 \pm 0.001$	$18 \pm 2$
<b>Binding to GGTase-I</b>					
KRas4B	CVIM	$200 \pm 30$	$0.008 \pm 0.001$	$0.0024 \pm 0.0009$	$300 \pm 100$

<sup>a</sup> Measured by biolayer interferometry as described in the Experimental Procedures and the legend of Figure 2.  $K_D$  was determined from a hyperbolic equation fit to the endpoint data from the BLI responses obtained during the association step between the small GTPases and SmgGDS-607 or prenyltransferase.  $k_{on}$  and  $k_{off}$  were determined from a one-phase exponential fit to the association and dissociation steps.  $K_{calc}$  is the calculated  $K_D$  assuming a simple binding step obtained using the following equation:  $K_{calc} = k_{off} / k_{on}$ .

**Table A2. Summary of parameters used for simulation of SmgGDS-607 concentration dependence for inhibition of small GTPase prenylation.**

KRas4B farnesylation reaction				
Simulation parameter	Empirical parameter	Value	Units	Notes
$k_1$	$k_{\text{on, FTase}}$	0.6	$\mu\text{M}^{-1}\text{s}^{-1}$	Value obtained from kinetic binding experiment (Table A1)
$k_{-1}$	$k_{\text{off, FTase}}$	0.0016	$\text{s}^{-1}$	Value obtained from kinetic binding experiment (Table A1)
$k_2$	$k_{\text{chem}}$	1.5	$\text{s}^{-1}$	Value obtained from $k_{\text{chem}} = (K_{\text{M}} \times k_{\text{on, FTase}}) - k_{\text{off, FTase}}$ , from which $K_{\text{M}}$ was obtained from multiple-turnover experiments with full-length protein (data not shown)
$k_{-2}$	---	0	---	---
$k_3$	$k_{\text{cat}}$	0.041	$\text{s}^{-1}$	Value obtained from multiple-turnover experiments with full-length protein (data not shown)
$k_{-3}$	---	0	---	---
$k_4$	$k_{\text{on, SmgGDS-607}}$	0.14	$\mu\text{M}^{-1}\text{s}^{-1}$	Value obtained from kinetic binding experiment (Table A1)
$k_{-4}$	$k_{\text{off, SmgGDS-607}}$	0.21	$\text{s}^{-1}$	Value obtained from $k_{\text{off, SmgGDS-607}} = K_{\text{D, SmgGDS-607}} \times k_{\text{on, SmgGDS-607}}$ (Table A1)
KRas4B geranylgeranylation reaction				
Simulation parameter	Empirical parameter	Value	Units	Notes
$k_1$	$k_{\text{on, GGTase-I}}$	0.008	$\mu\text{M}^{-1}\text{s}^{-1}$	Value obtained from kinetic binding experiment (Table A1)
$k_{-1}$	$k_{\text{off, GGTase-I}}$	0.0024	$\text{s}^{-1}$	Value obtained from kinetic binding experiment (Table A1)
$k_2$	$k_{\text{chem}}$	0.35	$\text{s}^{-1}$	Value obtained from single-turnover experiments performed with peptide TKCVIM (ref. 20)
$k_{-2}$	---	0	---	---

$k_3$	$k_{\text{cat}}$	0.082	$\text{s}^{-1}$	Value obtained from multiple-turnover experiments performed with peptide TKCVIM (ref. 20)
$k_{-3}$	---	0	---	---
$k_4$	$k_{\text{on, SmgGDS-607}}$	0.14	$\mu\text{M}^{-1}\text{s}^{-1}$	Value obtained from kinetic binding experiment (Table A1)
$k_{-4}$	$k_{\text{off, SmgGDS-607}}$	0.21	$\text{s}^{-1}$	Value obtained from $k_{\text{off, SmgGDS-607}} = K_{\text{D, SmgGDS-607}} \times k_{\text{on, SmgGDS-607}}$ (Table A1)

#### KRas4B M188L farnesylation reaction

Simulation parameter	Empirical parameter	Value	Units	Notes
$k_1$	$k_{\text{on, FTase}}$	0.13	$\mu\text{M}^{-1}\text{s}^{-1}$	Value obtained from kinetic binding experiment (Table A1)
$k_{-1}$	$k_{\text{off, FTase}}$	0.14	$\text{s}^{-1}$	Value obtained from $k_{\text{off, FTase}} = K_{\text{D, FTase}} \times k_{\text{on, FTase}}$ (Table A1)
$k_2$	$k_{\text{cat}}$	0.0032	$\text{s}^{-1}$	Value obtained from multiple-turnover experiments with full-length protein (data not shown)
$k_{-2}$	---	0	---	---
$k_3$	$k_{\text{on, SmgGDS-607}}$	0.41	$\mu\text{M}^{-1}\text{s}^{-1}$	Value obtained from kinetic binding experiment (Table A1)
$k_{-3}$	$k_{\text{off, SmgGDS-607}}$	0.045	$\text{s}^{-1}$	Value obtained from $k_{\text{off, SmgGDS-607}} = K_{\text{D, SmgGDS-607}} \times k_{\text{on, SmgGDS-607}}$ (Table A1)

#### DiRas1 farnesylation reaction

Simulation parameter	Empirical parameter	Value	Units	Notes
$k_1$	$k_{\text{on, FTase}}$	0.49	$\mu\text{M}^{-1}\text{s}^{-1}$	Value obtained from kinetic binding experiment (Table S1)
$k_{-1}$	$k_{\text{off, FTase}}$	0.02	$\text{s}^{-1}$	Value obtained from $k_{\text{off, FTase}} = K_{\text{D, FTase}} \times k_{\text{on, FTase}}$ (Table S1)
$k_2$	$k_{\text{chem}}$	0.372	$\text{s}^{-1}$	Value obtained from $k_{\text{chem}} = (K_{\text{M}} \times k_{\text{on, FTase}}) - k_{\text{off, FTase}}$ , from which $K_{\text{M}}$ was obtained from multiple-turnover experiments with full-length protein (data not shown)

$k_{-2}$	---	0	---	---
$k_3$	$k_{\text{on, SmgGDS-607}}$	0.19	$\mu\text{M}^{-1}\text{s}^{-1}$	Value obtained from kinetic binding experiment (Table S1)
$k_{-3}$	$k_{\text{off, SmgGDS-607}}$	0.0008	$\text{s}^{-1}$	Value obtained from kinetic binding experiment (Table S1)

---

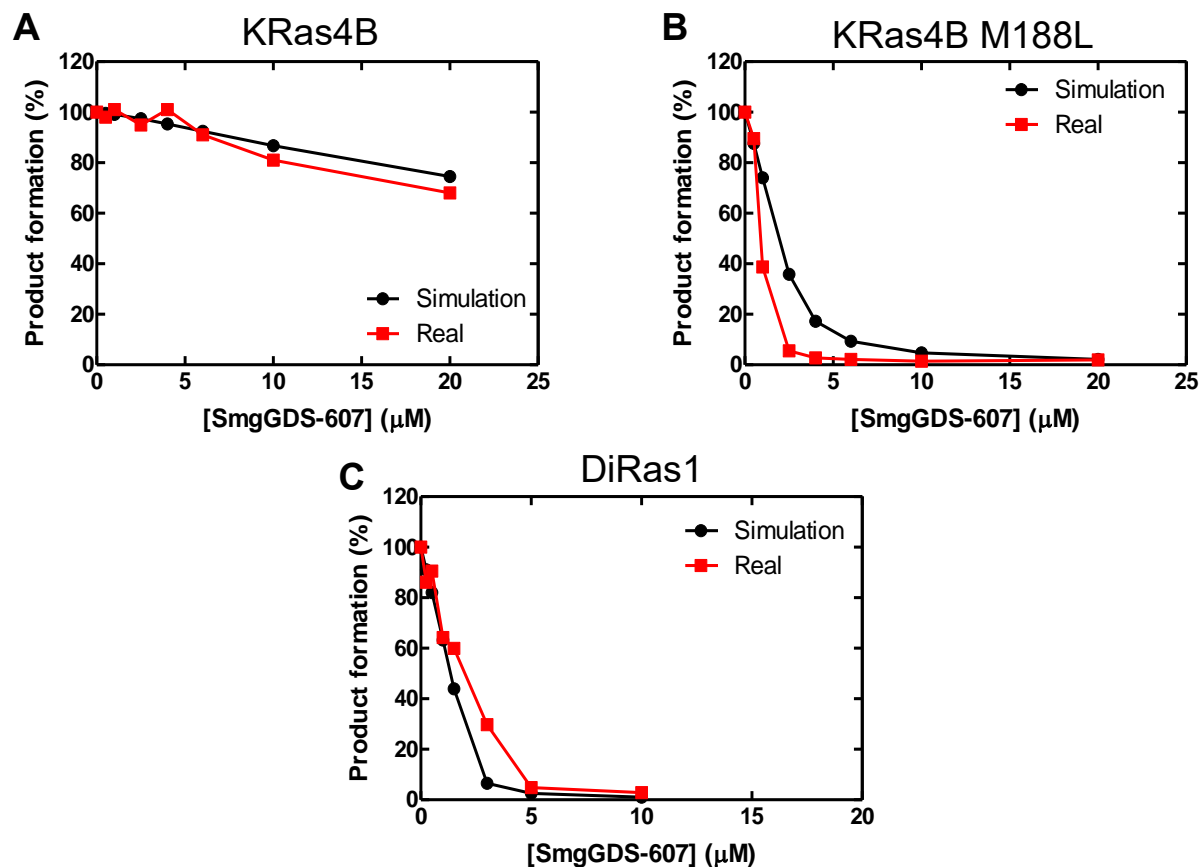


**Figure A1. Simulation of SmgGDS-607 concentration dependence for inhibition of small GTPase farnesylation using the KinTek Explorer Chemical Kinetics Software.** (A) Simulation was carried out following with a differential binding model (Figure 3) using the following equations: (1)  $E + S = ES = EP = E + P$  and (2)  $C + S = CS$ , where E represents the enzyme (FTase), S represents the substrate (KRas4B), P represents the product (farnesylated KRas4B), and C represents competitor (SmgGDS-607). Simulation was carried out using  $K_D^{FTase}$ ,  $K_D^{SmgGDS-607}$ ,  $k_{chem}$ , and  $k_{cat}$  values obtained empirically. (B) and (C) Simulation was carried out following a differential binding model using the following equations: (1)  $E + S = ES = E + P$  and (2)  $C + S = CS$ , where S represents the substrate (B, KRas4B M188L, and C, DiRas1). Simulation was carried out using  $K_D^{FTase}$ ,  $K_D^{SmgGDS-607}$ , and  $k_{chem}$  values obtained empirically.

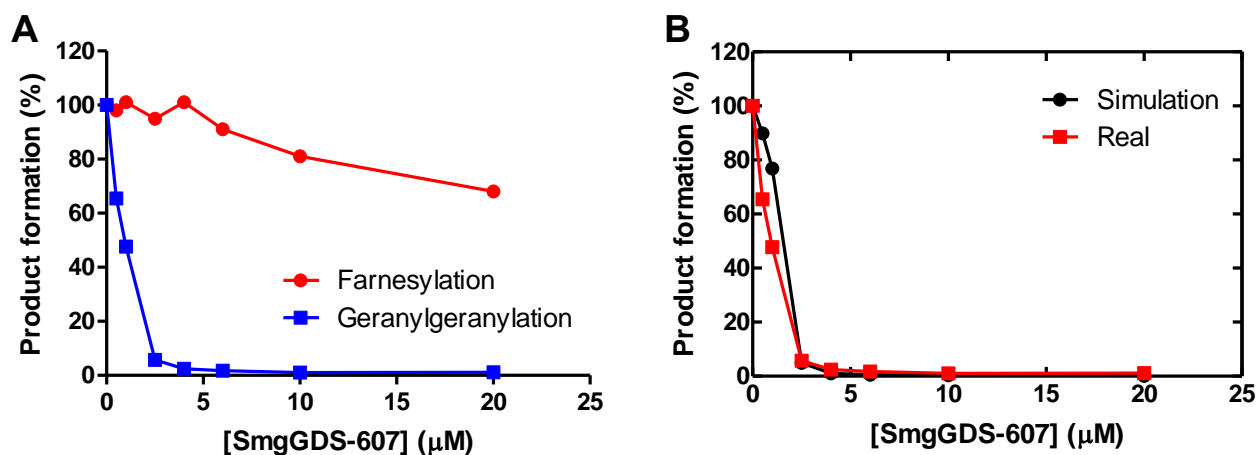
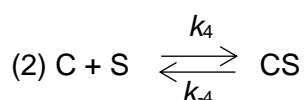
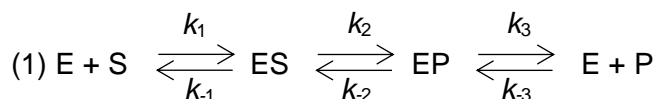


**Figure A2. SmgGDS-607 blocks the extent of geranylgeranylation of KRas4B.** (A) The KRas4B CAAX box (CVIM) is recognized by both FTase and GGTase-I, allowing for alternative geranylgeranylation when farnesylation is inhibited. KRas4B (2.5 μM) was incubated with GDP (25 μM), FTase or GGTase-I (25 nM), [<sup>3</sup>H]-GGPP (4 μM), and the indicated concentrations of SmgGDS-607. Reactions were stopped after 5 min (farnesylation) or 1 min (geranylgeranylation) and incorporation of radiolabeled farnesyl was measured as described in the methods. (B) Simulation of SmgGDS-607 effect on geranylgeranylation of KRas4B using the KinTek Explorer Chemical Kinetics Software. Simulation was carried out with a differential binding model using the following equations: (1)  $E + S = ES = EP = E + P$  and (2)  $C + S = CS$ , where E represents the enzyme (GGTase-I), S represents the substrate (KRas4B), P represents the product (geranylgeranylated KRas4B), and C represents competitor (SmgGDS-607). Kinetic values used for simulation include association and dissociation rate values obtained empirically (Table S1), while  $k_{chem}$  and  $k_{cat}$  values were taken from TKCVIM peptide data previously published (20);  $k_{on}^{GGTase-I} = 0.008 \mu M^{-1} s^{-1}$ ,  $k_{off}^{GGTase-I} = 0.0024 s^{-1}$ ,  $k_{on}^{SmgGDS-607} = 0.14 \mu M^{-1} s^{-1}$ ,  $k_{off}^{SmgGDS-607} = 0.01 s^{-1}$ ,  $k_{chem} = 0.35 s^{-1}$  and  $k_{cat} = 0.082 s^{-1}$ .

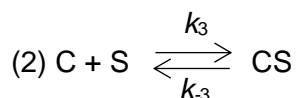
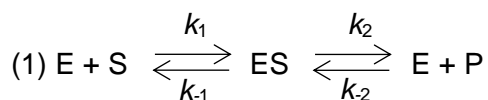
### ***Kinetic data modeling***

The simulations of SmgGDS-607 concentration dependence data for inhibition of small GTPase prenylation were performed using the KinTek Explorer Chemical Kinetics Software. For KRas4B, data simulations were performed using a three-step model to describe the farnesylation and geranylgeranylation reactions, while SmgGDS-607 binding is described by a single-step model:



where E represents the enzyme (FTase or GGTase-I), S represents the substrate (KRas4B), P represents the product (farnesylated or geranylgeranylated KRas4B), and C represents competitor (SmgGDS-607).

For KRas4B M188L and DiRas1, data simulations were performed using a two-step model to describe the farnesylation reaction, while SmgGDS-607 binding is described by a single-step model:



where E represents the enzyme (FTase), S represents the substrate (KRas4B M188L or DiRas1), P represents the product (farnesylated KRas4B M188L or DiRas1), and C represents competitor (SmgGDS-607).

The rate constants used for data simulation are listed in Table A2 and were either obtained empirically through kinetic binding experiments as described in the Experimental Procedures, steady-state kinetic experiments performed with full-length protein (data not

shown), or transient and steady-state kinetic experiments previously performed with TKCVIM peptide (ref. 20).

Simulation data was obtained as reaction progress curves. All curves were computed with 25 nM enzyme, 2.5  $\mu$ M Ras, and the indicated concentrations of SmgGDS-607. The percentage of product formed in the presence of SmgGDS-607 at specific time intervals was determined from the simulated progress curves using equation 7.

$$\% \text{ product} = \frac{\text{amount of product formed with SmgGDS-607 at a specific time}}{\text{amount of product formed without SmgGDS-607 at a specific time}} \times 100 \quad \text{Equation 7}$$

The time intervals used to calculate the simulated percentage of product formed for Ras substrates are 5 min for KRas4B (farnesylation), 1 min for KRas4B (geranylgeranylation), 6 min for DiRas1, and 30 min for KRas4B M188L.

The data modeling performed with kinetic and thermodynamic parameters obtained empirically offers qualitative validation of SmgGDS-mediated regulation defined by a differential binding model. It must be highlighted that for KRas4B M188L data (Figure A1, panel B), the  $k_{\text{off, SmgGDS-607}}$  value used in our model ( $k_{\text{off, SmgGDS-607}} = 0.045 \text{ s}^{-1}$ , Table A2) was obtained from the corresponding thermodynamic binding parameter,  $K_{\text{D}}$  ( $k_{\text{off, SmgGDS-607}} = K_{\text{D, SmgGDS-607}} \times k_{\text{on, SmgGDS-607}}$ ). However, modeling the data with the kinetic parameter obtained experimentally for SmgGDS-607 binding ( $k_{\text{off, SmgGDS-607}} = 0.0015 \pm 0.0004 \text{ s}^{-1}$ , Table A1) provides a better fit to the data. Similarly, for DiRas1 (Figure A1, panel C), the  $k_{\text{off, FTase}}$  parameter used in our model ( $k_{\text{off, FTase}} = 0.02 \text{ s}^{-1}$ , Table A2) was obtained from the corresponding thermodynamic binding parameter,  $K_{\text{D}}$  ( $k_{\text{off, FTase}} = K_{\text{D, FTase}} \times k_{\text{on, FTase}}$ ). However, modeling the data with the kinetic parameter obtained experimentally for FTase binding ( $k_{\text{off, FTase}} = 0.009 \pm 0.001 \text{ s}^{-1}$ , Table A1) provides a better fit to the data.

## REFERENCES

1. Cox, A. D., Fesik, S. W., Kimmelman, A. C., Luo, J., and Der, C. J. (2014) Drugging the undruggable RAS: mission possible? *Nat. Rev. Drug Discov.* **13**, 828–851
2. Nussinov, R., Tsai, C.-J., and Mattos, C. (2013) Pathway drug cocktail: targeting Ras signaling based on structural pathways. Targeting RAS–ERK signalling in cancer: promises and challenges. *Trends Mol. Med.* **19**, 695–704
3. Samatar, A. A., and Poulidakos, P. I. (2014) *Nat. Rev. Drug Discov.* **13**, 928–942
4. Cox, A. D., and Der, C. J. (2010) Ras history: The saga continues. *Small GTPases* **1**, 2-27
5. Berndt, N., Hamilton, A. D., and Sebti, S. M. (2011) Targeting protein prenylation for cancer therapy. *Nat. Rev. Cancer* **11**, 775–791
6. Liu, M., Sjogren, A. K., Karlsson, C., Ibrahim, M. X., Andersson, K. M., Olofsson, F. J., Wahlstrom, A. M., Dalin, M., Yu, H., Chen, Z., Yang, S. H., Young, S. G., and Bergo, M. O. (2010) Targeting the protein prenyltransferases efficiently reduces tumor development in mice with K-RAS-induced lung cancer. *Proc. Natl. Acad. Sci. U.S.A.* **107**, 6471–6476
7. Whyte, D. B., Kirschmeier, P., Hockenberry, T. N., Nunez-Oliva, I., James, L., Catino, J. J., Bishop, W. R., and Pai, J. K. (1997) K- and N-Ras are geranylgeranylated in cells treated with farnesyl protein transferase inhibitors. *J. Biol. Chem.* **272**, 14459–14464
8. Fiordalisi, J. J., Johnson, R. L., Weinbaum, C. A., Sakabe, K., Chen, Z., Casey, P. J., and Cox, A. D. (2003) High affinity for farnesyltransferase and alternative prenylation contribute individually to K-Ras4B resistance to farnesyltransferase inhibitors. *J. Biol. Chem.* **278**, 41718–41727
9. Lobell, R. B. et al. (2001) Evaluation of Farnesyl:Protein Transferase and Geranylgeranyl: Protein Transferase Inhibitor Combinations in Preclinical Models. *Cancer Res.* **61**, 8758–8768
10. deSolms, S.J. et al. (2003) Dual protein farnesyltransferase-geranylgeranyltransferase-I inhibitors as potential cancer chemotherapeutic agents. *J. Med. Chem.* **46**, 2973–2984
11. Williams, C. (2013) A new signaling paradigm to control the prenylation and trafficking of small GTPases, *Cell Cycle* **12**, 2933–2934
12. Berg, T. J., Gastonguay, A. J., Lorimer, E. L., Kuhnmuensch, J. R., Li, R., Fields, A. P., and Williams, C. L. (2010) Splice variants of SmgGDS control small GTPase prenylation and membrane localization. *J. Biol. Chem.* **285**, 35255–35266
13. Jennings, B. C., Lawton, A. J., Rizk, Z., and Fierke, C. A. (2018) SmgGDS-607 regulation of RhoA GTPase prenylation is nucleotide-dependent. *Biochemistry* **57**, 4289–4298
14. Vikis, H. G., Stewart, S., and Guan, K.-L. (2002) SmgGDS displays differential binding and exchange activity towards different Ras isoforms. *Oncogene* **21**, 2425–2432
15. Schuld, N. J., Vervacke, J. S., Lorimer, E. L., Simon, N. C., Hauser, A. D., Barbieri, J. T., Distefano, M. D., Williams, C. L. (2014) The chaperone protein SmgGDS interacts with small GTPases entering the prenylation pathway by recognizing the last amino acid in the CAAX motif. *J. Biol. Chem.* **289**, 6862–6876

16. Bergom, C., Hauser, A. D., Rymaszewski, A., Gonyo, P., Prokop, J. W., Jennings, B. C., Lawton, A. J., Frei, A., Lorimer, E. L., Aguilera-Barrantes, I., Mackinnon Jr., A. C., Noon, K., Fierke, C. A., Williams, C. L. (2016) The tumor-suppressive small GTPase DiRas1 binds the noncanonical guanine nucleotide exchange factor SmgGDS and antagonizes SmgGDS interactions with oncogenic small GTPases. *J. Biol. Chem.* **291**, 6534–6545
17. Ogita, Y., Egami, S., Ebihara, A., Ueda, N., Katada, T., and Kontani, K. (2015) Di-Ras2 protein forms a complex with SmgGDS protein in brain cytosol in order to be in a low affinity state for guanine nucleotides. *J. Biol. Chem.* **290**, 20245–20256
18. Ellis, C. A., Vos, M. D., Howell, H., Vallecorsa, T., Fults, D. W., and Clark, G. J. (2002) Rig is a novel Ras-related protein and potential neural tumor suppressor. *Proc. Natl. Acad. Sci. U.S.A.* **99**, 9876–9881
19. Abdiche, Y., Malashock, D., Pinkerton, A., and Pons, J. (2008) Determining kinetics and affinities of protein interactions using a parallel real-time label-free biosensor, the Octet. *Anal. Biochem.* **377**, 209–217
20. Hartman, H. L., Hicks, K. A., and Fierke, C. A. (2005) Peptide specificity of protein prenyltransferases is determined mainly by reactivity rather than binding affinity. *Biochemistry* **44**, 15314–15324
21. Hougland, J. L., Hicks, K. A., Hartman, H. L., Kelly, R. A., Watt, T. J., and Fierke, C. A. (2010) Identification of novel peptide substrates for protein farnesyltransferase reveals two substrate classes with distinct sequence selectivities. *J. Mol. Biol.* **395**, 176–190
22. Ochocki, J. D., and Distefano, M. D. (2013) Prenyltransferase Inhibitors: Treating Human Ailments from Cancer to Parasitic Infections. *MedChemComm* **4**, 476–492
23. Furfine, E.S., Leban, J.J., Landavazo, A., Moomaw, J.F., and Casey, P.J. (1995) Protein farnesyltransferase: kinetics of farnesyl pyrophosphate binding and product release. *Biochemistry* **34**, 6857–6862
24. Long, S. B., Casey, P. J., and Beese, L. S. (2000) The basis for K-Ras4B binding specificity to protein farnesyl-transferase revealed by 2 Å resolution ternary complex structures. *Structure* **8**, 209–222
25. Hicks, K. A., Hartman, H. L., and Fierke, C. A. (2005) Upstream polybasic region in peptides enhances dual specificity for prenylation by both farnesyltransferase and geranylgeranyltransferase type I. *Biochemistry* **44**, 15325–15333
26. Reid, T. S., Terry, K. L., Casey, P. J., and Beese, L. S. (2004) Crystallographic analysis of CaaX prenyltransferases complexed with substrates defines rules of protein substrate selectivity. *J. Mol. Biol.* **343**, 417–433
27. London, N., Lamphear, C. L., Hougland, J. L., Fierke, C. A., and Schueler-Furman O. (2011) Identification of a novel class of farnesylation targets by structure-based modeling of binding specificity. *PLoS Comput. Biol.* **7**, e1002170. doi:10.1371/journal.pcbi.1002170
28. Shimizu, H., Toma-Fukai, S., Saijo, S., Shimizu, N., Kontani, K., Katada, T., and Shimizu, T. (2017) Structure-based analysis of the guanine nucleotide exchange factor SmgGDS reveals armadillo-repeat motifs and key regions for activity and GTPase binding. *J. Biol. Chem.* **292**, 13441–13448

29. Wilson, J. M., Prokop, J. W., Lorimer, E., Ntantie, E., and Williams, C. L. (2016) Differences in the Phosphorylation-Dependent Regulation of Prenylation of Rap1A and Rap1B. *J. Mol. Biol.* **428**, 4929–4945
30. Hamel, B., Monaghan-Benson, E., Rojas, R. J., Temple, B. R., Marston, D. J., Burrige, K., and Sondek, J. (2011) SmgGDS is a guanine nucleotide exchange factor that specifically activates RhoA and RhoC. *J. Biol. Chem.* **286**, 12141–12148
31. Lanning, C. C., Ruiz-Velasco, R., and Williams, C. L. (2003) Novel mechanism of the co-regulation of nuclear transport of SmgGDS and Rac1. *J. Biol. Chem.* **278**, 12495–12506
32. Furfine, E. S., Leban, J. J., Landavazo, A., Moomaw, J. F., and Casey, P. J. (1995) Protein farnesyltransferase: kinetics of farnesyl pyrophosphate binding and product release. *Biochemistry* **34**, 6857–6862
33. Tschantz, W. R., Furfine, E. S., and Casey, P. J. (1997) Substrate binding is required for release of product from mammalian protein farnesyltransferase. *J. Biol. Chem.* **272**, 9989–9993
34. Wu, Z., Demma, M., Strickland, C. L., Syto, R., Le, H. V., Windsor, W. T., and Weber, P. C. (1999) High-level expression, purification, kinetic characterization and crystallization of protein farnesyltransferase  $\beta$ -subunit C-terminal mutants. *Protein Engineering* **12**, 341-348
35. Li, Y., and Sousa, R. (2012) Novel system for in vivo biotinylation and its application to crab antimicrobial protein scygonadin. *Biotechnol. Lett.* **34**, 1629–1635
36. Strassheim, D., Porter, R.A., Phelps, S.H., and Williams, C. L. (2000) Unique in vivo associations with SmgGDS and RhoGDI and different guanine nucleotide exchange activities by RhoA, dominant negative RhoAAsn-19, and activated RhoAVal-14. *J. Biol. Chem.* **275**, 6699–6702
37. Kirchner, J. (2001) Data Analysis Toolkit #5: Uncertainty Analysis and Error Propagation. Accessed March 11, 2019. [http://seismo.berkeley.edu/~kirchner/eps\\_120/Toolkits/Toolkit\\_05.pdf](http://seismo.berkeley.edu/~kirchner/eps_120/Toolkits/Toolkit_05.pdf).

## CHAPTER 3

### **Synergies Between the Upstream Polybasic Region and CAAX Identity in Ras Dictate Specificity of Prenylation and Interaction with SmgGDS-607**

#### INTRODUCTION

Members of the Ras protein family share several structural features, including four guanine nucleotide binding domains (I – IV), an effector binding domain, and a membrane targeting domain also identified as a hypervariable region (HVR). Some small GTPases in the Ras family contain a polybasic region (PBR) composed of multiple lysines or arginines that precedes the C-terminal CAAX motif in their HVR. Several studies confirm the importance of the PBR for Ras function, as the elimination or alteration of this domain influences membrane localization and cellular activity (1-3). This effect is mainly attributed to the signaling role of the PBR, since this domain can be recognized by a variety of Ras binding partners (1, 4-6). For some Ras proteins, the only distinctive features in their protein sequence are unique C-terminal PBR and CAAX sequences, suggesting that both affect protein-protein interactions. For example, protein farnesyltransferase (FTase) has weaker affinity for HRas, which lacks a PBR, compared to KRas4B, which contains a polylysine region before the CAAX sequence (7, 8). Consistent with these data, addition of the KRas4B PBR sequence to the C-terminus of HRas increases the FTase affinity compared to wild-type HRas (8). Similarly, an *in vitro* study with peptide substrates demonstrated that the polybasic region enhances the binding affinity of KRas4B-derived peptides for FTase (9). Furthermore, the presence of the upstream polylysine region in KRas4B is proposed to confer resistance to FTase inhibitors (FTIs) and allow for alternative geranylgeranylation (10).

The PBR is also proposed to regulate the interaction of Ras proteins with SmgGDS-607. In a previous study using KRas4B chimeras, the replacement of the polylysines with

a non-polybasic sequence in the C-terminus decreases interaction with SmgGDS-607, as measured by yeast two-hybrid screening (6). However, the exact nature of the PBR influence on SmgGDS-607 affinity is still a mystery. In Chapter 2 we demonstrate that SmgGDS-607 enhances farnesylation of HRas via the formation of a ternary FTase•HRas•SmgGDS-607 complex that enhances product release, suggesting that this behavior might be specific for GTPases lacking a PBR sequence. Hence, these data suggest that the role of the PBR sequence goes beyond modulating protein-protein interaction and may dictate regulation of Ras prenylation.

**Table 3.1. C-terminal sequence of FTase substrates used for this study.**

Ras protein	Hypervariable Region	CAAX
KRas4B-PBR <sub>KRas4B</sub> -CVIM (WT)	-DG <b>KKKKKK</b> S <b>K</b> TK	CVIM
KRas4B-HVR <sub>HRas</sub> -CVIM	-DGESGPGCMSCK	CVIM
KRas4B-PBR <sub>KRas4B</sub> -CVLS	-DG <b>KKKKKK</b> S <b>K</b> TK	CVLS
HRas-HVR <sub>HRas</sub> - CVLS (WT)	-PPDESGPGCMSCK	CVLS
HRas-PBR <sub>KRas4B</sub> -CVLS	-PPD <b>KKKKKK</b> S <b>K</b> TK	CVLS
HRas-HVR <sub>HRas</sub> -CVIM	-PPDESGPGCMSCK	CVIM
DiRas1	-DG <b>K</b> R <b>S</b> G <b>K</b> Q <b>K</b> R <b>T</b> D <b>R</b> V <b>K</b> G <b>K</b>	CTLM
DiRas2	-DG <b>K</b> <b>K</b> S <b>K</b> Q <b>K</b> R <b>K</b> E <b>K</b> L <b>K</b> G <b>K</b>	CVIM

polybasic residues

Here we investigate the molecular recognition of the PBR and CAAX motifs by both FTase and SmgGDS-607 to elucidate their function in regulation of Ras prenylation. The reactivity with FTase and affinity with SmgGDS-607 of various Ras substrates are examined using single turnover kinetics, steady state kinetics, and binding affinity assays. To further define the contributions of the PBR and CAAX sequences in regulation of Ras prenylation, we generated a set of Ras chimeric mutants that consists of different combinations of body, PBR (with and without), and CAAX motif (-CVIM and -CVLS) between KRas4B and HRas (Table 3.1). Additionally, we examine the contribution of charge distribution on the PBR by looking into two substrates that belong to a distinct subgroup of the Ras family, DiRas1 and DiRas2. Our data demonstrate that the presence of a PBR sequence in protein substrates enhances catalytic efficiency, indicated by higher values for both prenylation turnover ( $k_{cat}$ ) and substrate selectivity ( $k_{cat}/K_M$ ) compared to substrates lacking a PBR. The substrate selectivity is not contingent on the distribution of charge within the PBR, as DiRas1, DiRas2 and KRas4B exhibit similar  $k_{cat}/K_M$  values.

However, synergies between the CAAX sequence and the PBR influence the extent of enhancement of  $k_{cat}$  and the single-turnover rate, as CVLS exhibits faster turnover than CVIM. Additionally, this synergistic effect influences the affinity of substrates for SmgGDS-607, which ultimately dictates whether SmgGDS-607 will inhibit or enhance prenylation. Thus, the presence of a PBR dictates regulation of prenylation by both enhancing catalytic efficiency for farnesylation catalyzed by FTase and enhancing binding affinity for SmgGDS-607 in a sequence-specific manner.

## EXPERIMENTAL PROCEDURES

### ***Materials***

Purified, his-tagged SmgGDS-607 and biotinylated SmgGDS-607 were a gift from Dr. Benjamin C. Jennings (University of Michigan). Tritium labeled farnesyl pyrophosphate ( $[^3\text{H}]$ -FPP) was purchased from American Radiolabeled Chemicals, Inc. Primers were purchased from Integrated DNA Technologies.

### ***Preparation of KRas4B and HRas PBR chimera expression constructs***

Human KRas4B and HRas PBR chimera constructs were generated in pETM-11 vectors by overlap extension PCR using primers coding for the desired protein body and C-terminal sequences (Table 3.1). To construct plasmid pDG143 (KRas4B-HVR<sub>HRas</sub>-CVIM), a pair of primers was designed to amplify the KRas4B body coding region (F8: 5'-GAGGATCGAGATCTCGATCCC; F9: 5'-GCAGCTCATGCAGCCGGGGCCACTCTCACCATCTTTGCTCATCTTTTCTTTATGTTTC). Another pair of primers was used to amplify the KRas4B CAAX coding region with an overhang that encodes for the HRas PBR coding region (F10: 5'-GAGAGTGGCCCCGGCTGCATGAGCTGCAAGTGTGTAATTATGTAATAGCTCGAGC; F11: 5'-CTTTTAACAGCGATCGCGTATTTTCG). The resulting PCR products were gel-purified and used as template for the overlap PCR reaction. End primers (F8 and F11) were added to the overlap PCR reaction, followed by a gel purification. The resulting PCR product for the KRas4B-HVR<sub>HRas</sub>-CVIM chimera was

digested with *BglII/PvuI*. The DNA fragment was then ligated into a *BglII/PvuI*-digested pETM-11 vector.

A similar approach to pDG143 was used to construct plasmid pDG144 (HRas-PBR<sub>KRas4B</sub>-CVLS) with a few modifications. A pair of primers was used to amplify the HRas body coding region (F8 and F12: 5'-CTTTGTCTTTGACTTCTTTTTCTTCTTTTTCAGGAGGGTTCAGCTTCCG). Another pair of primers was used to amplify the HRas CAAX coding region with an overhang that encodes for the KRas4B PBR coding region (F11 and F13: 5'-AAAAAGAAGAAAAAGAAGTCAAAGACAAAGTGTGTGCTCTCCTGACTCG). The resulting PCR product for the HRas-PBR<sub>KRas4B</sub>-CVLS chimera was digested with *BglII/PvuI*. DNA sequencing verified the correct protein coding sequence.

### ***Preparation of KRas4B and HRas CAAX chimera expression constructs***

Human KRas4B and HRas CAAX chimera constructs were generated in pETM-11 vectors by site-directed mutagenesis using the QuickChange II site-directed mutagenesis kit (Agilent Technologies). To construct plasmid pDG145 (KRas4B-PBR<sub>KRas4B</sub>-CVLS), a pair of primers was used for site-directed point mutation (F14: 5'-GACAAAGTGTGTACTTATGTAATAGCTCGAG; F15: 5'-CTCGAGCTATTACATAAGTACACACTTTGTC), followed by a second round of site-directed amino acid mutation using another pair of primers (F16: 5'-GACAAAGTGTGTACTTAGTTAATAGCTCGAGCACC; F17: 5'-GGTGCTCGAGCTATTAATAAGTACACACTTTGTC). For plasmid pDG146 (HRas-HVR<sub>HRas</sub>-CVIM), a pair of primers was used for site-directed point mutation (F18: 5'-GCAAGTGTGTGATCTCCTGACTCGAG; F19: 5'-CTCGAGTCAGGAGATCACACACTTGC), followed by a second round of site-directed amino acid mutation using another pair of primers (F20: 5'-CTGCAAGTGTGTGATCATGTGACTCGAGCACCAC; F21: 5'-GTGGTGCTCGAGTCACATGATCACACACTTGCAG). DNA sequencing verified the correct protein coding sequence.

### ***FTase expression and purification***

Recombinant human FTase was expressed in BL21(DE3) *E. coli* cells, purified, quantified and assayed as described in Chapter 2 (11).

## **Ras expression and purification**

Ras proteins were expressed as described in Chapter 2 (11). BL21(DE3) *E. coli* cells were transformed with recombinant vectors encoding KRas4B (pBJ176), HRas (pBJ162), DiRas1 (pBJ173), DiRas2 (pBJ196), KRas4B-HVR<sub>HRas</sub>-CVIM (pDG143), KRas4B-PBR<sub>KRas4B</sub>-CVLS (pDG145), HRas-PBR<sub>KRas4B</sub>-CVLS (pDG144), or HRas-HVR<sub>HRas</sub>-CVIM (pDG146). Proteins were analyzed by SDS-PAGE to determine purity. Protein samples were concentrated, aliquoted, and stored at -80°C.

## **Steady-state kinetics**

The steady-state kinetic parameters,  $k_{cat}$ ,  $K_M$ , and  $k_{cat}/K_M$  were measured for human FTase with 8 different Ras substrates (KRas4B, KRas4B-HVR<sub>HRas</sub>-CVIM, KRas4B-PBR<sub>KRas4B</sub>-CVLS, HRas, HRas-PBR<sub>KRas4B</sub>-CVLS, HRas-HVR<sub>HRas</sub>-CVIM, DiRas1, and DiRas2) using a radiolabel-prenylation assay as described in Chapter 2 (11). The reactions contained a range of substrate concentrations spanning between 0.25 – 30  $\mu$ M, depending on the Ras protein. All reactions were performed at 30°C in 50 mM HEPPSO, pH 7.8, 5 mM TCEP, 5 mM MgCl<sub>2</sub>, 0.1% Triton X-100, 20 – 40  $\mu$ M GDP, 18 – 30  $\mu$ M 10% [<sup>3</sup>H]-FPP mix, and 50 nM FTase. Incubation times for the farnesylation reaction varied depending on the Ras protein while ensuring that the measurement was under initial product formation (<10%): KRas4B (3 min), HRas (20 min), DiRas1 (3 min), DiRas2 (3 min), KRas4B-HVR<sub>HRas</sub>-CVIM (8 min), KRas4B-PBR<sub>KRas4B</sub>-CVLS (3 min), HRas-PBR<sub>KRas4B</sub>-CVLS (4 min), and HRas-HVR<sub>HRas</sub>-CVIM (8 min). FPP Reactions were initiated by the addition of radiolabeled FPP mixture and incubated at 30°C before quenching the reactions by the addition of 1X Laemmli sample buffer. After resolving by SDS-PAGE and digesting the protein bands, samples were counted and the amount of prenylated product in pmol was determined using the specific activity (dpm/pmol) of tritium. The initial rate of farnesylation was determined from the amount of product formed divided by the incubation time, resulting in units of  $\mu$ M/s. The Michaelis-Menten equation (equation 1) was fit to the concentration dependence of the initial velocity ( $V/E$ ) to determine values of  $k_{cat}$  and  $K_M$  for FTase.

$$\frac{\text{Velocity}}{[\text{FTase}]} = \frac{k_{\text{cat}} \times [\text{substrate}]}{K_M + [\text{substrate}]} \quad \text{Equation 1}$$

### ***Transient kinetics***

Single turnover rate constants for FTase were determined as described in Chapter 2 using the radiolabel-prenylation assay (11). Reactions were carried out at 30°C in 50 mM HEPPSO, pH 7.8, 5 mM TCEP, 5 mM MgCl<sub>2</sub>, and 10 μM GDP. The reactions contained 750 nM FTase pre-incubated with 750 nM <sup>3</sup>H-FPP. Reactions initiated with the addition of substrate (2.5 μM Ras) were allowed to proceed for 30 - 60 min, depending on the Ras protein. Time points were taken by quenching the reaction at different time intervals by addition of 1X Laemmli sample buffer. The rate constant for product formation (*k*<sub>obs</sub>) was determined by fitting equation 2 to the time dependence of product formation (μM product/s), where P<sub>t</sub> is the product formed at time t, and P<sub>max</sub> is the reaction endpoint.

$$P_t = P_{\text{max}} \times (1 - e^{-k_{\text{obs}}t}) \quad \text{Equation 2}$$

### ***Binding assay***

Binding affinities were measured by biolayer interferometry (BLI) using a similar approach as in Chapter 2 (11) with the OctetRed96 instrument (Forte Bio). Assays were performed at 30°C in 96-well plates. Streptavidin (SA) biosensors were loaded with biotinylated SmgGDS-607 in 50 mM HEPES pH 7.8, 150 mM NaCl, 2 mM MgCl<sub>2</sub>, 20 – 30 μM GDP, 2 mM TCEP, and 0.25 mg/mL BSA. The loaded biosensors were washed in the same buffer before transferring the sensor tip to Ras protein solutions of various concentrations to carry out association measurements. Controls included a sensor probe without biotinylated SmgGDS-607 that was incubated in Ras protein solution and a sensor probe loaded with biotinylated SmgGDS-607 that was incubated only with buffer. Controls were subtracted from the binding data to correct for non-specific binding. The specific binding phase was fit to a single exponential (Equation 3) to determine the *k*<sub>obs</sub> at each concentration. R refers to the BLI response (nm), IR is the initial BLI response (nm), R<sub>eq</sub> represents the response at equilibrium or final BLI response, and t is the incubation time.

$$R = IR + (R_{\text{eq}} - IR) \times (1 - e^{-k_{\text{obs}}t}) \quad \text{Equation 3}$$

The dissociation constant,  $K_D$ , was determined by fitting the responses at equilibrium ( $R_{eq}$ ) for each Ras concentration to a binding isotherm (Equation 4), where  $K_D$  is the dissociation constant and  $X$  is the concentration of Ras. The data were fit using nonlinear regression in GraphPad Prism with the standard errors reported.

$$R_{eq} = \frac{R_{max}[X]}{K_D + [X]} \quad \text{Equation 4}$$

## RESULTS

### *The PBR sequence in Ras proteins enhances the steady-state kinetic parameters*

Previously, the steady-state parameter  $k_{cat}/K_M$  was measured for FTase with various peptide substrates that mimic the PBR and CAAX of the C-terminus in KRas4B (9), demonstrating that the addition of a PBR at the N-terminus (**KKKSKTKCVIM** versus **TKCVIM**) decreases the value of  $k_{cat}/K_M$  by ~6-fold and reduces the selectivity of FTase for catalyzing the farnesylation of a substrate containing a PBR. In contrast, a previous study performed with full-length Ras proteins demonstrated that KRas4B (ending in **KKKSKTKCVIM**) has the highest  $k_{cat}/K_M$  value compared to KRas4A (ending in **GCVKIKKCIIM**), NRas (ending in **QGCMGLPCVVM**), and HRas (ending in **PGCMSCKCVLS**) (7), suggesting that the PBR enhances selectivity. However, it is important to note that the CAAX sequences of the four Ras proteins vary, and these sequences could also contribute to the differences in  $k_{cat}/K_M$ . The contradicting results of the PBR influence on  $k_{cat}/K_M$  values for peptides compared to proteins call for a more controlled study to define the individual roles of the PBR and CAAX motifs in modulating prenylation.

**Table 3.2. Kinetic parameters for farnesylation of Ras proteins.**

Ras protein	$k_{cat}/K_M$ ( $\text{mM}^{-1} \text{s}^{-1}$ ) <sup>a</sup>	$k_{cat}$ ( $\text{s}^{-1}$ )	$K_M$ ( $\mu\text{M}$ )	$k_{obs}$ ( $\text{s}^{-1}$ )
KRas4B-PBR <sub>KRas4B</sub> -CVIM (WT)	17 ± 5	0.0117 ± 0.0008	0.7 ± 0.2	0.0107 ± 0.0004
KRas4B-HVR <sub>HRas</sub> -CVIM	0.3 ± 0.2	0.0008 ± 0.0005	3.0 ± 0.9	0.0014 ± 0.0002
KRas4B-PBR <sub>KRas4B</sub> -CVLS	5 ± 1	0.040 ± 0.005	8 ± 2	0.017 ± 0.002
HRas-HVR <sub>HRas</sub> -CVLS (WT)	0.07 ± 0.02	0.00016 ± 0.00001	2.2 ± 0.6	0.0021 ± 0.0002
HRas-PBR <sub>KRas4B</sub> -CVLS	11 ± 3	0.034 ± 0.003	3.2 ± 0.8	0.014 ± 0.004
HRas-HVR <sub>HRas</sub> -CVIM	0.9 ± 0.5	0.0044 ± 0.0005	5 ± 2	0.0026 ± 0.0004

<sup>a</sup>The errors in the  $k_{cat}/K_M$  values were calculated by error propagation (33).

To evaluate the individual and combined contributions of the PBR and/or the CAAX motif on substrate selectivity, the steady-state parameters  $k_{cat}$ ,  $K_M$ , and  $k_{cat}/K_M$  were measured using a radiolabel prenylation assay with a diverse set of full-length protein substrates that encompass wild type and chimeric Ras proteins (Table 3.2). The  $k_{cat}/K_M$  values were calculated from the dependence of the initial rate on the substrate concentration, as shown for wild-type KRas4B (Figure 3.1A). The specificity constant ( $k_{cat}/K_M$ ) is a useful metric to analyze enzymatic activity within a biological context, since comparing the relative rate for competing substrates indicates which substrate will be modified fastest (12). From our Ras chimeric substrates set, KRas4B exhibits the highest  $k_{cat}/K_M$  value of  $17 \pm 5 \text{ mM}^{-1}\text{s}^{-1}$ , which is comparable to the measured specificity constant

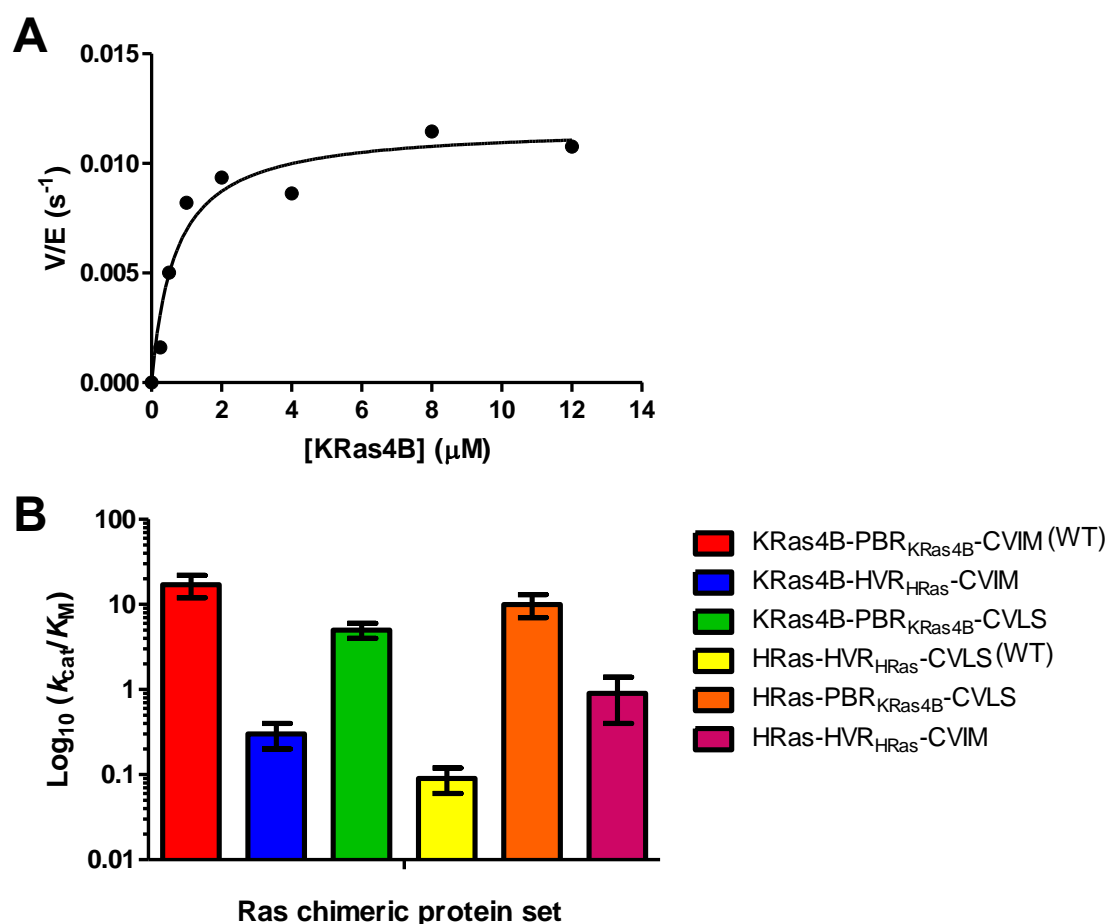


**Figure 3.1. Steady-state kinetics for FTase catalyzing prenylation of Ras substrates.** (A) Concentration dependence of farnesylation of KRas4B. Varied concentrations of KRas4B were incubated for 3 minutes with FTase (50 nM) and  $^3\text{H}$ -FPP (18  $\mu\text{M}$ ). Incorporation of radiolabeled farnesyl was measured as described in the methods. The Michaelis-Menten equation was fit to the data resulting in  $k_{cat} = 0.0117 \pm 0.0008 \text{ s}^{-1}$  and  $K_M = 0.7 \pm 0.2 \mu\text{M}$ . The data points are from single reactions at each KRas4B concentration. The results are representative of three independent experiment (B) Comparison of substrate specificity for FTase with various Ras substrates. The values of  $k_{cat}/K_M$ , measured as described in A, are listed in Table 3.2.

for the TKCVIM peptide with a  $k_{cat}/K_M$  value of  $16 \pm 2 \text{ mM}^{-1}\text{s}^{-1}$  (9). However, the **KKKSKTKCVIM** peptide ( $2.7 \pm 0.7 \text{ mM}^{-1}\text{s}^{-1}$ ) (9) exhibits a 6-fold lower value of  $k_{cat}/K_M$  than the full-length protein substrate, indicating that the additional three lysines from the endogenous hexalysine repeat in KRas4B contribute to this difference, possibly by altering the structure of the peptide substrate. The values of  $k_{cat}/K_M$  for the chimeric proteins vary by >200-fold, with KRas4B and HRas having the highest and lowest  $k_{cat}/K_M$  value, respectively. For KRas4B, the replacement of the PBR with the HVR from HRas renders the substrate less suitable for prenylation with a ~57-fold decrease in  $k_{cat}/K_M$ . Mutating the CAAX motif in KRas4B from CVIM to CVLS decreases  $k_{cat}/K_M$  less drastically by ~3-fold, suggesting that the PBR in KRas4B confers much of the specificity for FTase. On the other hand, replacing the HVR in the C-terminus in HRas with the KRas4B PBR sequence increases the value of  $k_{cat}/K_M$  by 157-fold, comparable to the value for WT KRas4B. In contrast, mutating the CAAX motif from CVLS to CVIM leads to a 10-fold increase. These results indicate that both the PBR and the CAAX sequences dictate specificity. Additionally, with or without a PBR, FTase catalyzes prenylation more rapidly with substrates ending in CVIM over CVLS, which contradicts the modestly increased value of  $k_{cat}/K_M$  observed with peptides ending in CVLS compared to CVIM (13). Nonetheless, KRas4B-PBR<sub>KRas4B</sub>-CVIM (WT), HRas-PBR<sub>KRas4B</sub>-CVLS, and KRas4B-

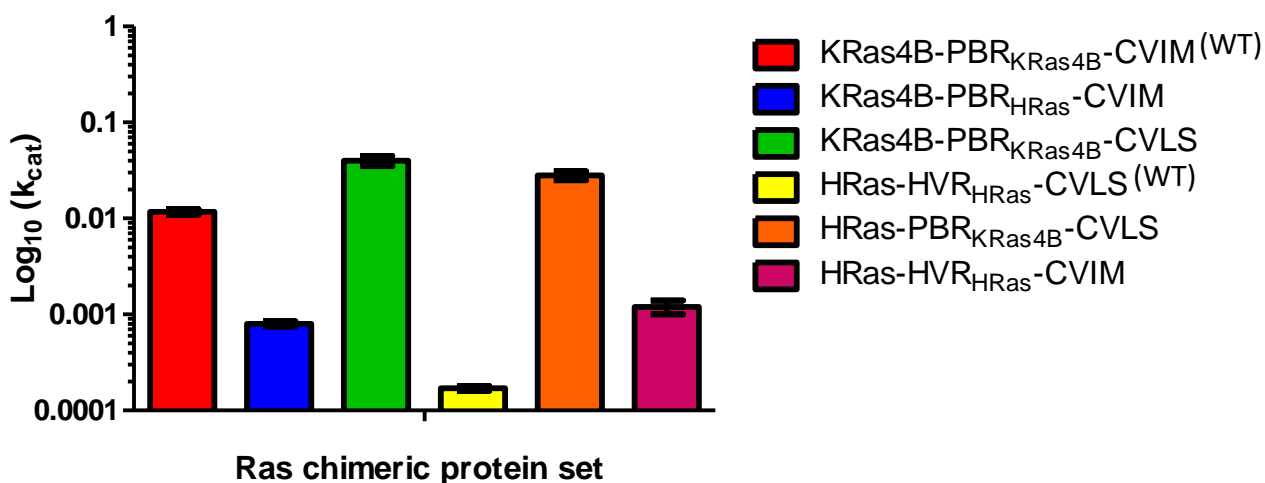


**Figure 3.2. Comparison of the turnover constant  $k_{cat}$  for FTase-catalyzed prenylation of various Ras substrates.** The  $k_{cat}$  values were determined for all Ras substrates using the radiolabel prenylation assay as described in the Experimental Methods and are listed in Table 3.2.

PBR<sub>KRas4B</sub>-CVLS are the best substrates from the set, indicating that the PBR plays an important role in enhancing prenylation (Figure 3.1B). Substrates containing a PBR have  $k_{cat}/K_M$  values above  $5 \text{ mM}^{-1}\text{s}^{-1}$ , while substrates lacking a recognized PBR have  $k_{cat}/K_M$  values in the range of  $0.07\text{-}0.9 \text{ mM}^{-1}\text{s}^{-1}$  (Table 3.2). These data support previous observations with full-length Ras substrates – FTase is most selective for catalyzing prenylation of Ras substrates containing a PBR.

For FTase catalyzing farnesylation of peptide substrates, the rate-determining step for FTase turnover,  $k_{cat}$ , is product dissociation (14, 15). The value of  $k_{cat}$  for farnesylation of small GTPases is equal to or smaller than the rate constant for product dissociation, providing insight into the role of the PBR sequence. The  $k_{cat}$  values vary by >200-fold; product release is faster for KRas4B-PBR<sub>KRas4B</sub>-CVIM (WT), KRas4B-PBR<sub>KRas4B</sub>-CVLS and HRas-PBR<sub>KRas4B</sub>-CVLS ( $k_{cat} > 0.01 \text{ s}^{-1}$ ), and slower for KRas4B-HVR<sub>HRas</sub>-CVIM, HRas-HVR<sub>HRas</sub>-CVLS (WT), and HRas-HVR<sub>HRas</sub>-CVIM ( $k_{cat} < 0.005 \text{ s}^{-1}$ ) (Table 3.2, Figure 3.2). The substrates tested in this study can be divided into two classes: [1] those that contain a PBR where product release is faster and [2] those that do not contain a PBR where product release is slower, suggesting that the PBR sequence enhances product release. Interestingly, within the substrates that contain a PBR,  $k_{cat}$  is faster when the C-terminus ends in CVLS. A similar trend was observed in a previous study with GCVXX peptides, where the  $k_{cat}$  for GCVLS ( $0.40 \pm 0.08 \text{ s}^{-1}$ ) is 8-fold faster than for GCVIM ( $0.05 \pm 0.01 \text{ s}^{-1}$ ), albeit no PBR is present in these peptide substrates (18). Addition of a PBR to HRas (HRas-PBR<sub>KRas4B</sub>-CVLS) leads to a >200-fold enhancement in  $k_{cat}$ , while mutating CVLS to CVIM (HRas-HVR<sub>HRas</sub>-CVIM) in HRas increases  $k_{cat}$  by ~26-fold. Similarly, removing the PBR in KRas4B (KRas4B-HVR<sub>HRas</sub>-CVIM) leads to a ~15-fold decrease in the turnover rate. These data indicate that the presence of a PBR sequence enhances the rate of product dissociation from FTase; the value of  $k_{cat}$  is higher for proteins that contain a PBR sequence. Furthermore, both the PBR and the CAAX sequences dictate the value of  $k_{cat}$  and by inference, the rate of product dissociation.

### ***PBR sequences enhance the transient kinetics catalyzed by FTase***

To further understand the role of the PBR on catalysis and to evaluate the rate-limiting step in  $k_{cat}$ , the rate constants for farnesylation of Ras chimeric substrates were measured

under single turnover conditions. A single exponential equation was fit to the reaction progress curves to generate the observed rate constants,  $k_{obs}$ , as represented in Figure 3.3A. Interestingly, the lack of a PBR in KRas4B causes a significant decrease in the farnesylation rate constant,  $k_{obs}$ , by ~8-fold (Table 3.2), while the mutation of the CAAX from CVIM to CVLS causes a modest increase by 1.6-fold (Figure 3.3B). A similar trend is observed in HRas. The presence of a PBR in the C-terminus of HRas causes a 6.5-fold increase in  $k_{obs}$ , while the  $k_{obs}$  for HRas-HVR<sub>HRas</sub>-CVIM is similar to wild-type HRas. Substrates lacking a PBR exhibit slower prenylation rate constants ( $<0.003 \text{ s}^{-1}$ , Table 3.2), demonstrating that the PBR sequence also enhances the observed rate constant for farnesylation.

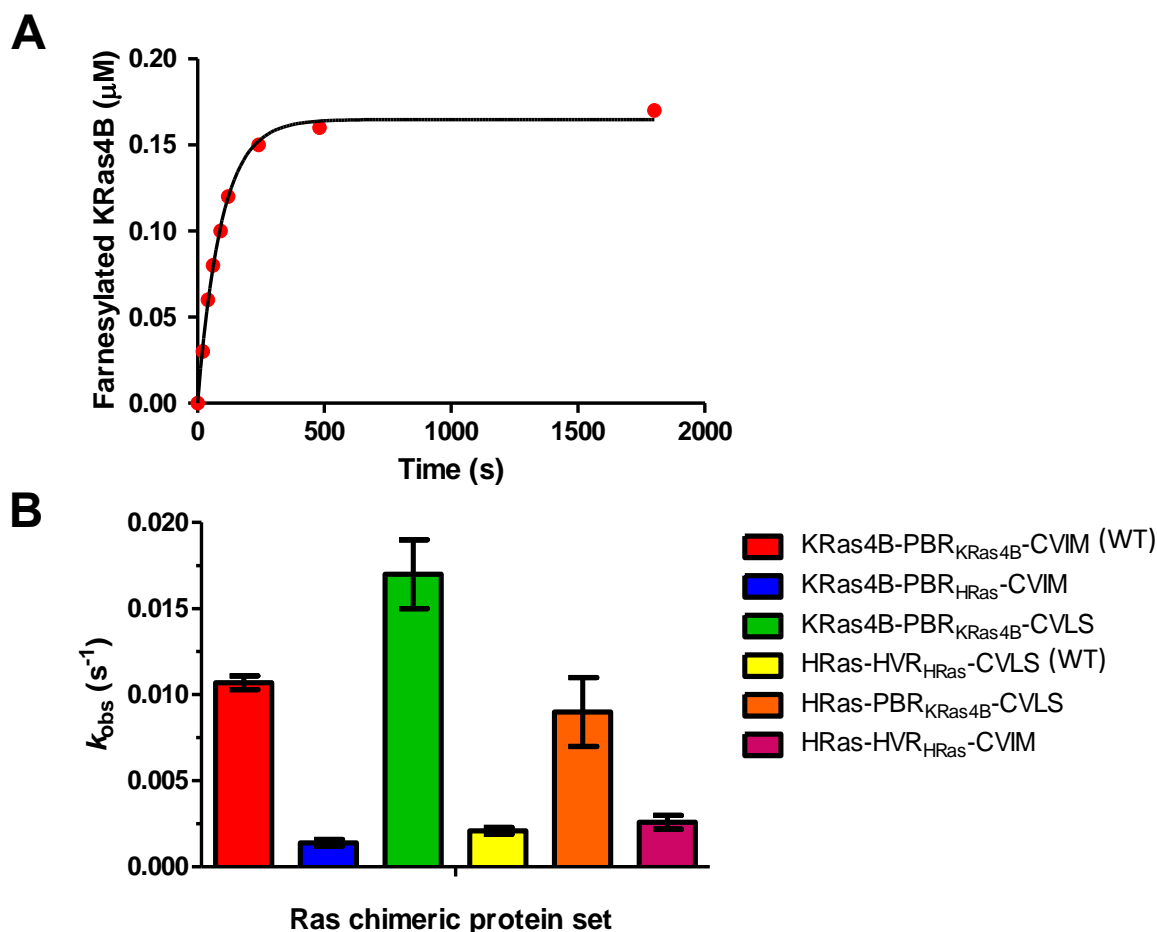


**Figure 3.3. Single-turnover rate for farnesylation of Ras substrates.** (A) Representative single turnover kinetics for FTase farnesylation of KRas4B. Under these conditions, FTase (500 nM) reacts with 2.5  $\mu\text{M}$  KRas4B, 25  $\mu\text{M}$  GDP, and limiting  $^3\text{H-FPP}$  (250 nM). The farnesylation rate constant  $k_{obs}$  was calculated by a fit of equation 2 to the data as  $0.0107 \pm 0.0004 \text{ s}^{-1}$ . (B) Comparison of single turnover rate constant for various Ras substrates.

For peptide substrates, the farnesylation step ( $k_{\text{obs}}$ ) is frequently faster than product dissociation (32). This is also true for wild-type HRas (HRas-HVR<sub>HRas</sub>-CVLS) where the value of  $k_{\text{obs}}$  is 13-fold faster than  $k_{\text{cat}}$ . Similarly, for KRas4B-HVR<sub>HRas</sub>-CVIM the single turnover rate constant is faster than  $k_{\text{cat}}$ , suggesting that product release is the rate-limiting step in steady-state turnover. Unexpectedly, the  $k_{\text{obs}}$  and  $k_{\text{cat}}$  values for WT KRas (KRas4B-PBR<sub>KRas4B</sub>-CVIM) are comparable, indicating that farnesylation is the rate-limiting step. These data indicate that the effect of the PBR on enhancing the product dissociation rate is significantly larger than the increase in the value of  $k_{\text{cat}}$ . For comparison, a peptide substrate (dns-KKKS<sub>TKCVIM</sub>) comparable to the C-terminus of KRas has rate constants that are faster than the full-length protein ( $k_{\text{obs}} = 1.1 \pm 0.1 \text{ s}^{-1}$  and  $k_{\text{cat}} = 0.052 \pm 0.008 \text{ s}^{-1}$ ) and product dissociation is rate-limiting (9). Interestingly, for KRas4B-HVR<sub>HRas</sub>-CVIM and HRas-HVR<sub>HRas</sub>-CVIM the value of  $k_{\text{obs}}$  is within a factor of 2 of  $k_{\text{cat}}$  (Table 3.2), suggesting that product dissociation is faster for substrates ending in CVIM compared to CVLS and product release is not the main rate-limiting step for turnover. Curiously, for the KRas-PBR<sub>KRas4B</sub>-CVLS and HRas-PBR<sub>KRas4B</sub>-CVLS mutants, the  $k_{\text{cat}}$  value is ~2-fold faster than the single turnover rate constant. This cannot be true if the kinetic mechanisms are the same under the two conditions thereby suggesting some modest alteration in the mechanism between single and multiple turnover conditions.

### ***Charge distribution in the PBR affects FTase kinetics***

So far, most studies conducted to understand the role of the PBR sequence in Ras activity and FTase activity has been solely focused on the “classic” sequence of an upstream PBR described by KRas4B (Table 3.1) (1, 7-9). However, there is no consensus sequence for a PBR, as some Ras family members contain stretches of positively charged amino acids (KRas4B, Rap1A, Rap1B, RalA), while others contain spaced residues (KRas4A, DiRas1, DiRas2, DiRas3, RalB). To ascertain the effect of a PBR with dispersed charge distribution in regulating prenylation, we examined the activity of FTase toward DiRas1 and DiRas2, Ras-like proteins belonging to a distinct subgroup of the Ras family. Both proteins contain a number (7 to 8) of positively charged residues in their PBR sequences similar to KRas4B, yet the distribution of charge is dispersed throughout the

polybasic tail (Table 3.1). Additionally, both proteins end with a methionine in their CAAX motif, and DiRas2 shares the CVIM sequence found in KRas4B.

**Table 3.3. Kinetics parameters for farnesylation of DiRas proteins.**

Ras protein	$k_{cat}/K_M$ ( $\text{mM}^{-1} \text{s}^{-1}$ ) <sup>a</sup>	$k_{cat}$ ( $\text{s}^{-1}$ )	$K_M$ ( $\mu\text{M}$ )	$k_{obs}$ ( $\text{s}^{-1}$ )
DiRas1	$19 \pm 7$	$0.0075 \pm 0.0006$	$0.4 \pm 0.2$	$0.039 \pm 0.008$
DiRas2	$14 \pm 7$	$0.013 \pm 0.002$	$0.9 \pm 0.4$	$0.05 \pm 0.01$

<sup>a</sup>The errors in the  $k_{cat}/K_M$  values were calculated by error propagation (33).

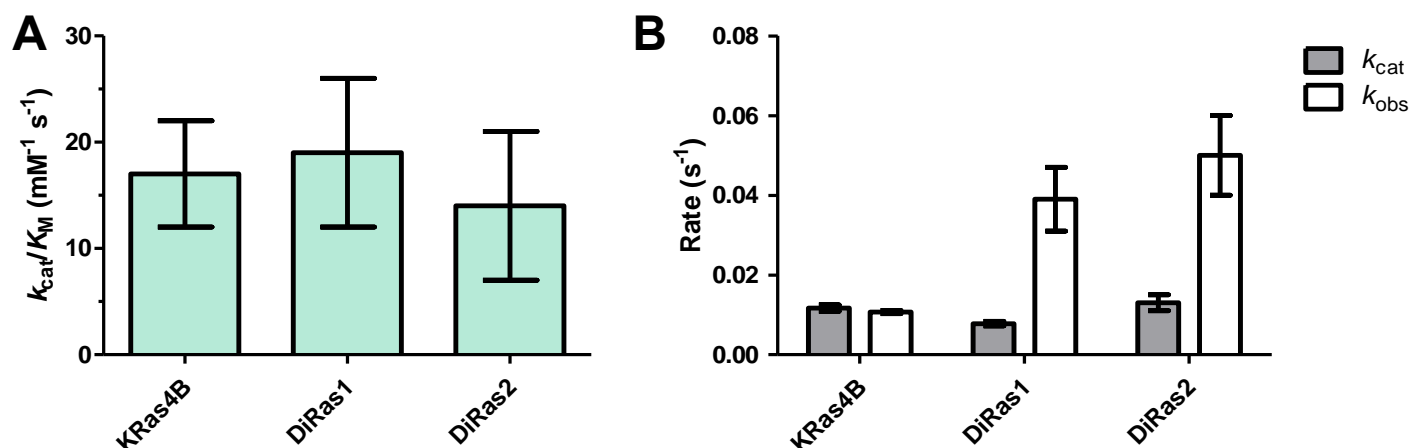


**Figure 3.4. Comparison of steady-state and single-turnover kinetic parameters of FTase-catalyzed prenylation of KRas4B and DiRas proteins.** (A) Comparison of substrate specificity for FTase with KRas4B and DiRas proteins. The values of  $k_{cat}/K_M$ , measured as described in the experimental procedures, are listed in Table 3.3. (B) Comparison between  $k_{cat}$  and the single-turnover rate constant ( $k_{obs}$ ) values for KRas4B and DiRas proteins.

Interestingly, DiRas1 and DiRas2 exhibit similar  $k_{cat}/K_M$  values of  $19 \pm 7 \text{ mM}^{-1}\text{s}^{-1}$  and  $14 \pm 7 \text{ mM}^{-1}\text{s}^{-1}$  (Table 3.3), respectively, although their PBR and CAAX sequences differ from one another. Additionally, their  $k_{cat}/K_M$  values are comparable to that of KRas4B (Figure 3.4A), suggesting that having a PBR and a C-terminal methionine is sufficient for high specificity. Moreover, the specificity constant for full length DiRas1 is 17-fold higher than the measured specificity constant for the TKCTLM peptide ( $1.1 \pm 0.3 \text{ mM}^{-1}\text{s}^{-1}$ ) (16), supporting the prediction that the PBR enhances selectivity. The  $k_{cat}$  values for DiRas1 and DiRas2 are  $0.0075 \pm 0.0006 \text{ s}^{-1}$  and  $0.013 \pm 0.002 \text{ s}^{-1}$ , respectively (Table 3.3). Furthermore, the  $k_{cat}$  values for DiRas2 and KRas4B are comparable, demonstrating that the distribution of charge in the PBR does not alter the rate of product release when the PBR is followed by a CVIM sequence. DiRas1 and DiRas2 exhibit single turnover rates that are comparable (Table 3.3), but faster than values measured for other proteins (Table 3.2). These data suggest that dispersed arginine and lysine residues are optimal for

enhancing the farnesylation reaction. However, in contrast to KRas4B, the  $k_{obs}$  values for both DiRas1 and DiRas2 are faster than  $k_{cat}$  (Figure 3.4B), suggesting that product release is rate-limiting for turnover. Furthermore, the difference in rate-limiting step between KRas4B and DiRas proteins suggests that the concentrated charge in the KRas4B C-tail has a larger effect on product dissociation than the dispersed charge in DiRas proteins.

### ***Synergies between CAAX and PBR dictate binding affinities of Ras substrates for SmgGDS-607***

In Chapter 2, it was established that SmgGDS-607 binds DiRas1 >300-fold tighter than KRas4B (11), although both end in methionine and contain a PBR. These data suggest that the sequence identity of both the PBR and CAAX affect the affinity with SmgGDS-607. To further investigate the effects of the PBR and the importance of sequence identity in modulating the interaction of Ras with SmgGDS-607, we measured the affinities of SmgGDS-607 for the Ras chimeras using bio-layer interferometry (BLI, OctetRed96) with biotinylated SmgGDS-607 and varying concentrations of Ras (26). From our set of Ras proteins, DiRas1 binds SmgGDS-607 with the highest affinity, as previously seen in Chapter 2 (Table 3.4) (11). Interestingly, although both DiRas proteins contain dispersed polybasic residues in their PBR and end in methionine, the affinity of DiRas2 for SmgGDS-607 is 10-fold weaker than DiRas1, suggesting that other factors contribute to binding, such as sequence identity of the protein body. Similarly, although both end in CVIM, DiRas2 binds to SmgGDS-607 30-fold tighter than KRas4B, suggesting that the dispersed charge in the PBR and/or the body sequence identity of DiRas2 enhances binding.

**Table 3.4. Binding affinity of SmgGDS-607 for Ras proteins.**

<b>Ras protein</b>	<b><math>K_D</math> (<math>\mu</math>M)</b>
DiRas1	0.005 $\pm$ 0.001
DiRas2	0.05 $\pm$ 0.02
KRas4B-PBR <sub>KRas4B</sub> CVIM	1.5 $\pm$ 0.4
KRas4B-HVR <sub>HRas</sub> -CVIM	8 $\pm$ 2
KRas4B-PBR <sub>KRas4B</sub> CVLS	14 $\pm$ 5
HRas-HVR <sub>HRas</sub> -CVLS	>9
HRas-PBR <sub>KRas4B</sub> -CVLS	14 $\pm$ 5
HRas-HVR <sub>HRas</sub> -CVIM	>12

In Chapter 2, we also established that the binding affinity for SmgGDS-607 and HRas is weaker than for KRas4B and DiRas1. We hypothesized that this weaker binding is due to the lack of a PBR in HRas. Therefore, we predicted that the Ras chimeric proteins that lack a PBR will exhibit binding affinities similar to HRas, while the Ras chimeric proteins that contain the KRas4B PBR sequence will exhibit binding affinities similar to KRas4B. As expected, the dissociation constant for KRas4B-HVR<sub>HRas</sub>-CVIM is comparable to that of HRas with a  $K_D$  value of  $8 \pm 2 \mu\text{M}$ , while HRas-HVR<sub>HRas</sub>-CVIM exhibits a  $K_D$  of  $>12 \mu\text{M}$  (Table 3.4). Conversely, both KRas4B-PBR<sub>KRas4B</sub>-CVLS and HRas-PBR<sub>KRas4B</sub>-CVLS exhibit similar  $K_D$  values at  $14 \pm 5 \mu\text{M}$ , which is ~9-fold weaker than KRas4B. This result demonstrates that the combination of a polylysine sequence in the PBR and -CVLS decreases the affinity for SmgGDS-607. In all, our binding studies support the hypothesis that the PBR promotes direct interaction of small GTPases with SmgGDS-607 and that a dispersed charge sequence, as observed in DiRas, enhances this interaction.

### ***PBR in Ras influences SmgGDS-607-mediated regulation***

In Chapter 2, we established the differential effects of SmgGDS-607 on KRas4B, DiRas1 and HRas farnesylation (11). For substrates containing a PBR, the levels of SmgGDS-607-mediated inhibition of farnesylation depend on which protein, FTase or SmgGDS-607, has the highest affinity for the substrate. For KRas4B, SmgGDS-607 minimally inhibits farnesylation due to KRas4B binding to FTase 700-fold tighter than to SmgGDS-607. For DiRas1, SmgGDS-607 drastically inhibits farnesylation due to SmgGDS-607 binding DiRas1 ~9-fold tighter than FTase. Interestingly, for HRas, a substrate lacking a PBR, SmgGDS-607 enhances farnesylation. To further understand the role of the PBR in SmgGDS-607-mediated regulation of Ras prenylation, we used a radiolabel competition assay to assess the effects of SmgGDS-607 on the levels of farnesylation of the Ras chimeras. The amount of farnesylated Ras chimeras formed by incubation with FTase and FPP was measured with and without  $6 \mu\text{M}$  SmgGDS-607 (Figure 3.5A). Based on our previous data in Chapter 2 and our binding data with the Ras chimeras, we predicted that for the chimeras containing the KRas4B PBR sequence

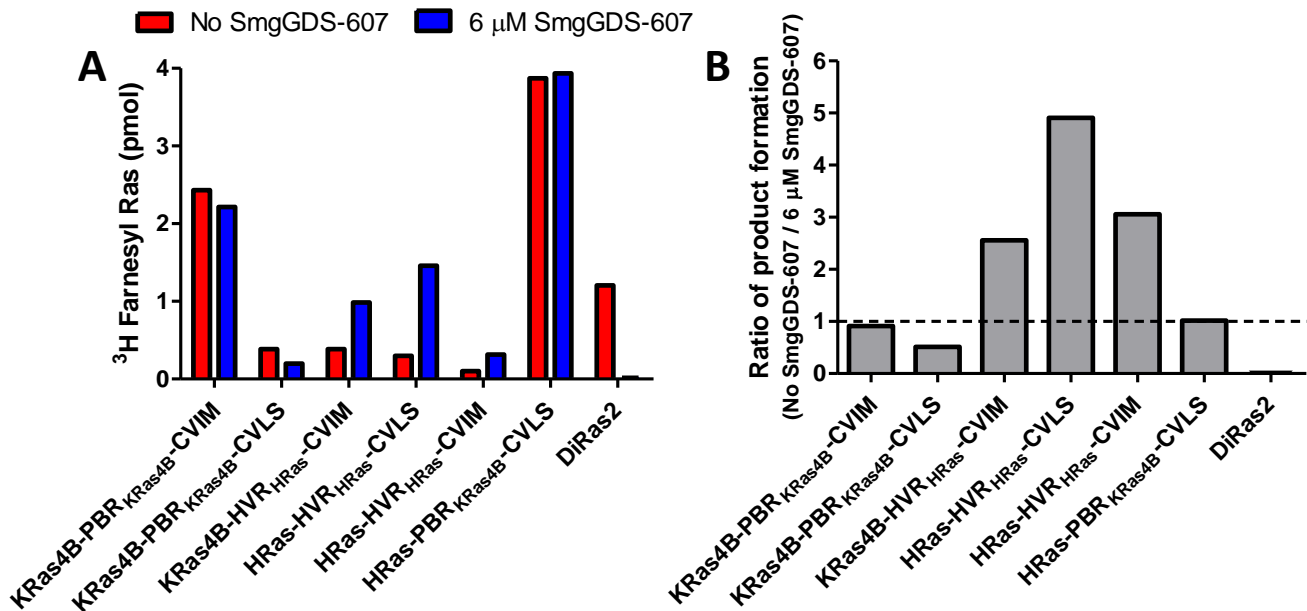


**Figure 3.5. SmgGDS-607 exhibits differential effects on farnesylation of Ras substrates.** (A) SmgGDS-607 enhances the extent of farnesylation of substrates lacking a PBR, while inhibiting or having no effect on substrates containing a PBR. The SmgGDS-607 concentration used is below saturating conditions for all substrates except KRas4B-PBR<sub>KRas4B</sub>-CVIM and DiRas2. (B) The ratios of product formation for different Ras substrates comparing conditions with no SmgGDS-607 and 6 μM SmgGDS-607.

farnesylation would not be inhibited by SmgGDS-607, while for those containing the HRas HVR sequence farnesylation would be enhanced.

As predicted, farnesylation of 2.5 μM HRas-PBR<sub>KRas4B</sub>-CVLS was not inhibited by addition of 6 μM SmgGDS-607 (Figure 3.5). Interestingly, the levels of farnesyl incorporation are higher for HRas-PBR<sub>KRas4B</sub>-CVLS than for wild-type KRas4B. However, the presence of 6 μM SmgGDS-607 leads to inhibition of KRas4B-PBR<sub>KRas4B</sub>-CVLS farnesylation by ~2-fold. In contrast, farnesylation of KRas4B-HVR<sub>HRas</sub>-CVIM and HRas-HVR<sub>HRas</sub>-CVIM was *enhanced* by 2.6-fold and 3-fold, respectively, in the presence of SmgGDS-607 (Figure 3.5B), demonstrating that the HVR sequence from HRas determines enhancement of farnesylation. Therefore, the PBR sequence influences whether farnesylation will be inhibited or enhanced. To determine whether this trend extends to PBRs containing dispersed charge, we tested the effect of SmgGDS-607 on farnesylation of DiRas proteins. As previously observed in Chapter 2, DiRas1 exhibits 8.5-fold difference in binding affinity between SmgGDS-607 and FTase, favoring interaction with SmgGDS-607. Our data shows that 6 μM SmgGDS-607 leads to complete inhibition of farnesylation of DiRas2 catalyzed by FTase, suggesting that similar to

DiRas1, DiRas2 has higher affinity for SmgGDS-607 than FTase and that this behavior might be due to the dispersed charge in the PBR sequence.

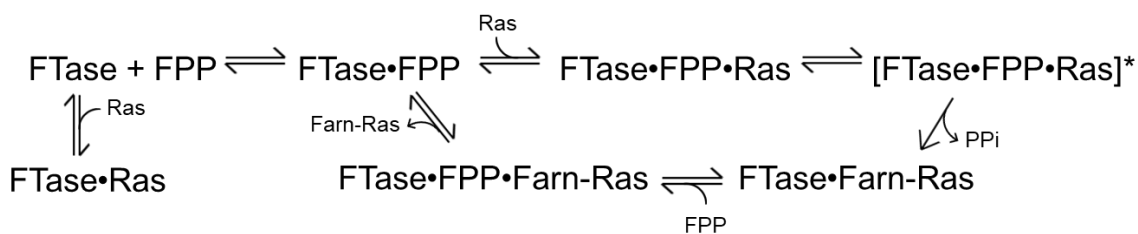
## DISCUSSION

The C-terminal hypervariable region (HVR) sequence plays a critical role in the correct membrane localization of the different Ras isoforms within the cell (2,3,17,34). Membrane localization of these proteins is dynamic and influenced by different factors, such as GDP/GTP status, interacting proteins, and post-translational modifications. Constitutive association with membranes is made possible by farnesylation and palmitoylation of Ras GTPases (17). Our data demonstrate that the polybasic residues in the HVR of Ras and DiRas proteins contribute significantly to the regulation of farnesylation by SmgGDS. Previously, a study with Ras chimeras demonstrated that a lower concentration of wild-type KRas4B is required to reach maximal FTase activity, suggesting that this effect is due to the presence of the polylysine sequence in the PBR and the C-terminal CVIM sequence (8). In our work we expand upon these data to demonstrate that the PBR sequence regulates prenylation of Ras isoforms by both influencing farnesylation kinetics and interactions with the chaperone protein SmgGDS-607.

Our results demonstrate that interaction with the PBR sequence aids product release for the FTase•Ras-farnesyl complex, as demonstrated with the KRas4B and HRas chimeras. However, the extent of product release mediation is synergistically dependent on both the PBR and the CAAX motif sequences. Interestingly, our data shows that the  $k_{cat}$  and the single-turnover rate constant ( $k_{obs}$ ) values for KRas4B are similar, suggesting that farnesylation or a prior step is the rate-limiting step for turnover of this substrate. In contrast, a previous study demonstrated that product release is the rate-limiting step for the corresponding KKKS~~TK~~CVIM peptide, based on a 10-fold increase in the farnesylation rate constant ( $k_{obs}$ ) for the peptide substrate (9) and an apparent increase in the dissociation rate constant for the KRas4B substrate ( $k_{dissociation} > k_{cat}$ ). Based on the crystal structure of KKKS~~TK~~CVIM bound to FTase, the residues S4K5T6K7 form a type I  $\beta$  turn to properly accommodate the lysine residues within the hydrophobic cavity of the FTase active site, allowing Lys5 and Lys7 to make favorable interactions with Asp359

and Glu161, respectively, in FTase (5). For full-length KRas4B, this C-terminal amino acid sequence is attached to a globular body that may both interact with the FTase interface and constrain mobility of the C-terminus. Kinetic studies with peptide substrates indicate that there is a conformational change prior to farnesylation (5,14,31). For KRas4B, the presence of the body may lead to a spatial orientation of the C-terminal tail that is favorable for interactions with the polylysine residues but that consequently leads to a less optimal configuration of reactants for catalysis. Likewise, it is possible that the equilibrium with peptide substrates favors the reactive structural conformation, but with protein, it favors an unreactive conformation. This would lead to a decrease in the apparent farnesylation rate constant. Nonetheless, although a step at or before catalysis is rate-limiting in the KRas4B farnesylation reaction, the PBR aids in product release as indicated by a decrease in  $k_{cat}$  and a shift of the rate-limiting step to product release upon substitution of the HVR sequence from HRas.

Surprisingly, three of the Ras chimeras exhibit  $k_{cat}$  values that are faster than the single-turnover values. In our single-turnover experiments, the concentration of substrate used was above the  $K_M$ , allowing for favorable conditions for E•S complex formation. Yet, with FTase, other variables come into play that allow for a reactive E•S complex formation, such as the FPP concentration. In a previous kinetic study, it was determined that the E•FPP complex enhances affinity for FTase with HRas and KRas4B (31). Therefore, the reactive FPP molecule also plays a part in modulating the rate of Ras farnesylation. Additionally, for HRas-PBR<sub>KRas4B</sub>-CVLS, HRas-HVR<sub>HRas</sub>-CVIM, and KRas4B-PBR<sub>KRas4B</sub>-CVLS, substrate inhibition could explain why we observe slower single-turnover rate values. Under multiple-turnover conditions, the FPP concentration is 400-fold higher than FTase concentration, pushing the reaction to proceed via the



favourable FTase•FPP•Ras pathway. However, our data suggest that under single-

Figure 3.6. Kinetic Pathway for the FTase-catalyzed prenylation of Ras substrates.

turnover conditions, the rate of E•FPP formation becomes the rate-limiting step of the reaction and the excess Ras concentration results in the formation of the E•Ras complex, depleting the amount of free FTase that is available for reacting with FPP (Figure 3.6). Hence, the rate-limiting steps of the Ras chimeras farnesylation reaction under multiple- and single-turnover conditions may differ. However, the observed effect is modest (<3-fold) and does not alter the overall conclusion that the PBR enhances product release. As mentioned above, certain positively charged residues in the C-terminus of KRas4B make favorable electrostatic interactions with negatively charged residues in FTase for binding in the active site (5), and this might be true for other PBR-containing substrates. However, enzymes not only require a conformational fit upon substrate binding, but dynamic structural changes occur to drive catalysis and product release. For FTase, it has been demonstrated that an additional FPP molecule needs to bind after catalysis to enhance dissociation of prenylated peptide (Figure 3.6) (35). With PBR-containing substrates, the conformation of the FTase:product complex could favor the binding of a new FPP molecule that aids in release of product, while for substrates without a PBR, this conformation might not be favored.

In recent years, kinetic studies performed to understand FTase substrate selectivity and catalysis have been done using peptides as surrogates for full-length protein substrates. Some advantages to this approach are faster throughput and the ability to measure a wider range of substrates. However, one of the biggest limitations to this approach is the lack of distal protein interactions that could contribute to effective binding between the enzyme and multiple substrates, which impact the enzyme kinetics, as our data suggest. A comparison of our DiRas1 data with a previous peptide study done with TKCTLM peptide (16) demonstrates comparable rates for turnover ( $k_{cat}$ ) for the peptide and protein. However, higher concentrations of peptide are required to reach maximal activity, as observed from a 16-fold higher  $K_M$  value. Consequently, the substrate selectivity ( $k_{cat}/K_M$ ) for the peptide is 18-fold lower than for protein. Given that our data demonstrate that the PBR sequence plays a role throughout the farnesylation reaction in both catalysis and product release, the absence of the PBR in the TKCTLM peptide substrate might contribute to the differences observed. In contrast, with particular CAAX sequences, the absence of an upstream sequence can lead to kinetic advantages. For

example, catalysis of HRas turnover ( $k_{cat}$ ) is 2,500-fold slower than for the GCVLS peptide while the value of  $K_M$  is unaltered (13), leading to ~2,500-fold increase in substrate selectivity ( $k_{cat}/K_M$ ) for the peptide. In comparison with HRas-PBR<sub>KRas4B</sub>-CVLS, GCVLS peptide turnover is ~12-fold faster, while the value of  $K_M$  is modestly lower, leading to ~15-fold increase in  $k_{cat}/K_M$  for the peptide. In cells, the differences in substrate selectivity and kinetics for farnesylation between Ras GTPase isoforms might contribute to the different membrane trafficking pathways observed for these GTPases. The farnesyl group is not the only modification that promotes interaction of Ras with membranes. An adjacent set of motifs that vary among Ras isoforms is also needed for proper localization, such as di-palmitoylation of cysteines in HRas or the hexalysine PBR found in KRas4B. Nonetheless, our data demonstrate that synergies between the HVR and the CAAX motif contribute to regulation of the initial step in the membrane trafficking pathway.

The SmgGDS interaction with small GTPases has been presumed to be selective for proteins that contain a PBR. This claim was supported by studies demonstrating that SmgGDS proteins pulldown with RhoA family members and multiple Ras family members, such as KRas4B, Rap1A, Rap1B, and Rac1 (6,11,18-24). The ability of SmgGDS proteins to interact with a number of small GTPases that contain PBRs suggests that this structural feature enhances the affinity of these proteins with SmgGDS. However, SmgGDS proteins are proposed to carry out multiple roles within the cell, such as regulation of prenylation by sequestering proteins from the prenyltransferases (11, 18), stimulation of GDP release via guanine exchange factor (GEF) activity (20), and protection of cancer cells from nucleolar stress (25). In Chapter 2, we demonstrated that SmgGDS-607 can enhance prenylation of HRas and suggested that this functional role might be limited to substrates that lack a PBR sequence. These data also suggested that enhancement occurs via the formation of a ternary complex, FTase•HRas•SmgGDS-607. This mode of binding allows other interactions to compensate for the loss of favorable binding interactions between SmgGDS-607 and GTPases lacking a PBR. Our binding studies with the Ras chimeric proteins demonstrate that SmgGDS-607 has higher affinity for proteins containing a PBR sequence. However, this interaction has sequence selectivity, since SmgGDS-607 exhibits a stronger affinity for substrates that contain dispersed positive residues in the PBR. Furthermore, the sequence of the CAAX

sequence also alters the degree of affinity for SmgGDS-607, as observed with the Ras chimeric proteins.

The overall sequence of the C-terminus in small GTPases not only affects the direct contact with SmgGDS-607, but it also affects intramolecular interactions within the GTPase. These interactions may explain differences in the farnesylation kinetics between peptides and proteins. A structural study demonstrated that the PBR of KRas4B interacts with the catalytic domain in the KRas4B body when GDP is bound, preferentially interacting with the effector binding site of the protein and making it unavailable for protein-protein interactions (26). Consistent with this, the interaction of calmodulin with the PBR of KRas4B is inhibited upon GDP binding, confirming this PBR sequestration model (27). The >30-fold difference in binding affinities observed in our study between DiRas proteins and KRas4B for SmgGDS-607 could be explained by this PBR sequestration model, in which the PBR of KRas4B, but not DiRas, is not readily accessible for interaction with the electronegative patch in the SmgGDS-607 structure. In contrast, although the HVR affects backbone dynamics of the catalytic domain, HRas has not been observed to exhibit HVR sequestration, possibly due to the lack of polylysine residues (28). Therefore, the PBR sequestration model might be specific to KRas4B. Nonetheless, the lack of a PBR sequence leads to weak binding affinities for SmgGDS-607, as observed with HRas and Ras chimeric mutants.

In Chapter 2 we demonstrated that the relative affinities between FTase and SmgGDS-607 for DiRas and Ras proteins dictate regulation of farnesylation. Furthermore, we discovered a novel role for SmgGDS-607 in enhancing farnesylation of HRas. Our studies with Ras chimeric mutants confirm that the lack of a PBR sequence leads to SmgGDS-607-mediated enhancement of farnesylation. In contrast, SmgGDS-607 does not affect the levels of farnesylation for KRas4B and HRas-PBR<sub>KRas4B</sub>-CVLS presumably because these proteins have higher affinity for FTase than for SmgGDS-607 under our experimental conditions. However, SmgGDS-607 completely obstructs farnesylation of DiRas proteins, consistent with the high affinity observed between these proteins (11, 29-30). Our findings validate the role of SmgGDS-607 in regulating prenylation of FTase substrates and demonstrate that this regulation is modulated by the

PBR and CAAX motifs of the substrates, which affects affinity for both SmgGDS-607 and FTase. Furthermore, in a cellular context, small GTPases compete for binding to FTase and SmgGDS-607 depending on concentration and thermodynamic and kinetic forces, contributing to the complexity of this regulation. The complexity of the protein-protein interactions in the Ras membrane trafficking pathway allows for a greater regulation of this process and additional steps that can be altered to block the delivery of oncogenic Ras to membranes. Hence, understanding the intricacies in the molecular factors that dictate regulation of Ras prenylation sheds light into possible avenues that can be investigated to target Ras for novel therapeutics.

## REFERENCES

1. Jackson, J.H., Li, J.W., Buss, J.E., Der, C.J., Cochrane, C.G. (1994) Polylysine domain of K-ras 4B protein is crucial for malignant transformation. *Proc. Natl. Acad. Sci. USA* **91**, 12730–12734
2. Hancock, J.F., Paterson, H., Marshall, C.J. (1990) A polybasic domain or palmitoylation is required in addition to the CAAX motif to localize p21ras to the plasma membrane. *Cell* **63**, 133–139
3. Hancock, J.F., Cadwallader, K., Paterson, H., Marshall, C.J. (1991) A CAAX or a CAAL motif and a second signal are sufficient for plasma membrane targeting of ras proteins. *EMBO J.* **10**, 4033–4039
4. Chen, Z., Otto, J.C., Bergo, M.O., Young, S.G., Casey, P.J. (2000) The C-terminal polylysine region and methylation of K-Ras are critical for the interaction between K-Ras and microtubules. *J. Biol. Chem.* **270**, 41251–41257
5. Long, S.B., Casey, P.J., Beese, L.S. (2000) The basis for K-Ras4B binding specificity to protein farnesyltransferase revealed by 2 Å resolution ternary complex structures. *Structure* **8**, 209–222
6. Vikis, H.G., Stewart, S., Guan, K.L. (2002) SmgGDS displays differential binding and exchange activity towards different Ras isoforms. *Oncogene* **21**, 2425–2432
7. Zhang, F.L., Kirschmeier, P., Carr, D., James, L., Bond, R.W., Wang, L., Patton, R., Windsor, W.T., Syto, R., Zhang, R., Bishop, W.R. (1997) Characterization of Ha-Ras, N-Ras, Ki-Ras4A, and Ki-Ras4B as in vitro substrates for farnesyl protein transferase and geranylgeranyl protein transferase type I. *J. Biol. Chem.* **272**, 10232–10239
8. James, G.L., Goldstein, J.L., Brown, M.S. (1995) Polylysine and CVIM sequence of K-RasB dictate specificity of prenylation and confer resistance to benzodiazepine peptidomimetic in vitro. *J. Biol. Chem.* **270**, 6221–6226
9. Hicks, K.A., Hartman, H.L., Fierke, C.A. (2005) Upstream polybasic region in peptides enhances dual specificity for prenylation by both farnesyltransferase and geranylgeranyltransferase type I. *Biochemistry* **44**, 15323–15333
10. Fiordalisi, J.J., Johnson, R.L., Weinbaum, C.A., Sakabe, K., Casey, P.J., Cox, A.D. (2003) High affinity for farnesyl transferase and alternative prenylation contribute individually to K-ras4B resistance to farnesyl transferase inhibitors. *J. Biol. Chem.* **278**, 41718–41727
11. García-Torres, D., Fierke, C. A. (2019) SmgGDS-607 exhibits dual effects in regulating farnesylation of small GTPases: activation and inhibition. *J. Biol. Chem.* (Under revision)
12. Fersht, A. (1999) *Structure and mechanism in protein science: A guide to enzyme catalysis and protein folding*, W. H. Freeman and Company, New York
13. Hougland, J.L., Lamphear, C.L., Scott, S.A., Gibbs, R.A., Fierke, C.A. (2009) Context-dependent substrate recognition by protein farnesyltransferase. *Biochemistry* **48**, 1691–1701
14. Furfine, E.S., Leban, J.J., Landavazo, A., Moomaw, J.F., and Casey, P.J. (1995) Protein farnesyltransferase: kinetics of farnesyl pyrophosphate binding and product release. *Biochemistry* **34**, 6857–6862

15. Reigard, S.A., Zahn, T.J., Haworth, K.B., Hicks, K.A., Fierke, C.A., Gibbs, R.A. (2005) Interplay of isoprenoid and peptide substrate specificity in protein farnesyltransferase. *Biochemistry* **44**, 11214–11223
16. Hougland, J.L., Hicks, K.A., Hartman, H.L., Kelly, R.A., Watt, T.J., Fierke, C.A. (2010) Identification of novel peptide substrates for protein farnesyltransferase reveals two substrate classes with distinct sequence selectivities. *J. Mol. Biol.* **395**, 176–190
17. Hancock, J.F. (2003) Ras proteins: different signals from different locations. *Nat. Rev. Mol. Cell Biol.* **4**, 373–384
18. Jennings, B.C., Lawton, A.J., Rizk, Z., and Fierke, C.A. (2018) SmgGDS-607 regulation of RhoA GTPase prenylation is nucleotide-dependent. *Biochemistry* **57**, 4289–4298
19. Shimizu, H., Toma-Fukai, S., Saijo, S., Shimizu, N., Kontani, K., Katada, T., and Shimizu, T. (2017) Structure-based analysis of the guanine nucleotide exchange factor SmgGDS reveals armadillo-repeat motifs and key regions for activity and GTPase binding. *J. Biol. Chem.* **292**, 13441–13448
20. Hamel, B., Monaghan-Benson, E., Rojas, R. J., Temple, B. R., Marston, D. J., Burrige, K., and Sondek, J. (2011) SmgGDS is a guanine nucleotide exchange factor that specifically activates RhoA and RhoC. *J. Biol. Chem.* **286**, 12141–12148
21. Berg, T. J., Gastonguay, A. J., Lorimer, E. L., Kuhnmuensch, J. R., Li, R., Fields, A. P., and Williams, C. L. (2010) Splice variants of SmgGDS control small GTPase prenylation and membrane localization. *J. Biol. Chem.* **285**, 35255–35266
22. Lanning, C. C., Ruiz-Velasco, R., and Williams, C. L. (2003) Novel mechanism of the co-regulation of nuclear transport of SmgGDS and Rac1. *J. Biol. Chem.* **278**, 12495–12506
23. Schuld, N. J., Vervacke, J. S., Lorimer, E. L., Simon, N. C., Hauser, A. D., Barbieri, J. T., Distefano, M. D., Williams, C. L. (2014) The chaperone protein SmgGDS interacts with small GTPases entering the prenylation pathway by recognizing the last amino acid in the CAAX motif. *J. Biol. Chem.* **289**, 6862–6876
24. Wilson, J.M., Prokop, J.W., Lorimer, E., Ntantie, E., Williams, C.L. (2016) Differences in the phosphorylation-dependent regulation of prenylation of Rap1A and Rap1B. *J. Mol. Biol.* **428**, 4929–4945
25. Gonyo, P., Bergom, C., Brandt, A.C., Tsaih, S.W., Sun, Y., Bigley, T.M., Lorimer, E.L., Terhune, S.S., Rui, H., Flister, M.J., Long, R.M., Williams, C.L. (2017) SmgGDS is a transient nucleolar protein that protects cells from nucleolar stress and promotes the cell cycle by regulating DREAM complex gene expression. *Oncogene* **36**, 6873–6883
26. Chavan, T.S., Jang, H., Khavrutskii, L., Abraham, S.J., Banerjee, A., Freed, B.C., Johannessen, L., Tarasov, S.G., Gaponenko, V., Nussinov, R., Tarasova, N.I. (2015) High-affinity interaction of the K-Ras4B hypervariable region with the Ras active site. *Biophys J.* **109**, 2602–2613
27. Abraham, S.J., Nolet, R.P., Calvert, R.J., Anderson, L.M., Gaponenko, V. (2009) The hypervariable region of K-Ras4B is responsible for its specific interactions with calmodulin. *Biochemistry* **48**, 7575–7583

28. Thapar, R., Williams, J.G., Campbell, S.L. (2004) NMR characterization of full-length farnesylated and non-farnesylated H-Ras and its implications for Raf activation. *J Mol Biol.* **343**, 1391–1408
29. Bergom, C., Hauser, A. D., Rymaszewski, A., Gonyo, P., Prokop, J. W., Jennings, B. C., Lawton, A. J., Frei, A., Lorimer, E. L., Aguilera-Barrantes, I., Mackinnon Jr., A. C., Noon, K., Fierke, C. A., Williams, C. L. (2016) The tumor-suppressive small GTPase DiRas1 binds the noncanonical guanine nucleotide exchange factor SmgGDS and antagonizes SmgGDS interactions with oncogenic small GTPases. *J. Biol. Chem.* **291**, 6534–6545
30. Ogita, Y., Egami, S., Ebihara, A., Ueda, N., Katada, T., and Kontani, K. (2015) DiRas2 protein forms a complex with SmgGDS protein in brain cytosol in order to be in a low affinity state for guanine nucleotides. *J. Biol. Chem.* **290**, 20245–20256
31. Pompliano, D. L., Schaber, M. D., Mosser, S. D., Omer, C. A., Shafer, J. A., Gibbs, J. B. (1993) Isoprenoid diphosphate utilization by recombinant human farnesyl:protein transferase: Interactive binding between substrates and a preferred kinetic pathway. *Biochemistry* **32**, 8341–8347
32. Hartman, H. L., Hicks, K. A., Fierke, C. A. (2005) Peptide specificity of protein prenyltransferases is determined mainly by reactivity rather than binding affinity. *Biochemistry* **44**, 15314–15324
33. Kirchner, J. (2001) Data Analysis Toolkit #5: Uncertainty Analysis and Error Propagation. Accessed March 11, 2019. [http://seismo.berkeley.edu/~kirchner/eps\\_120/Toolkits/Toolkit\\_05.pdf](http://seismo.berkeley.edu/~kirchner/eps_120/Toolkits/Toolkit_05.pdf).
34. Plowman, S. J., Hancock, J. F. (2005) Ras signaling from plasma membrane and endomembrane microdomains. *Biochimica et Biophysica Acta* **1746**, 274–283
35. Tschantz, W. R., Furfine, E. S., Casey, P. J. (1997) Substrate binding is required for release of product from mammalian protein farnesyltransferase. *J. Biol. Chem.* **272**, 9989–9993

## CHAPTER 4

### Conclusions and Future Directions

Ras proteins have been the center of cancer research for the past 30 years because of their role in initiating signaling pathways via their GTP/GDP exchange cycle. Particularly, KRas4B has been the focus of many research efforts towards understanding the mechanisms of action for proper Ras function. Although targeting farnesylation, the first step in the Ras membrane trafficking pathway, through FTIs seemed like an infallible approach for cancer therapy, KRas4B circumvents this approach by restoration of Ras membrane insertion via alternative prenylation. However, targeting Ras membrane localization remains a viable scientific rationale. The recent discovery of SmgGDS proteins and their involvement in regulating transport through prenylation of small GTPases has opened the possibility for targeting the SmgGDS:Ras interaction as a novel approach to cancer treatment. In this thesis, we have identified the sequence requirements at the C-terminus of Ras proteins for recognition by FTase and SmgGDS-607. We characterized the roles of the polybasic region and CAAX identity in modulating FTase kinetics. We elucidated the mechanism employed by SmgGDS-607 in inhibiting Ras prenylation through substrate sequestration. Excitingly we identified a novel function of SmgGDS-607 for enhancing prenylation of GTPases that lack a PBR. Finally, we made progress toward understanding regulation of Ras entry into the prenylation pathway. Here we summarize the results of this work and the implications in human cancer.

#### ***The role of SmgGDS-607 in Ras prenylation***

Cell-based experiments provide evidence that SmgGDS-607 immunoprecipitates with non-prenylated KRas4B (1). However, when comparing levels of prenylated versus non-prenylated KRas4B upon SmgGDS-607 overexpression in cells, there were no observed changes in the ratio of the different species. In contrast, overexpression of SmgGDS-607 caused an accumulation of non-prenylated small GTPases that become

geranylgeranylated, such as RhoA, Rap1A, and Rac1. These observations led to the hypothesis that SmgGDS-607 effectively regulates the prenylation of GTPases that will become geranylgeranylated, but not of GTPases that will become farnesylated, such as KRas4B. However, this observation only considered one of many small GTPases that are farnesylated in cells. Therefore, we sought to define the role of SmgGDS-607 in regulating farnesylation of various small GTPases, particularly those that belong to the Ras family. We developed *in vitro* experiments to determine the direct effects of SmgGDS-607 on farnesylation kinetics, and more importantly, to elucidate a mechanism to explain why regulation of geranylgeranylation is observed in various small GTPases, while regulation of KRas4B farnesylation by SmgGDS-607 seems to be non-existent.

To define the role of SmgGDS-607 in regulating farnesylation, we examined three representative FTase substrates, KRas4B, HRas and DiRas1. We performed competition experiments, in which we measured the levels of protein prenylation at different concentrations of SmgGDS-607, along with binding assays to measure the binding affinities of Ras proteins for the FTase and SmgGDS-607. These studies indicate that, in fact, addition of SmgGDS-607 either decreases or increases the levels of farnesylation depending on the small GTPase identity. For proteins that contain a PBR, SmgGDS-607 has an inhibitory effect on farnesylation. In contrast, for proteins that lack a PBR, SmgGDS-607 enhances farnesylation by catalyzing product release. Collectively, the data elucidated a mechanism for SmgGDS-607-mediated regulation of farnesylation of FTase substrates in which inhibition of farnesylation depends on which protein, FTase or SmgGDS-607, has the highest affinity for the substrate. Our data demonstrate that although SmgGDS-607 binds to KRas4B, the “lack” of regulation in prenylation is due to a >600-fold difference in binding affinity favoring FTase interaction. Given that SmgGDS-607 can inhibit or enhance farnesylation, these differential effects on small GTPases can significantly alter the dynamics and levels of Ras farnesylation in cells. Furthermore, small GTPases contribute to the cellular complexity of GTPase regulation by: differential expression and post-translational modifications, shifting nucleotide status, and continuous involvement in different pathways and protein-protein interactions that affect the relative concentration of these proteins in the cell.

At the start of this research, the consensus in the field was that SmgGDS proteins only interact with small GTPases containing a PBR (2-5). This theory stemmed from early experiments suggesting that SmgGDS could act as a GEF for a variety of small GTPases that contain a PBR, such as RhoA (6), Rac1 (7), Cdc42 (8), Rap1A (9), Rap1B (10), KRas4B (9), but not for HRas (11,12). However, a recent study demonstrated that this GEF activity is only true for RhoA and RhoC (2), calling for further investigation into the structural features needed for the interaction between small GTPases and SmgGDS proteins. In this thesis, we demonstrate that SmgGDS-607 can interact with GTPases (with and without a PBR) in various ways, including via a ternary complex with the prenyltransferase. Now that a crystal structure has been determined for one of the SmgGDS splice variants (4,13), a number of site-directed mutagenesis studies could be done to elucidate the structure/function relation of SmgGDS in this newly discovered interaction with Ras. For example, computer modeling of the SmgGDS-558 structure suggests that there is a putative binding interface in which many GTPases, like RhoA, Rap1A, DiRas1, and KRas4B, could bind in a similar manner (14). Particularly, the residues of SmgGDS-607 that influence Rap1A co-immunoprecipitation are D239, E242, E246, D253, E255, N394, K395, N387, N342, R345 (5). Due to the armadillo repeat motifs in the SmgGDS structure, it is predicted that SmgGDS acts as a scaffold protein. We demonstrate that SmgGDS does not directly interact with FTase. However, for HRas, SmgGDS could be regulating both HRas and FTase in the HRas:FTase complex to increase the dissociation rate constant. Because the binding mechanism of SmgGDS:HRas is distinct to the other small GTPases, one could prepare and analyze these SmgGDS mutations individually and in combination to elucidate which residues are involved in ternary complex formation for HRas in comparison to those residues that enhance the binding affinity of RhoA. We predict that residues involved in recognition of PBR might not play a significant role for the interaction with HRas.

This work revealed a novel function of SmgGDS-607 with a small GTPase that lacks a PBR, however, this function might be specific for enhancing farnesylation of HRas. Therefore, investigating the effects of wild-type and SmgGDS-607 mutants on prenylation of other endogenous FTase substrates that lack a PBR, such as NRas and Rap2A, or GGTase-I substrates that lack a PBR, such as Rap2B and RhoB, would test whether this

observed function is general for PBR-lacking substrates and expand our understanding of the role of SmgGDS in prenylations of small GTPases.

### ***The role of the PBR in protein binding and catalysis***

The presence of the upstream polylysine region in KRas4B has been proposed to increase binding affinity of FTase to this substrate, which along with its ability to be alternatively prenylated has been suggested to cause FTI resistance (15,16). Our data demonstrate that not only does the PBR enhance binding affinity, but the presence of a PBR enhances catalytic efficiency. Interestingly, our data differs from previous studies performed with peptide substrates, in which the presence of an upstream PBR decreases the farnesylation rate constant and  $k_{cat}/K_M$  (17). Our study with Ras chimeras demonstrate that the presence of a PBR enhances  $k_{cat}$  by >10-fold and  $k_{cat}/K_M$  by >50-fold, suggesting that additional contacts not contained in the peptide play a significant role in the FTase:Ras interaction. Furthermore, our studies show that the catalytic enhancement is not limited to the “classical” C-terminal sequence KKKKKKSKTKCVIM, but it is also observed in substrates with longer and varied PBR sequences and different CAAX identities, such as DiRas1 and DiRas2. Collectively, our multiple- and single-turnover kinetic experiments demonstrate that the PBR aids in product dissociation as indicated by a decrease in  $k_{cat}$  and a shift of the rate-limiting step to product release upon substitution of the PBR sequence in KRas4B to the HVR sequence from HRas. Our binding studies with Ras chimeras establish that synergies between the PBR and CAAX motif dictate binding affinity for SmgGDS-607. Furthermore, as observed in Chapter 2 with HRas, SmgGDS-607 enhances farnesylation of substrates that lack a PBR. Yet, the extent of enhancement is also dependent on the CAAX identity.

To better understand the role of the PBR (or lack thereof) in protein binding and catalysis, efforts should be directed towards elucidating the mechanism that dictates SmgGDS-mediated farnesylation of substrates without a PBR. Based on the competition experiments discussed in Chapter 2 and Chapter 3, we developed two preliminary mechanisms to describe our observations with Ras substrates (wild-type and chimeras) (Figure 4.1). Based on previous peptide data (17), PBR-containing substrates most likely follow a mechanism described in Figure 4.1A. FTase needs to bind an FPP molecule

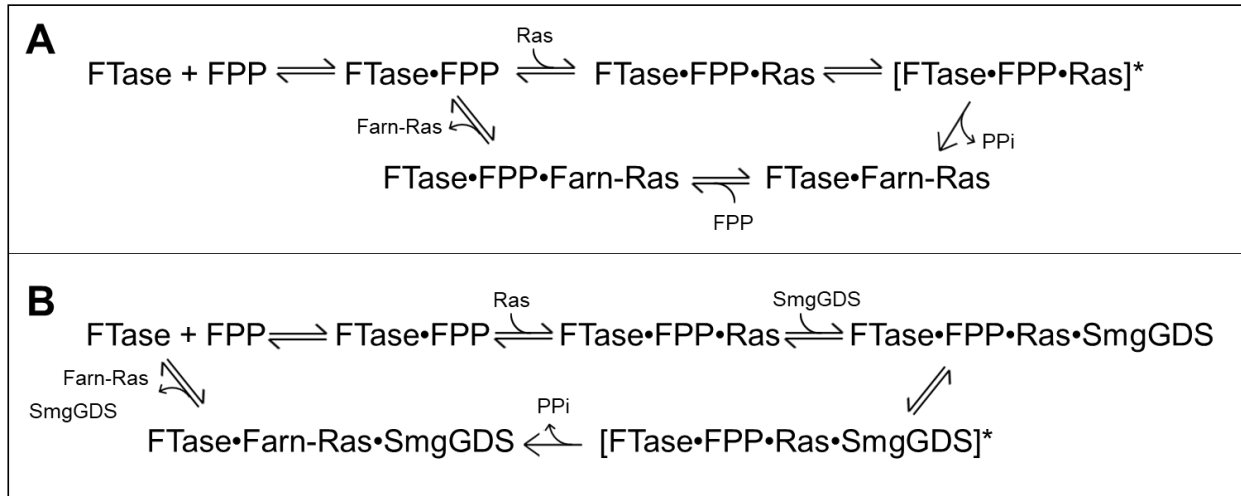


**Figure 4.1. Proposed kinetic mechanisms for FTase catalytic cycle.** (A) Farnesylation of PBR-containing Ras substrates. (B) SmgGDS-mediated farnesylation of Ras substrates lacking a PBR.

before binding Ras, followed by a change in conformation that allows for farnesylation. After this step, FTase binds to a new FPP molecule, which promotes the release of product. For substrates without a PBR, like HRas, SmgGDS enhances catalysis and product release (Figure 4.1B). Similar to Figure 4.1A, FTase binds both an FPP molecule and Ras to initiate the reaction. However, the FTase:Ras:SmgGDS-607 complex needs to be formed to promote formation of FTase active conformation and catalyze the incorporation of the farnesyl group. After this step, SmgGDS replaces the role of FPP and enhances product dissociation. To confirm if this is the path followed by substrates that lack a PBR, additional thermodynamic and kinetic experiments need to be done. We currently have only measured the binding affinity of the Ras chimeras with SmgGDS-607. To further explore this mechanism, binding experiments with Ras chimeras, FTase and SmgGDS-607 should be done to determine whether substrates that lack a PBR form a ternary complex. Additionally, competition experiments with SmgGDS-607 against farnesylation of Ras chimeras should be performed with different SmgGDS-607 concentrations.

The mutational analysis of SmgGDS-607 with RhoA reveals that residues in the electronegative patch of SmgGDS are crucial for interacting with the PBR (2). With computational modeling, residues D119, E200, E211, E213, E217, E237, D239, E242, E246, E253, D255, E288, D294, D303, and E304 have been identified to make up the electronegative patch in SmgGDS-607 (14). Given that the PBR of RhoA (ARRGKKKKSG)

is different to that of KRas4B (KKKKKKSKTK) and that the binding affinities between RhoA and KRas4B for SmgGDS-607 differ by >1,000-fold, we hypothesize that differences in contacts come into play for interaction with SmgGDS-607. Site-directed mutagenesis studies can provide a better understanding of the role of the electronegative patch in SmgGDS-607 in recognizing the distinctive polylysine region in KRas4B. For example, an *in-silico* docking and mutational analysis study suggested that residues D239, E242, E246, E253, and D255 of SmgGDS-607 are responsible for Rap1 PBR binding (5). Therefore, mutational analysis of these residues and other residues corresponding to the electronegative patch in SmgGDS-607 could determine which residues are responsible for KRas4B PBR binding. As previously done in the Fierke laboratory, we can measure the binding affinity with these mutants using fluorescence anisotropy and a fluorescently labeled peptide that represents the PBR and CAAX motif of KRas4B (18). Furthermore, mutational analysis of the polylysine region in KRas4B can elucidate which residues on the C-terminus PBR contribute to farnesylation and/or to SmgGDS binding.

The effects of the PBR in FTase kinetics have been presented in this work. However, investigating the effects of the PBR in GGTase-I kinetics could expand our understanding on protein prenylation, specifically the factors that dictate recognition of substrates and catalysis by GGTase-I. FTase and GGTase-I are distinct heterodimers composed of a common  $\alpha$ -subunit and differing  $\beta$ -subunits that contain most of the catalytic residues. The differences in sequence of the  $\beta$ -subunits allow for each enzyme to endogenously modify separate pools of small GTPases. Because the CAAX motif is essential for substrate recognition and catalysis, much efforts in understanding GGTase-I substrate specificity have resorted to peptides that mimic this region. However, given that other PBR-containing small GTPases undergo geranylgeranylation for proper membrane localization and function, performing multiple- and single-turnover experiments with different PBR-containing peptides and full-length protein substrates can expand our understanding of how structural and sequence motifs contribute to the regulation of small GTPase geranylgeranylation.

### ***Implications of thesis work in cancer treatment***

The implications of Ras in cancer have been extensively explored by the scientific and medical community in the last 30 years. Unfortunately, although researchers have made great progress in understanding the Ras signaling pathways, Ras proteins are still considered to be an “undruggable” target. One approach to abolishing aberrant signaling caused by mutations in Ras has been to block farnesylation, the first step in the Ras membrane trafficking pathway, via small molecules that inhibit FTase. However, this approach has not been successful due to alternative prenylation of KRas4B, the most commonly mutated isoform, in the presence of FTIs. One way to circumvent the limitations of FTI treatment can be through use of combination therapy. This thesis work sheds light into the factors that dictate the interaction of Ras proteins with the prenyltransferases and a newly discovered small GTPase chaperone protein identified as SmgGDS-607. Particularly, this work highlights the binding and catalytic mechanisms made possible by the recognition of important structural and sequence motifs found in Ras, such as the PBR and CAAX motifs. Identifying which residues come into contact and how they aid in regulating prenylation can be of great importance for the development of small molecules that target these specific motifs. For example, since DiRas1 binds >300-fold tighter than KRas4B to SmgGDS-607, developing a small molecule that can disrupt the SmgGDS-607:DiRas1 interaction might render free SmgGDS-607 in the cell that is available to interact with KRas4B. Given that SmgGDS-607 can inhibit alternative prenylation of KRas4B, a combination therapy that includes an FTI and a small molecule that blocks the SmgGDS-607:DiRas1 interaction might allow KRas4B to be preserved in a non-prenylated state and might disrupt the oncogenic signaling of this isoform. Ultimately, the results of these studies provide insight into possible avenues that can be explored for effective treatment of Ras-related cancer.

## REFERENCES

1. Schuld, N. J., Vervacke, J. S., Lorimer, E. L., Simon, N. C., Hauser, A. D., Barbieri, J. T., Distefano, M. D., Williams, C. L. (2014) The chaperone protein SmgGDS interacts with small GTPases entering the prenylation pathway by recognizing the last amino acid in the CAAX motif. *J. Biol. Chem.* **289**, 6862–6876.
2. Hamel, B., Monaghan-Benson, E., Rojas, R. J., Temple, B. R. S., Marston, D. J., Burridge, K., Sondek, J. (2011) SmgGDS is a guanine nucleotide exchange factor that specifically activates RhoA and RhoC. *J. Biol Chem.* **286**, 12141–12148.
3. Williams, C. L. (2003) The polybasic region of Ras and Rho family small GTPases: a regulator of protein interactions and membrane association and a site of nuclear localization signal sequences. *Cell Signal.* **15**, 1071–1080.
4. Shimizu, H., Toma-Fukai, S., Saijo, S., Shimizu, N., Kontani, K., Katada, T., Shimizu, T. (2017) Structure-based analysis of the guanine nucleotide exchange factor SmgGDS reveals armadillo repeat motifs and key regions for activity and GTPase binding. *J. Biol Chem.* **292**, 13441–13448.
5. Wilson, J. M., Prokop, J. W., Lorimer, E., Ntantie, E., Williams, C. L. (2016) Differences in the phosphorylation-dependent regulation of prenylation of Rap1A and Rap1B. *J. Mol. Biol.* **428**, 4929–4945.
6. Isomura, M., Kaibuchi, K., Yamamoto, T., Kawamura, S., Katayama, M., Takai, Y. (1990) Partial purification and characterization of GDP dissociation stimulator (GDS) for the proteins from bovine brain cytosol. *Biochem. Biophys. Res. Commun.* **169**, 652–659.
7. Hiraoka, K., Kaibuchi, K., Ando, S., Musha, T., Takaishi, K., Mizuno, T., Asada, M., Ménard, L., Tomhave, E., Didsbury, J., Snyderman, R. Takai, Y. (1992) Both stimulatory and inhibitory GDP/GTP exchange proteins, smgGDS and rhoGDI, are active on multiple small GTP-binding proteins. *Biochem. Biophys. Res. Commun.* **182**, 921–930.
8. Yaku, H., Sasaki, T., Takai, Y. (1994) The Dbl oncogene product as a GDP/GTP exchange protein for the Rho family: its properties in comparison with those of SmgGDS. *Biochem. Biophys. Res. Commun.* **198**, 811–817.
9. Mizuno, T., Kaibuchi, K., Yamamoto, T., Kawamura, M., Sakoda, T., Fujioka, H., Matsuura, Y., Takai, Y. (1991) A stimulatory GDP/GTP exchange protein for smg p21 is active on the post-translationally processed form of c-Ki-ras p21 and rhoA p21. *Proc. Natl. Acad. Sci. U S A* **88**, 6442–6446.
10. Yamamoto, T., Kaibuchi, K., Mizuno, T., Hiroyoshi, M., Shirataki, H., Takai, Y. (1990) Purification and characterization from bovine brain cytosol of proteins that regulate the GDP/GTP exchange reaction of smg p21s, ras p21-like GTP-binding proteins. *J. Biol. Chem.* **265**, 16626–16634.
11. Orita, S, Kaibuchi, K., Kuroda, S., Shimizu, K., Nakanishi, H., Takai, Y. (1993) Comparison of kinetic properties between two mammalian ras p21 GDP/GTP exchange proteins, ras guanine nucleotide-releasing factor and smg GDP dissociation stimulation. *J. Biol. Chem.* **268**, 25542–25546.
12. Vikis, H. G., Stewart, S., Guan, K. L. (2002) SmgGDS displays differential binding and exchange activity towards different Ras isoforms. *Oncogene.* **21**, 2425–2432.

13. Shimizu, H., Toma-Fukai, S., Kontani, K., Katada, T., Shimizu, T. (2018) GEF mechanism revealed by the structure of SmgGDS-558 and farnesylated RhoA complex and its implication for a chaperone mechanism. *Proc. Natl. Acad. Sci. U S A.* **115**, 9563–9568.
14. Bergom, C., Hauser, A. D., Rymaszewski, A., Gonyo, P., Prokop, J. W., Jennings, B. C., Lawton, A. J., Frei, A., Lorimer, E. L., Aguilera-Barrantes, I., Mackinnon, A. C., Noon, K., Fierke, C. A., Williams, C. L. (2016) The tumor-suppressive small GTPase DiRas1 binds the noncanonical guanine nucleotide exchange factor SmgGDS and antagonizes SmgGDS interactions with oncogenic small GTPases. *J. Biol. Chem.* **291**, 6534–6545.
15. James, G. L., Goldstein, J. L., Brown, M. S. (1995) Polylysine and CVIM sequences of K-RasB dictate specificity of prenylation and confer resistance to benzodiazepine peptidomimetic *in vitro*. *J. Biol. Chem.* **270**, 6221–6226.
16. Fiordalisi, J. J., Johnson II, R. L., Weinbaum, C. A., Sakabe, K., Chen, Z., Casey, P. J., Cox, A. D. (2003) High affinity for farnesyltransferase and alternative prenylation contribute individually to K-Ras4B resistance to farnesyltransferase inhibitors. *J. Biol. Chem.* **278**, 41718–41727.
17. Hicks, K. A., Hartman, H. L., Fierke, C. A. (2005) Upstream polybasic region in peptides enhances dual specificity for prenylation by both farnesyltransferase and geranylgeranyltransferase type I. *Biochemistry* **44**, 15325–15333.
18. Jennings, B. C., Lawton, A. J., Rizk, Z., Fierke, C. A. (2018) SmgGDS-607 regulation of RhoA GTPase prenylation is nucleotide-dependent. *Biochemistry* **57**, 4289–4298.